Performance Evaluation of Wireless Medium Access Control Protocols for Internet of Things

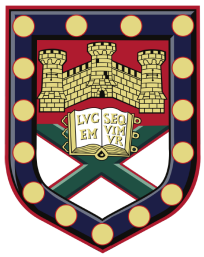

Ning Wang

College of Engineering, Mathematics and Physical Sciences
University of Exeter

Submitted by Ning Wang to the University of Exeter as a thesis for the degree of
Doctor of Philosophy in Computer Science

I certify that all material in this thesis which is not my own work has been identified and that any material that has previously been submitted and approved for the award of a degree by this or any other University has been acknowledged.

Department of Computer Science February 2023

I would like to dedicate this thesis to my loving parents.

I also wish to dedicate it to all I lost during the study period.

Declaration

I hereby declare that except where specific reference is made to the work of others, the contents of this dissertation are original and have not been submitted in whole or in part for consideration for any other degree or qualification in this, or any other university. This dissertation is my own work and contains nothing which is the outcome of work done in collaboration with others, except as specified in the text and Acknowledgements. This dissertation contains fewer than 65,000 words including appendices, bibliography, footnotes, tables and equations and has fewer than 150 figures.

Ning Wang
February 2023

Acknowledgements

First and foremost, I would like to express my most profound appreciation to my supervisor Dr. Jia Hu who gave me the extremely precious opportunity to do this wonderful project. Moreover, his invaluable supervision, support and tutelage are all indispensable for me to complete this project. He has been and will always be not only a supervisor of my academic work but also a director of my life.

Many thanks also to my second supervisor Prof. Geyong Min for all his help. I have learned a lot from his enthusiasm and wisdom.

I would like to extend my sincere thanks to Prof. Shusen Yang. His guidance enlightened me the real academia and research. Without his help, I would never know more than the textbooks and exams.

Thanks should also go to my colleagues in the lab over the years: Dr. Zhengxin Yu, Dr. Chengqiang Huang, Dr. Haozhe Wang, Dr. Miao Wang, Dr. Zhiwei Zhao, Dr. Yuan Zuo, Dr. Jin Wang, Dr. Lejun Chen, Dr. Ke Li, Ms. Yang Mi, Mr. Dongya Wang, Mr. Zheyi Chen, Mr. Han Xu, and all members in the lab who offer me lots of help and care for me. It was a wonderful time with their accompany.

Words cannot express my gratitude to my friends Dr. Hao Yang, Dr. Yumeng Yang, Dr. Taiming Chen, Mr. Henry Chen, Mr. Yanlin Wu, Mr. Yizhuo Sun, Mr. Guohua Yang, Mr. Kunihiko Kanasaki, and all the fantastic guys. This endeavour would not have been possible without their help during my research time in the UK. It is a small world, after all.

Special thanks to all who may not be able to receive my appreciation in this world. We will meet again.

Finally, I am deeply grateful to my great parents and families, who always support me and love me. A new day will begin, and my heart will be with you forever.

Abstract

The Internet of Things makes the residents in Smart Cities enjoy a more efficient and high-quality lifestyle by wirelessly interconnecting the physical and visual world. However, the performance of wireless networks is challenged by the ever-growing wireless traffic data, the complexity of the network structures, and various requirements of Quality of Service (QoS), especially on the Internet of Vehicle and wireless sensor networks. Consequently, the IEEE 802.11p and 802.11ah standards were designed to support effective inter-vehicle communications and large-scale sensor networks, respectively. Although their Medium Access Control protocols have attracted much research interest, they have yet to fully consider the influences of channel errors and buffer sizes on the performance evaluation of these Medium Access Control (MAC) protocols. Therefore, this thesis first proposed a new analytical model based on a Markov chain and Queuing analysis to evaluate the performance of IEEE 802.11p under imperfect channels with both saturated and unsaturated traffic. All influential factors of the Enhanced Distributed Channel Access (EDCA) mechanism in IEEE 802.11p are considered, including the backoff counter freezing, Arbitration Inter-Frame Spacing (AIFS) defers, the internal collision, and finite MAC buffer sizes. Furthermore, this proposed model considers more common and actual conditions with the influence of channel errors and finite MAC buffer sizes. The effectiveness and accuracy of the developed model have been validated through extensive ns-3 simulation experiments.

Second, this thesis proposes a developed analytical model based on Advanced Queuing Analysis and the Gilbert-Elliot model to analyse the performance of IEEE 802.11p with burst error transmissions. This proposed analytical model simultaneously describes transmission queues for all four Access Categories (AC) queues with the influence of burst errors. Similarly, this presented model can analyse QoS performance, including throughputs and end-to-end delays with the unsaturated or saturated load traffics. Furthermore, this model operates under more actual bursty error channels in vehicular environments. In addition, a series of simulation experiments with a natural urban environment is designed to validate the efficiency and accuracy of the presented model. The simulation results reflect the reliability and effectiveness of the presented model in terms of throughput and end-to-end delays under various channel conditions.

Third, this thesis designed and implemented a simulation experiment to analyse the performance of IEEE 802.11ah. These simulation experiments are based on ns-3 and an extension. These simulation experiments' results indicate the Restricted Access Window (RAW) mechanism's influence on the throughputs, end-to-end delays, and packet loss rates. Furthermore, the influences of channel errors and bursty errors are considered in the simulations. The results also show the strong impact of channel errors on the performance of IEEE 802.11ah due to urban environments.

Finally, the potential future work based on the proposed models and simulations is analysed in this thesis. The proposed models of IEEE 802.11p can be an excellent fundamental to optimise the QoS due to the precise evaluation of the influence of factors on the performance of IEEE 802.11p. Moreover, it is possible to migrate the analytical models of IEEE 802.11p to evaluate the performance of IEEE 802.11ah.

List of Publications

N. Wang and J. Hu, "Performance Analysis of the IEEE 802.11p EDCA for Vehicular Networks in Imperfect Channels," *2021 20th International Conference on Ubiquitous Computing and Communications (IUCC/CIT/DSCI/SmartCNS)*, 2021, pp. 535-540

N. Wang and J. Hu, “Performance analysis of the IEEE 802.11p for vehicular networks with bursty packet errors”, *2022 IEEE International Conference on Trust, Security and Privacy in Computing and Communications (TrustCom)*, 2022, pp. 1440-1445

N. Wang and J. Hu, "A Comprehensive Performance Analysis of the IEEE 802.11p MAC under Imperfect Channels and Finite Buffer Sizes Conditions," Submitted to *Computer Communications*.

N. Wang and J. Hu, "Modelling and Performance Analysis of the IEEE 1609.4 WAVE/DSRC for Vehicle Network with Burst Error Transmission," To be submitted.

N. Wang and J. Hu, "A simulation study of the performance of the IEEE 802.11ah with bursty packet errors", To be submitted.

Table of contents

List of figures

List of tables

Chapter 1

Introduction

1.1 Overview

Smart Cities focus on improving the quality of life for urban residents with a wireless-connected environment. In a future Smart City structure, data is collected by a massive number of sensors equipped on smartphones, tablets, wearable devices, vehicles, buildings, and everywhere around the city [1]. In return, the collected information is processed and analysed in the cloud to help various potential and existing applications, including traffic management, auto-driving systems, environment monitoring, crime detection, community services, and urban planning [2]. These applications require high efficiency and reliable wireless network environments to exchange data among devices. Therefore, the wireless network connection is indispensable to Smart City structures. The network of sensors on physical objects is called the Internet of Things (IoT). More specially, the networks particularly designed for vehicles are defined as the Internet of Vehicles (IoV). Moreover, both IoT and IoV provide services to multifarious users, such as moving pedestrians and vehicles, immovable buildings, and even drones flying in the sky [3]. As a result, wireless networks handle a major transmission responsibility in IoT and IoV.

However, the performance of wireless networks is challenged by the myriad Quality of Service (QoS) requirements demanded by extensive and ever-growing applications. It is because of not only the continuously rising wireless traffic data but also the complex network structure of Smart Cities. For the former one, wireless traffic data is expected to boost sevenfold from 2017 to 2022, according to the Cisco Visual Networking Index [4]. Thus, the throughput performance of the wireless networks of IoT and IoV is required to deal with the explosive growth of data. For the latter one, the safety-related services of IoV, such as emergency electronic brake warnings and hazardous location notifications, have very

stringent real-time requirements. Hence, the wireless network of IoT and IoV is required to deliver messages with low latency and high reliability.

In order to support the IoV services, IEEE 802.11p was designed as a standard that enables data exchanges between high-speed vehicles and the roadside infrastructure. Similar to IEEE 802.11e, IEEE 802.11p employs the Enhanced Distributed Channel Access (EDCA) mechanism in its Medium Access Control (MAC) protocol [5]. Applications with different QoS requirements are assigned to one of four Access Categories (ACs). The QoS of each AC is differentiated by specific EDCA parameters, including the Contention Window (CW) and Arbitrary Inter-frame Space (AIFS). Thus, the probability that an AC wins the channel's contention depends on the deferring and back-off time decided by the value of the AIFS and CW. Nevertheless, IEEE 802.11p disables the Transmission Opportunity (TXOP) limit and utilises different EDCA parameters due to the unique environment of IVC [6].

Moreover, unlike other WLAN environments, wireless channels of IEEE 802.11p are significantly influenced by the obstacles and the movement in vehicular environments due to the high Doppler shift and large delay spread [7, 8]. Furthermore, vehicles' physical surroundings are ever-changing within urban environments, affecting packet transmissions. Thus, the channel status, including the path loss and channel error rate, can significantly change during driving [9, 10]. To enhance the transmission channel for vehicular environments, the PHY protocol of IEEE 802.11p was developed based on IEEE 802.11a PHY with a higher carrier frequency, 5.9 GHz [11]. However, although the higher carrier frequency can improve the rapid channel variations caused by the mobility of vehicles, the influences of realistic physical environments are still underestimated.

IEEE 802.11ah (Wi-Fi HaLow) standard is designed to meet the requirements of large-scale, low-energy consumption sensor networks for the Internet of Things. Different from the other standard of IEEE 802.11 families, IEEE 802.11ah focuses on improving the performance of a wireless network composed of hundreds or even thousands of low-power sensors [12]. Therefore, IEEE 802.11ah introduced several innovative concepts, including Restricted Access Window (RAW), Target Wake Time (TWT), Traffic Indication Map (TIM), and Association IDentification (AID). Moreover, it takes advantage of both low-power networks and Wi-Fi technologies. For example, IEEE 802.11ah employs Distributed Coordination Function (DCF), which has already been proven in other IEEE 802.11 protocols [13]. Consequently, it is considered one of the best solutions as a unified standard for Smart Cities. Hence, the performance of IEEE 802.11ah has drawn the attention of both academia and industry. However, the existing studies of the performance of IEEE 802.11ah need to be more comprehensive and ignore the influences of channel errors.

The remainder of this paper is organised as follows. First, the motivations and challenges of this research are discussed in Section 1.2. Second, the research aims and objectives of this thesis are introduced in Section 1.3. Third, The main contributions of this thesis are presented in Section 1.4. Finally, the outline of this thesis is provided in Section 1.5.

1.2 Motivation and challenges

The performance of IEEE 802.11p and IEEE 802.11ah is vital for both academia and industry. However, although some studies have been proposed to evaluate the performances of these standards, multiple weaknesses and challenging issues are still underestimated. The main challenging issues for the performance modelling of IEEE 802.11p are listed as follows:

- A reliable and accurate analytical model of the performance of IEEE 802.11p. The most typical method to evaluate the performance of IEEE 802.11p is using simulations. However, the time cost of using simulation tools of IEEE 802.11p could be very high. As a result, the practicality of simulation is poor. Thus, a reliable and accurate analytical model with significantly lower computational complexity is vital.

- The comprehensibility of the analytical model. Most of the existing works on the performance modelling of IEEE 802.11p neglect some of the mechanisms of IEEE 802.11p, such as the AIFS deferring procedure, internal collisions, and back-off counter freezing. It is because considering each of these mechanisms would increase the complexity and difficulty of the analytical model. However, neglecting these mechanisms, which are defined in the standard, will result in significant errors in performance evaluations.

- The impact of channel errors. The packet losses and transmission failures caused by channel errors are wildly ignored in the performance evaluation of IEEE 802.11p. However, the impact of channel errors is much more significant in IEEE 802.11p than in other IEEE 802.11 families due to the dynamic topology of high-speed vehicles and the high Doppler shift.

- The impact of the actual operating urban environments of IEEE 802.11p. Vehicles' physical surroundings are ever-changing within urban environments, affecting packet transmissions. Thus, the channel status can change dramatically during driving in urban environments. Consequently, channel errors are usually bursty in vehicular environments. Nevertheless, the impact of the bursty error transmissions has never been considered as far as we know.

- The influence of the buffer size. Most of the existing works unreally assumed infinite or zero buffer sizes. However, the buffer size can significantly influence the performance of IEEE 802.11p, especially for high-priority messages.
- The unsaturated or saturated load traffics. The throughput performance of IEEE 802.11p can change dramatically while the offered load alters. As a result, the peak and saturated throughputs can be very different. Nonetheless, many existing works only considered the latter due to the complexity.

For the performance analysis of IEEE 802.11ah, the main challenging issues are listed as follows:

- The influence of the grouping, RAW mechanism and TWT on the performance of IEEE 802.11ah. The current works need to be more comprehensive to analyse the throughputs, latency and reliability of IEEE 802.11ah. Remarkably, the influence of the RAW mechanism is underestimated.
- The impact of channel errors on the performance of IEEE 802.11ah. Due to the urban operation environment, the impact of the channel errors on the throughputs, end-to-end delays and packet loss should be addressed.

1.3 Research aims and objectives

Based on the discussion above, it is clear that many research gaps exist in the performance analysis of IEEE 802.11p and IEEE 802.11ah. First, a comprehensive analytical model of the performance of IEEE 802.11p is needed. Second, a thorough performance study of IEEE 802.11ah is worthy. Therefore, the main objectives of this research are listed as follows:

- To do a literature review of IEEE 802.11p and IEEE 802.11ah. First, this research project aims to understand the mechanism of IEEE 802.11p and IEEE 802.11ah. Second, this research project aims to study the related works of the performance evaluation of IEEE 802.11p and IEEE 802.11ah.
- To design an analytical model for the performance of IEEE 802.11p. This research project aims to design an analytical model comprehensively describing the EDCA mechanism of IEEE 802.11p. Furthermore, we aim to evaluate the performance of IEEE 802.11p under unsaturated or saturated load traffic with various MAC buffer sizes. In addition, this research project also aims to investigate the influence of channel errors.

- To improve the analytical model to evaluate the performance of IEEE 802.11p with burst error transmissions. This research project aims to model the channel status and analyse the influences of bursty errors on the performance of IEEE 802.11p.
- To design and implement simulation experiments to analyse the performance of IEEE 802.11ah. This research project aims to evaluate the RAW mechanism's influence on the throughputs, end-to-end delays, and packet loss rates with the simulation. In addition, we aim to include the channel error model and the bursty error model to study the influence on the performance of IEEE 802.11ah.

1.4 Contributions

To achieve the above objectives, this research proposes a complete analytical model for IEEE 802.11p under imperfect channels and burst error transmissions. Also, this research proposed a set of simulation studies of the performance of IEEE 802.11ah. In detail, the major contributions of this research are summarised as follows:

- A new analytical model based on 3-D Markov Chain and Queuing analysis is presented to analyse the performance of IEEE 802.11p under imperfect channels. This proposed analytical model comprehensively describes the CW backoff and AIFS deferring procedure for all four AC queues simultaneously within one 3-D Markov Chain. As a comprehensive model, all influential factors, including backoff counter freezing, AIFS deferring and internal collisions, are mathematically included. Furthermore, this model considers finite MAC buffer sizes with unsaturated or saturated load traffic. More specially, this model operates under more common imperfect channels with potential errors due to channel fading and modulation errors. In addition, a series of simulation experiments with a real urban environment is designed to validate the efficiency and accuracy of the presented model. The simulation results reflect the reliability and effectiveness of the presented model in terms of throughput and end-to-end delays under various channel conditions.
- An improved analytical model based on Advanced Queuing Analysis and the Gilbert-Elliot model is presented to analyse the performance of IEEE 802.11p with burst error transmissions. This proposed analytical model simultaneously describes transmission queues for all four AC queues with the influence of burst errors. Similarly, This presented model can analyse QoS performance, including throughputs and end-to-end delays with the unsaturated or saturated load traffics. Furthermore, this model operates

under more actual bursty error channels in vehicular environments. In addition, a series of simulation experiments with a real urban environment is designed to validate the efficiency and accuracy of the presented model. The simulation results reflect the reliability and effectiveness of the presented model in terms of throughput and end-to-end delays under various channel conditions.

- A series of simulation experiments are designed to analyse the performance of IEEE 802.11ah. These simulation experiments are based on ns-3 and an extension. These simulation experiments' results indicate the RAW mechanism's influence on the throughputs, end-to-end delays, and packet loss rates. In addition, the influences of channel errors and bursty errors are considered in the simulations. The results also show the strong impact of channel errors on the performance of IEEE 802.11ah due to urban environments.

1.5 Thesis organisation

The rest of this thesis is organised as follows:

- In Chapter 2, the background knowledge of this thesis will be introduced. First, the features and related work of the Internet of Vehicles and IEEE 802.11p will be analysed. Second, the characteristics and related work of the Internet of Things and IEEE 802.11ah will be demonstrated. Finally, a conclusion will be drawn at the end of this chapter.

- In Chapter 3, a new analytical model and the performance analysis of IEEE 802.11p for the Internet of Vehicles in imperfect channels will be proposed. First, the analytical model will be presented with the mathematical analysis and derivations. Second, this model will be validated by a series of simulations. After that, the performance of IEEE 802.11p will be evaluated. Finally, a conclusion will be drawn at the end of this chapter.

- In Chapter 4, an improved analytical model and the performance analysis of IEEE 802.11p for the Internet of Vehicles with bursty error transmissions will be developed. First, the two-state continuous-time Markov chain channel model for bursty errors will be presented. Second, the improved analytical model will be presented with mathematical analysis and derivations. Third, this improved model will be validated by a series of simulations. Fourth, the performance of IEEE 802.11p with bursty error

transmissions will be evaluated. Finally, a conclusion will be drawn at the end of this chapter.

- In Chapter 5, a simulation study of the performance analysis of IEEE 802.11ah will be proposed. First, the mechanism of the RAW will be introduced. Second, the simulation design and implementation of IEEE 802.11ah based on ns-3 will be introduced. Third, the performance of IEEE 802.11ah will be analysed regarding the throughputs, end-to-end delays and packet loss rates. Finally, a conclusion will be drawn at the end of this chapter.
- In Chapter 6, this thesis and the research works will be concluded. First, a summary of this thesis will be presented. Second, future work will be discussed.

Chapter 2

Background

With a wireless-connected environment in the future Smart City structure, the Internet of Things plays an essential role in enabling the wireless connections of users in the urban area. This chapter presents a detailed background introduction to the Internet of Vehicles and the Internet of Things. Meanwhile, this chapter proposed an in-depth review of the related work of IEEE 802.11p and IEEE 802.11ah. The rest of this chapter is organised as follows. First, the background knowledge of the IEEE 802.11p and the Internet of Vehicles will be introduced in Section 2.1. Second, the EDCA mechanism utilised in the MAC layer of IEEE 802.11p will be analysed in Section 2.2. Third, the related works of the performance evaluation of IEEE 802.11p will be discussed in Section 2.3. Fourth, the background knowledge of the Internet of Things will be presented in Section 2.4. Fifth, the related works of the performance simulation of IEEE 802.11p will be analysed in Section 2.5. Finally, a summary will be drawn in Section 2.6.

2.1 IEEE 802.11p and Internet of Vehicles

In recent years, intelligent connected vehicle systems have drawn a great deal of attention from both academia and vehicle manufacturers. It is because of its significant potential in the Intelligent Transportation Systems (ITS), especially for the safety services[14]. For instance, the intelligent connected vehicle systems enable the active safety control of the transport system of Smart Cites[15]. Furthermore, the fundamental of intelligent connected vehicle systems is to share position, speed and other information among every vehicle and pedestrian [16, 17]. Therefore, the intelligent connected vehicle systems require vehicles, pedestrians and roadside infrastructures to communicate wirelessly with each other, which is called the Internet of Vehicles (IoV).

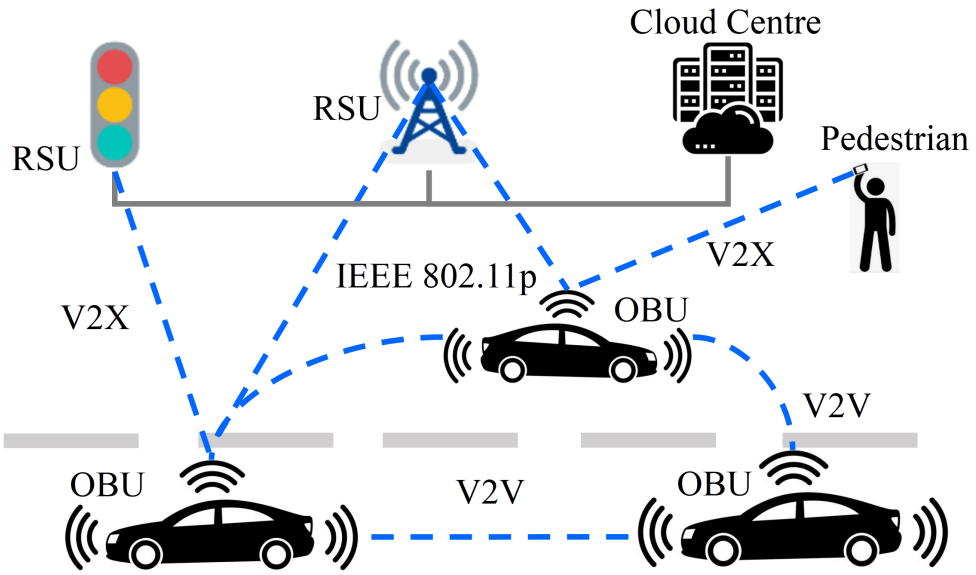

Fig. 2.1 The structure of the Inter of Vehicles

The concept of the Internet of Vehicles was first proposed at the International Telecommunication Union — Telecommunication Standardization Sector (ITU-T) Automotive Communications Standardization Conference in 2003 [18]. Initially, it was named the vehicular ad hoc network (VANET) to distinguish it from the mobile ad hoc network (MANET) in the conveyance field [19]. Later, VANET experienced an evolution with expanded applications and was renamed the Internet of Vehicles [20].

IoV enables the ability of wireless communication for not only vehicles but also infrastructures and pedestrians. Therefore, the structure of IoV is considerably complex. In detail, a typical IoV topology is composed of On-Board Units (OBUs) and Roadside Units (RSUs) [21, 22]. Firstly, the OBUs usually refer to vehicles moving on the road [23]. Recently, crewless aerial vehicles, Smart Bikes, and pedestrians with smartphones or wearable devices are also classified OBUs [24–28]. Hence, nodes with mobility are the main characteristic of OBUs. By contrast, the RSUs are immobile physical instruments built along the roadside, such as traffic lights or buildings [21, 29, 30]. Furthermore, different from OBUs, RSUs usually equip a wired connection to the Internet [31, 32]. Therefore, an RSU can be the intermediate node between OBUs and the cloud [33, 34, 23]. Fig. 2.1 illustrates a typical structure of IoV. As shown in Fig. 2. 1, OBUs and RSUs are connected by wireless networks. Moreover, communication among only vehicles is defined as Vehicle to Vehicle (V2V),

whereas communications among multiple types of users are called Vehicle to Everything (V2X) [35, 36].

IoV plays a vital role in the future Smart City structure for its potential for traffic management and public safety [37]. In an ideal intelligent connected vehicle system, both OBUs and RSUs can exchange safety messages and traffic management information for collision avoidance and auto-driving systems wirelessly through the Internet of Vehicles [38]. However, the network structure of such an intelligent connected vehicle system could be very complex as the devices use various communication methods [39]. For instance, the vehicles equipped are connected by In-Vehicle networks [40], which commonly utilise heterogeneous architectures and protocols [41]. Nevertheless, the RSUs or smartphones might use utterly different network protocols to transfer data. Hence, it leads to problems in privacy and communication efficiency [42]. Consequently, the efficiency and Quality of Services are worsened.

Moreover, with the extensive and ever-growing applications designed for Intelligent Transportation Systems and Smart Cities, the IoV is indispensably required to simultaneously accommodate multiple Quality of Service (QoS) conditions. So it is because RSUs and OBUs are communicating both safety and non-safety messages through the applications of IoV at the same time [43]. For example, according to the U.S. National Intelligent Transportation Systems (ITS) Architecture (NITSA), the safety applications of IoV include emergency electronic brake, warnings, hazardous location notifications, arterial and freeway management, crash prevention and safety, broadway operations and maintenance, and traffic incident management [44]. Meanwhile, although the IoV emphasises safety applications, there are also many common non-safety services in IoV structures, such as infotainment services, payment services, and internet access.

The IEEE 802.11p standard has a set of specifications in order to achieve communication in the ever-changing vehicular environment. It was proposed as a standard to support V2V and V2X communications by IEEE and the Federal Communication Commission (FCC) [5]. IEEE 802.11p defined the PHY and MAC layer of the Wireless Access in Vehicular Environment (WAVE) [45]. The protocol suite supports the IPv6 stack in parallel using Wave Short Message Protocol (WSMP) [46] and operates in the 5.9GHz band with a 75MHz spectrum dedicated to IoV services [47].

Similar to IEEE 802.11e, IEEE 802.11p employs the Enhanced Distributed Channel Access (EDCA) mechanism in its Medium Access Control (MAC) protocol in order to support differentiated QoS [48]. Applications with different QoS requirements are assigned to one of four Access Categories (ACs). The QoS of each AC is differentiated by specific EDCA parameters, including the Contention Window (CW) and Arbitrary Inter-frame Space

(AIFS). Thus, the probability that an AC wins the channel's contention depends on the deferring and backoff time decided by the value of the AIFS and CW [5]. Nevertheless, IEEE 802.11p disables the Transmission Opportunity (TXOP) limit and utilises different EDCA parameters due to the unique environment of IoV [6].

Most of the services and applications of IEEE 802.11p are specially developed for vehicular environments. Different from other WLAN environments, it worsened the channel fading by the Doppler spread on Orthogonal Frequency Division Multiplex (OFDM) [49]. Therefore, the obstacles and movement in vehicular environments are significantly influenced by wireless channels due to the high Doppler shift and large delay spread [50]. As a result, the channel error rate is higher and significantly impacts the performance of IEEE 802.11p [51, 50]. Moreover, vehicles' physical surroundings are ever-changing within urban environments, affecting packet transmissions [52–57]. To enhance the transmission channel for vehicular environments, the PHY layer of IEEE 802.11p was developed based on IEEE 802.11a PHY with a higher carrier frequency [5, 58]. However, although the higher carrier frequency can improve the rapid channel variations caused by the mobility of vehicles, the influences of realistic physical environments still need to be underestimated.

Furthermore, the applications of IEEE 802.11p usually have stringent QoS requirements. Thus, it is necessary to estimate the performances of IEEE 802.11p based on the actual vehicular environments. However, most of the existing research for the performance analysis of IEEE 802.11p used an unreal assumption with ideal channels similar to the analysis of other IEEE 802.11 families. Nonetheless, this assumption ignored the particular operation environments of IEEE 802.11p. For example, the performance of the transmission channel can be much poorer than expected when the vehicle passes through tunnels or builds. Such a case is usual in vehicular environments but unusual in traditional WLAN environments. Therefore, it is valuable to accurately estimate the performance by considering the influences of vehicular environments.

2.2 The EDCA mechanism in IEEE 802.11p

In the IEEE 802.11p standard, the Enhanced Distributed Channel Access (EDCA) is employed in order to support prioritised QoS services. As shown in Fig. 3.1, four ACs with priorities of high to low are defined in the IEEE 802.11p standard: Voice - AC_VO, Video - AC_VI, Best Effort - AC_BE, and Background - AC_BK (see Fig. 2.2). The ACs with higher priorities are designed for applications with higher time or throughput requirements, whereas lower-priority ACs are for non-emergency messages. Each AC works on an independent transmission queue installed in each station. The differentiated QoS is achieved by assigning

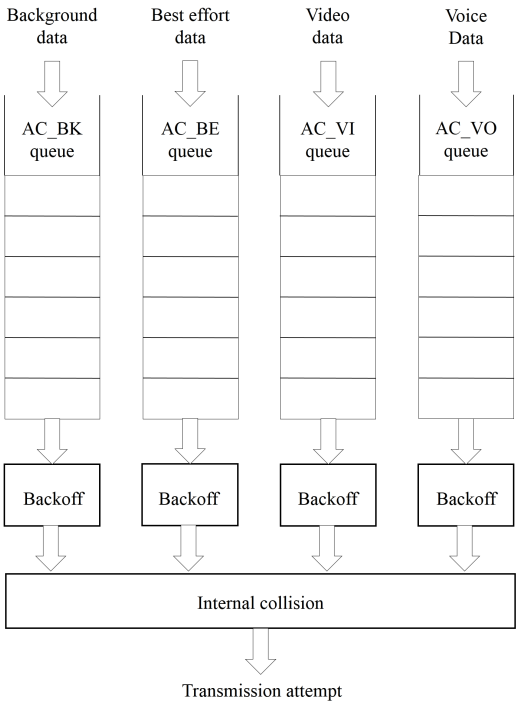

Fig. 2.2 EDCA mechanism

a unique set of distinct channel access parameters, including CW and AIFS. Generally, a larger value of CW or AIFS means less probability of winning the contention to access the channel and a long time of delays. Therefore, messages with high QoS demands can be achieved by assigning high-priority ACs.

The EDCA uses carrier sense multiple access with collision avoidance (CSMA/CA) mechanism to reduce the collisions caused by multiple nodes intended to transmit frames simultaneously. It means that a station must sense the channel's status before a transmission attempt. Therefore, transmission can only start when the channel is sensed idle and kept for an AIFS. An AIFS is defined by:

$$AIFS_{[AC]} = SIFS + AIFSN_{[AC]} * aSlotTime \tag{2.1}$$

where $AIFSN_{[AC]}$ stands for the number of time slots in $AIFS_{[AC]}$ and $aSlotTime$ is the duration of a time slot.

Otherwise, this transmission attempt defers a random backoff counter, which follows a uniform distribution within the range of $[0, CW_{AC}]$. In the beginning, the value of CW_{AC} equals CW_{min}. After experiencing a transmission failure due to a collision or a packet error, it doubles until it reaches CW_{max}. If the transmission succeeds or it reaches the retry limit,

the value of CW_{AC} is reset to CW_{min}. During the backoff procedure, the station keeps sensing the channel status. Once the channel is idle for a time slot, the backoff counter decreases for one. Otherwise, the backoff counter freezes until the channel is sensed idle continuously for an AIFS. When the backoff counter becomes zero, the AC attempts to transmit the packets. However, if it happens with multiple ACs simultaneously in one station, an internal collision occurs, and the frame from the AC with the highest priority is chosen to be transmitted.

Different from the EDCA mechanism in IEEE 802.11e, IEEE 802.11p disabled the TXOP burst transmission. Therefore, the TXOP limit for all four ACs is set to zero in the IEEE 802.11p protocol. It is due to the particular topology of IoV, in which the links between vehicles are dramatically changing. This operating environment is significantly distinct from IEEE 802.11e, including traditional Wireless Local Area Networks (WLANs) and sensor networks, which immovable or low mobility stations usually construct. As a result, each AC is allowed to transmit one frame only after it wins the contention. Moreover, the value of the CW and AIFS of each ACs is updated. This adaption is to guarantee the QoS requirements of the higher ACs.

2.3 Related work of IEEE 802.11p

The performance of the IEEE 802.11p has been a hot topic in academia. Nevertheless, the mechanism of IEEE 802.11 is complicated and challenging to model. [59] is the pioneer introduced the stochastic process and Markov process analysis into the performance analysis of IEEE 802.11. This paper primarily proved the Markov property of the process of the back-off counter decreasing [60], [61]. Furthermore, it designed a Markov chain model to estimate the behaviour of the backoff process under saturated traffic for IEEE 802.11b. Therefore, based on [59], the Markov chain model has been utilised to analyse the performance of IEEE 802.11 protocols, such as [62] and [63].

However, drawing significant attention, the EDCA mechanism was introduced in IEEE 802.11e. As a result, much fewer presented analytical models based on [59] can operate with the EDCA mechanism. Furthermore, most existing works were developed under the assumption of ideal channels and MAC buffer conditions. For example, [62] proposed a unified model of the IEEE 802.11e EDCA mechanism by combining several different approaches. The throughputs and end-to-end delays can be estimated under the assumption of saturated traffic conditions. However, this model failed to consider the impact of internal collisions. Moreover, [63] constructed a comprehensive 3-D discrete-time Markov chain model that considered the CW, AIFS and TXOP as a combination with unsaturated traffic.

However, all of these works are conceived based on IEEE 802.11e rather than on IEEE 802.11p.

Due to the unique vehicular operating environments, the EDCA mechanism in IEEE 802.11p is updated from 802.11e. Consequently, [48] made a primary attempt to compare the performance differences between IEEE 802.11e and 802.11p. It employed an analytical model to investigate the throughput under saturated traffic conditions. Primarily, it presented the contention zones, which can be the nonsynchronous AIFS deferring procedure. However, it neglected the backoff freezing mechanism and can only work under the assumption of saturated traffic. By contrast, [64] developed an analytical model which can operate under both saturated and unsaturated conditions. Nevertheless, it assumed that only one of the four AC queues is working. Similarly, [65] presented a model considering only two AC queues existing.

The mobility of vehicles is the most crucial difference between IEEE 802.11e and 802.11p. Therefore, [66] introduced a stochastic traffic model describing vehicles' mobility behaviours in IoV. Nonetheless, the work did not consider the EDCA mechanism of IEEE 802.11p. Similarly, [67] modelled the vehicles with a fluid-flow mobility model to analyse the vehicular network's time-varying behaviour. Nonetheless, this work did not consider four AC queues either. Moreover, although these two papers developed vehicle mobility models, they need to work in a more realistic traffic environment.

Given that IoV safety applications are usually highly time-sensitive, the end-to-end delays are the critical performance of QoS in IEEE 802.11p. For instance, [68] provided a study of the end-to-end delay analysis with the broadcast scheme in IEEE 802.11p by modelling the backoff and queueing processes. However, similar to the above, the EDCA mechanism is still ignored in this model. In [69], a combination of two Markov Chains analysed the delay distributions of safety messages. Nevertheless, this model assumed only two AC priorities. Based on [69], [70] analysed the reliability of the transmission of the safety messages of IEEE 802.11p. However, these two models neglected the backoff counter freezing in the MAC layer, which can significantly influence performance and reliability.

As a paramount improvement, [71] proposed an analytical model that considered the backoff counter freezing. This model combines two discrete-time Markov chains to estimate the throughputs and end-to-end delays for all four ACs queues. [72] presented another accurate analytical model with updated parameters of the IEEE 802.11p protocol. However, both models were designed with a 2-D Markov chain and another separate 1-D Markov chain. As a result, these two models cannot analyse the AIFSN deferring procedure and CW backoff jointly, which seriously increases complexity. Moreover, they ignored the influence of the buffer sizes. As another approach, [6] suggested the potential impact of the TXOP in IEEE

802.11p. However, the TXOP has been set to 0 in the 802.11p protocol due to the high-speed vehicular ad-hoc network environment. In addition, none of the works above considered the impact of the buffer sizes and channel errors.

The influences of channel errors have been considered in many existing models of IEEE 802.11e. For example, [73] presented an analytical model of 802.11e, which assumed fixed packet error rates. Nevertheless, this model was based on the analysis of the IEEE 802.11e protocol. In addition, the fixed packet error rates are unsuitable for wireless modulation. After that, [74] analysed the performance of 802.11p under an error-prone channel condition. Meanwhile, [70] also considered the influence of channel errors for the adaptive Multi-Channel assignment and coordination scheme in IEEE 802.11p. Especially, [69] considered various channel error conditions for the transmissions of IEEE 802.11p. However, these works were outside of four AC queues. By contrast, [68] proposes an analytical model with Bit Error Rates for four ACs. However, it ignored the asynchronous AIFSN deferring process of all of the four ACs queues, clearly distinct from the 802.11p protocol. Finally, as a major improvement, [50] presented a comprehensive analytical model that can estimate the QoS performance, including throughputs and end-to-end delays for four ACs queues under the impact of channel errors. This work modelled the mechanism of IEEE 802.11p with all critical factors by a 3-D Markov chain. Nonetheless, this model cannot operate with burst error transmission, which is vital in vehicular environments.

In practical vehicular environments, channel errors usually happen bursty and are highly correlated due to fading and shadowing of wireless channels. However, the realistic channel status effects are widely ignored or highly abstracted and simplified. The Gilbert-Elliot model is believed to be a reliable approach to modelling burst error transmissions. [75] and [76] introduced the Gilbert-Elliot model into the performance analysis of IEEE 802.11 families. They assumed that the channel status switches between a good and a bad state. Furthermore, [77–82] also considered the two-state Gilbert-Elliot model to increase the reliability and accuracy of the performance analysis of IEEE 802.11e. Moreover, [83] proposed an analytical model for IEEE 802.11e. This model considered not only the bursty errors but also the bursty transmissions with advanced queuing analysis. However, all the works above are not developed for vehicular networks. [84] is the first one that considered the burst error transmission in IEEE 802.11p. It utilised the Gilbert-Elliot model to abstract the channel status of IEEE 802.11p. Nonetheless, it did not analyse the influence on the performance.

The impact of the MAC buffer size is another practical problem that has not drawn enough attention to academia. Most of the existing models assumed a very small or infinite MAC buffer size. For instance, [85] and [86] designed an analytical model of the EDCA mechanism

Table 2.1 COMPARISON OF THE RELATED WORKS

	Standard	ACs	AIFSN	MAC buffer	Imperfect channel	Bursty error
[48]	802.11p	4	Yes	Infinite	No	No
[89]	802.11p	1	Yes	Finite	No	No
[90]	802.11p	1	Yes	Infinite	Yes	No
[70]	802.11p	2	Yes	Infinite	No	No
[71]	802.11p	4	Yes	Infinite	No	No
[72]	802.11p	4	Yes	Infinite	No	No
[68]	802.11p	4	No	Infinite	Yes	No
[69]	802.11p	2	No	Infinite	Yes	No
[83]	802.11e	4	Yes	Finite	Yes	Yes

for IEEE 802.11e under no buffer condition. However, this assumption ignores the influence of the queuing delay. By contrast, [87] proposed a different model, which assumed an infinite queue size for IEEE 802.11e. However, the assumption of an infinite queue is obviously not practical and unattainable. Outstandingly, [63] suggested the significance of the MAC buffer size of all four AC queues for IEEE 802.11e. This model can calculate the throughputs and end-to-end delays under a finite buffer size.

Considering the practical operation environment of vehicular networks, the nodes of IEEE 802.11p are more unlikely to implement a huge buffer size. However, as shown in Table 2.1, the majority of existing models are based on the assumption of infinite queue size[69, 70, 68, 74, 72, 71, 66]. By contrast, [88] introduced an analytical model that considered the influence of a finite queue size on the delay in IEEE 802.11p. However, this model is based on Distributed Coordination Function (DCF). Therefore, only one queue is considered in this model. Overall, the existing works on the performance analysis for IEEE 802.11p under imperfect channel conditions and finite MAC queue size are preliminary and uncompleted.

2.4 IEEE 802.11ah and Internet of Things

Modern information and communication technology introduces a novel dimension to the world where connectivity is available anytime and anywhere. This structure is widely known as the Internet-of-Thing (IoT). IoT connects people and the physical world [91]. In other words, IoT broke the boundaries limiting information dissemination [92, 93]. Meanwhile, new applications and services of IoT are boosting sharply due to the variety of smart things

being invented [94–96], including sensors, robots, vehicles, phones, and wearable devices. According to Cisco, the total number of devices in IoT will have passed 50 billion by 2020 [4].

On the one hand, the IoT enables Smart Cities and Smart Homes, which greatly improves our daily life [97–99]. On the other hand, it brings many challenges to wireless communication technologies, such as large-scale connectivity, low power consumption, long transmission range, bounded delay, and high throughput [100–102]. As a result, the current IoT solutions are argued to be insufficient to IoT. For example, ZigBee and Bluetooth are unable to provide stable connectivity and high throughput of large-scale sensor networks [103, 104]. Moreover, other solutions, such as WiMAX and LTE, are unsuitable due to the high energy consumption [105–107]. Consequently, IEEE proposed a new Wi-Fi standard, IEEE 802.11ah, also named Wi-Fi HaLow, to fill this gap, as it has sufficient throughputs with lower energy consumption.

IEEE 802.11ah is developed based on IEEE 802.11 families. Therefore, it shares the advantages of Wi-Fi technologies, which have been proven successful. For example, similar to IEEE 802.11b, IEEE 802.11ah also employ the Distributed Coordination Function (DCF) mechanism based on Carrier-Sense Multiple Access with Collision avoidance (CSMA/CA) for channel access [108]. Furthermore, it also uses a modulation method modified from orthogonal frequency division multiplexing (OFDM) [109].

However, IEEE 802.11ah introduces a number of new features to make it unique. First, IEEE 802.11ah introduced a new PHY layer. Unlike traditional Wi-Fi operating in the 2.4 GHz and 5GHz frequency bands, IEEE 802.11ah works on the sub 1 GHz (S1G) frequency bands [110]. Therefore, the transmission range of IEEE 802.11ah is vastly expanded from other IEEE 802.11 protocols [111]. The S1G is inherited from IEEE 802.11ac [112]. Nevertheless, IEEE 802.11ac was designed to serve only applications requiring a low data rate. By contrast, the data rate ranges of IEEE 802.11ah from 150 kb/s to 346.6667 Mb/s by the modulation order and the coding rate [113]. Thus, IEEE 802.11ah is able to support various data rate requirements in IoT.

Furthermore, the MAC layer of IEEE 802.11ah consists of a variety of new characteristics to improve performance and energy efficiency. First, IEEE 802.11ah introduces a grouping sectorization mechanism in its MAC layer. The nodes of IEEE 802.11ah are divided into sectors in order to solve the hidden node problem and mitigate the contention [114]. This grouping mechanism is achieved by the access point (AP) transmitting or receiving through a set of antenna beams [100]. Usually, the groups are made according to the positions of stations (STAs). Hence, the grouping sectorization can work in linkage with the RAW mechanism. The Restricted Access Window (RAW) mechanism is the most significant

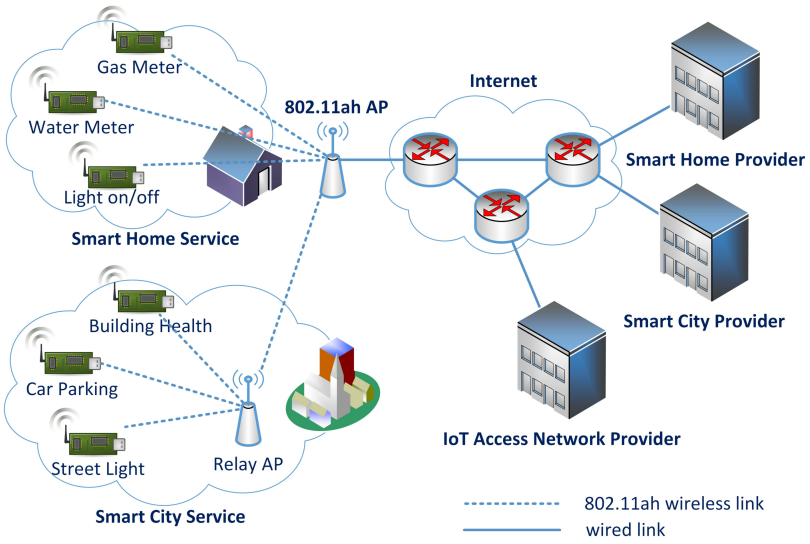

Fig. 2.3 The structure of IEEE 802.11ah for IoT [88].

characteristic of IEEE 802.11ah. RAW is a combination of time division multiple access (TDMA) and CSMA/CA [115]. In detail, each group of STAs should assign to a certain RAW slot. This is implemented by a special beacon frame which carries the RAW parameter set (RPS) information element [13]. The RPS details the group ascription of each STA and the RAW slot's start and end time [116]. The STAs assigned to a RAW slot can only access the channel during the RAW slot. Therefore, compared to the traditional IEEE 802.11 series, which allowed all nodes to contend for the medium, only the STAs within the same group are involved in the contention in IEEE 802.11ah [117]. As a result, the intensity of contention is significantly mitigated. In addition, IEEE 802.11ah also employs the Target Wake Time (TWT) mechanism in order to achieve lower energy consumption [118]. Since the RAW limited the channel access out of the RAW slot, STAs can keep in sleep or snooze mode until it is wakened up by an AP when the RAW slot starts [119]. Consequently, energy is saved due to the decreasing working time. Moreover, with the coordination of the grouping sectorization, RAW and TWT, IEEE 802.11ah is able to support more nodes, up to 8192, than traditional IEEE 802.11 protocols.

With the strong ability in energy saving and large-scale sensor networks, the applications of IEEE 802.11ah are vast. A typical structure of IEEE 802.11ah is shown in Fig. 2.3. Hence, as Fig. 2.3 illustrates, the potential usages of IEEE 802.11ah are various. For instance, the expected applications of IEEE 802.11ah are environmental and agricultural monitoring, smart meters and grids, production automation, indoor and outdoor location, and COVID-19 monitoring [118, 120, 121].

2.5 Related work of IEEE 802.11ah

With its great potential in IoT and industrial internet, the performance of the IEEE 802.11ah standard has been studied for years before it was officially published in 2017. However, most of the existing research concentrates on the unique modulation structure of IEEE 802.11ah. For example, [122] proposed a performance study of IEEE 802.11ah with multiple antennas and Multiple-Input Multiple-Output (MIMO) schemes in 2013. It demonstrated simulation outputs of the end-to-end delays and throughputs with the S1G PHY layer. However, this work assumed a MAC protocol similar to IEEE 802.11n because the IEEE 802.11ah had not been standardised then. Therefore, the influences of the new features in the MAC layer are neglected, including the grouping, RAW and TWT mechanisms. Moreover, [123] presented an in-depth throughput analysis with various modes of operation. It analysed the influence on throughputs of the Modulation and Coding Scheme (MCS) from MCS 0 up to MCS 10. In addition, it compared the effective throughputs multiband of IEEE 802.11ah. Also, this work provided a BER evaluation of multiple modulations. Nonetheless, the latency and reliability of IEEE 802.11ah were not mentioned.

Furthermore, [124] designed a comparison study of the performances of IEEE 802.11ah and Bluetooth. It compared the delays and packet loss probabilities in an indoor scenario of the two different protocols. However, IEEE 802.11ah emphasises the performance and low-energy consumption of large-scale sensor networks in urban environments. Thus, the in-door scenario is incapable of demonstrating the principal advantages of IEEE 802.11ah. By contrast, [125] proposed a simulation work to analyse the behaviour of IEEE 802.11ah with an outdoor scenario. As a result, it indicated the impact on packet loss probabilities of various outdoor long transmission ranges. Nevertheless, same as all the works mentioned above, it ignored the influences of the unique MAC layer of IEEE 802.11ah.

As a vital improvement, [126] introduced a simulation study of the RAW mechanism in the MAC layer of IEEE 802.11ah. However, it only demonstrated the packet loss rates with two different traffics. Therefore, the performance of throughputs and delays were not contained. Furthermore, [127] presented a more detailed performance analysis of the RAW mechanism of IEEE 802.11ah. It discussed the impact on the throughputs and packet loss rates of the number of STAs and the number of groups of the RAW mechanism. In addition, it also indicated the influence of the duration of a RAW slot. Based on [127], [128] developed a further study to improve the performance of the MAC layer of IEEE 802.11ah. However, the current IEEE 802.11ah standard defines a fixed duration of a RAW slot which is different from its assumption. Moreover, [129] designed a simulation to analyse the performance of the MAC layer of IEEE 802.11ah with multiple APs. As a result, it demonstrated throughputs of

up to 9 APs. Nevertheless, it used only one grouping method, which neglected the influences of different numbers of STAs in a RAW group.

Furthermore, [130] proposed an uncomplicated performance analysis of the RAW mechanism in IEEE 802.11ah. It evaluated the throughputs and delays of IEEE 802.11ah with the DCF mechanism. This work used a DCF analytical model based on the classic model proposed in [59]. However, the model of [59] was designed for IEEE 802.11b, and it did not validate its model with simulation results. Meanwhile, [131] also developed a performance analysis with a similar model. It evaluated the influence of the number of STAs on the throughputs. Nonetheless, the paper was proposed before the official presentation of IEEE 802.11ah. Therefore, the features and assumptions of IEEE 802.11ah in this work are outdated, especially the length of a RAW slot defined in the standard. Furthermore, the influence of channel errors was widely ignored. None of the works above has taken the channel errors into consideration.

In contrast, [132] primarily analysed the achievable data rate under the impact of a fixed Bit Error Rate (BER). It also evaluated the influence of transmission ranges. However, it did not consider the bursty error transmission. Moreover, [133] discussed the packet loss rates due to the Doppler Effect of IEEE 802.11ah. However, it considered the channel errors of only movable STAs. In fact, the movable environment is not the primary utilisation environment of IEEE 802.11ah because it is the territory of IEEE 802.11p. In addition, again, the bursty error transmission is ignored. Overall, there is a significant gap in the performance analysis for IEEE 802.11ah under the imperfect channel conditions and bursty error transmissions.

2.6 Conclusion

To conclude, first, an accurate analytical model must consider all influential factors following the IEEE 802.11p protocol and actual conditions. Nevertheless, although academia has concentrated on the performance analysis of IEEE 802.11p since it was proposed, all of the existing models, to the best of our knowledge, are inadequate or do not capture realistic operation conditions. Second, the simulation and performance analysis of IEEE 802.11ah is insufficient. The existing simulation works of the performance of IEEE 802.11ah ignore either the influences of the new mechanism of IEEE 802.11ah or the impact of the channel status.

Chapter 3

Modelling and Performance Analysis of IEEE 802.11p for Internet of Vehicles in Imperfect Channels

3.1 Introduction

The Internet of Vehicles plays a crucial role in future Intelligent Transportation Systems (ITS). IoV provides the Vehicle to Vehicle (V2V) and Vehicle to Everything (V2X) wireless network connections to exchange safety, traffic management and infotainment information for automobiles in Smart Cities. The equipment in a typical IoV topology is composed of Road-Side Units (RSUs) and On-Board Units (OBUs). RSUs and OBUs are expected to communicate multiple safety or non-safety messages through applications of IoV. However, the myriad applications demand various Quality of Services (QoS).

In order to support differentiated QoS, IEEE 802.11p has been designed for the rapidly increasing applications in IoV. Similar to IEEE 802.11e, IEEE 802.11p employs the Enhanced Distributed Channel Access (EDCA) mechanism in its Medium Access Control (MAC) protocol. Applications with different QoS requirements are assigned to one of four Access Categories (ACs). The QoS of each AC is differentiated by specific EDCA parameters, including the Contention Window (CW) and Arbitrary Inter-frame Space (AIFS). Thus, the probability that an AC wins the channel's contention depends on the deferring and backoff time decided by the value of the AIFS and CW. Nevertheless, IEEE 802.11p disables the Transmission Opportunity (TXOP) limit and utilizes different EDCA parameters due to the unique environment of IoV.

Furthermore, unlike the traditional wireless network, the dynamic topology of IoV is connected by vehicles moving at high speeds, which worsens the channel fading by the Doppler spread on Orthogonal Frequency Division Multiplex (OFDM). As a result, the channel error rate is higher and significantly impacts the performance of IEEE 802.11p. Therefore, with the specific characteristics described above of IEEE 802.11p, a complete, reliable and effective analytical model of the IEEE 802.11p EDCA mechanism for vehicular networks is required.

3.2 Analytical model

3.2.1 Modelling of the backoff procedure

In this section, we present a 3-D discrete-time Markov Chain to analyze the EDCA mechanism in IEEE 802.11p. This 3-D Markov chain demonstrates the procedure of the CW backoff and AIFS deferring schemes. The notations utilized in the proposed model can be found in Table 3.1. The AC_BK AC_BE, AC_VI, and AC_VO are denoted by subscripts $AC_v, (v = 0, 1, 2, 3)$, respectively. First, we consider some assumptions in our work.

- The collision probability, p_v, is irrelevant to the number of retries. Therefore, p_v is unchanged after any unsuccessful transmission.
- The packet arrival traffic for each AC_v follows a Poisson Process with the rate λ_v. Therefore, the packet interval follows an Exponential distribution with the expectation equation to $\frac{1}{\lambda_v}$.
- The impact of channel fading and modulation is modelled by Bit Error Rates (BER) for simplicity. It means that each bit of a frame shares the same error rate. If a packet with errors is received, the packet is discarded at the destination. Then, retransmission is required until the retry limit is reached. In addition, we assume the MAC header, PHY header, and Acknowledgement (ACK) are error-free. Thus, the probability of receiving an erroneous packet is:

$$p_e = 1 - (1 - BER^L) \tag{3.1}$$

where L stands for the frame payload length.

Table 3.1 NOTATIONS OF THE ANALYTICAL MODEL

Notations	Definition
AC_v	Access Catagory v
BER	Bit Error Rates
d_v	The differences between $AIFS_v$ and $AIFS_{min}$
D_v	End-to-end delay of AC_v
DQ_v	Mean of the queuing delay of AC_v
DS_v	Mean of the service delay of AC_v
D_v^s	Mean of the service delay if a packet of AC_v is received
D_v^f	Mean of the service delay if a packet of AC_v is discarded
$\overline{D}_v^a$	Mean of the channel access delay if a packet of AC_v is received
$\overline{D}_v^b$	Mean of the channel access delay if a packet of AC_v is discarded
k	MAC buffer size of AC_v
L	Packet size
m	Retry limit
n	Number of vehicles
p_b	Collision probability of AC_v
p_e	Error probability of a frame
p_{bv}	Probability of the channel is idle during the CW backoff period of the AC_v
p_{tv}	Probability of the channel is idle during the $AIFS$ period of the the AC_v after $AIFS_{min}$
P_{0v}	Probability of the transmission queue of AC_v is empty
P_{Kv}	Probability of the MAC buffer of AC_v is full
T_v^A	Average time spent on deferring the AIFS period of AC_v
T_v^a	Average time spent for each attempt during the AIFS period of the AC_v
T_v^{col}	Transmission delay of AC_v when an internal collision happens
T_v^{tr}	Transmission delay of AC_v when the packet is received
W_{iv}	Current CW value after i times failed transmission
S_v	Throughput put of AC_v
α_v	Probability of at least one of ACs transmits in a given time slot during AC_v is in the backoff procedure
β_a	Probability of the packet of the transmission of AC_a is received during AC_v is in the backoff procedure
$\overline{\alpha}_v$	Probability of at least one of ACs transmits in a given time slot during AC_v is in the AIFS deferring procedure
$\overline{\beta}_a$	Probability of the packet of the transmission of AC_a is received during AC_v is in the AIFS deferring procedure
$\overline{\sigma_v}$	Average length of a time slot
τ_v'	Transmission probability of AC_v under the saturation condition
τ_v	Transmission probability of AC_v under the non-saturation condition
λ_v	Packet arrival rate of AC_v
μ_v	Mean service rate of AC_v
μ_{sv}	Mean service rate of a frame is transmitted successfully of the AC_v
μ_{fv}	Mean service rate of a frame is discarded of AC_v

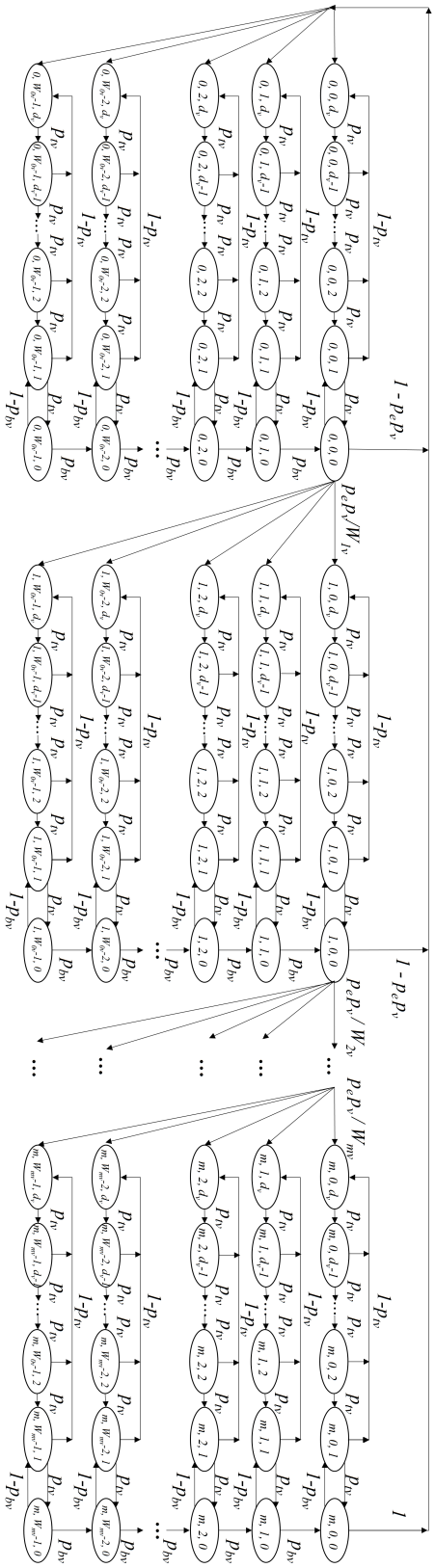

Fig. 3.1 3-D Markov Chain.

With the assumptions above, we construct the 3-D discrete-time Markov chain. Let s(t) represent the stochastic process of the backoff stage, b(t) denote the stochastic process of the backoff counter for a given AC, and c(t) stands for the stochastic process of the AIFS backoff counter from the AIFS of current AC to minimum AIFS. In this Markov chain, we define a time slot as the variable time interval between the starts of two consecutive decrements of the backoff counter. To avoid ambiguity, the fixed time slot (unit time) defined in [5] is called the physical time slot. Then, we model these three stochastic processes s(t), b(t), c(t) as a 3-D discrete-time Markov chain which illustrating in Fig. 3.1.

The state transition probabilities of this 3-D Markov chain are demonstrated as follows:

$$
\begin{cases}
P_{\{i,j,0|i,j+1,0\}} = p_{bv}, & i \in [0,m]\ ,\ j \in [1, W_{iv}-1] \quad (3.2a)\\
P_{\{i,j,d_v|i,j,0\}} = 1-p_{bv}, & i \in [0,m]\ ,\ j \in [1, W_{iv}-1] \quad (3.2b)\\
P_{\{i,j,0|i,j,1\}} = p_{tv}, & i \in [0,m]\ ,\ j \in [0, W_{iv}-1] \quad (3.2c)\\
P_{\{i,j,k|i,j,k+1\}} = p_{tv}, & k \in [0, d_v-1] \quad (3.2d)\\
P_{\{i,j,d_v|i,j,k\}} = 1-p_{tv}, & k \in [0, d_v] \quad (3.2e)\\
P_{\{i,j,d_v|i-1,0,0\}} = \frac{p_v p_e}{W_{iv}}, & i \in [1,m]\ ,\ j \in [0, W_{iv}-1] \quad (3.2f)\\
P_{\{0,j,d_v|i,0,0\}} = \frac{(1-p_v p_e)}{W_{iv}}, & i \in [0,m-1]\ ,\ j \in [0, W_{iv}-1] \quad (3.2g)\\
P_{\{0,j,d_v|m,0,0\}} = \frac{1}{W_{0v}}, & j \in [0, W_{iv}-1] \quad (3.2h)
\end{cases}
\tag{3.2}
$$

where p_v is the collision probability of the Head-of-Queue (HoQ) frame of the AC_v. p_{bv} stands for the probability that the channel is sensed idle for a time slot after the AIFS period of the AC_v. p_{tv} denotes the probability the channel is sensed idle for a time slot within the AIFS period of the AC_v.m is the retry limit. Furthermore, d_v denotes the difference of the AIFS value of the current AC between the minimal value of AIFSN. Hence, $d_v = AIFS_v - AIFS_{min}$. W_{iv} represents the current CW value after i times failed transmission. According to the IEEE

802.11p protocol [5], the W_{iv} can be calculated as follow:

$$W_{iv} = \begin{cases} CW_{min}+1, & i=0 \\ 2^{i}W_{0v}, & i \in [1,m') \\ CW_{max}+1, & i \in [m',m] \end{cases} \tag{3.3}$$

where m' is the maximum backoff stage for the AC_v, and m is the retry limit. The equations of the state transition probabilities are explained as follows:

- Equation (3.2a) accounts for the case that the channel is sensed idle for a time slot, and the backoff counter decreases one.
- Equation (3.2b) accounts for the case that the channel is sensed busy and the backoff counter freezes.
- Equation (3.2c) accounts for the case that the backoff counter is activated after the AIFS deferring period.
- Equation (3.2d) accounts for the case that the channel is sensed idle during the AIFS deferring period, and the remaining slots for the backoff counter start to decrease one.
- Equation (3.2e) accounts for the case that the channel is sensed busy during the AIFS deferring period, and the AC returns to the beginning of the AIFS deferring period.
- Equation (3.2f) accounts for the case that an unsuccessful transmission occurs due to either a collision or an erroneous packet, and the backoff stage goes up.
- Equation (3.2g) accounts for the case that a successful transmission occurs and the value of CW is rest to CW_{min}.
- Equation (3.2h) accounts for the case that the retry limit has been reached and the value of CW is rest to CW_{min}.

Hence, let $b_{i,j,k}$ stand for the stationary distribution of the 3-D Markov chain above. The $b_{i,j,k}$ satisfies the following normalization condition with $i \in [0,m], j \in [0,W_{iv}-1], k \in [0,d_v]$:

$$1 = \sum_{i=0}^{m}\sum_{j=0}^{W_{iv}-1} b_{i,j,0} + \sum_{i=0}^{m}\sum_{j=0}^{W_{iv}-1}\sum_{k=1}^{d_v} b_{i,j,k} \tag{3.4}$$

Now, we can derive the expression of the initial state $b_{0,0,0}$ by solving this 3-D Markov process:

$$b_{0,0,0} = \left\{ \frac{(1-p_{tv}^{d_v})}{(1-p_{tv})p_{tv}^{d_v}}[(1-p_{bv})\sum_{i=0}^{m}\frac{W_{iv}-1}{2p_{bv}}(p_v p_e)^i + \sum_{i=0}^{m}\frac{(p_v p_e)^i}{W_{iv}}] + \sum_{i=0}^{m}\frac{W_{iv}-1}{2p_{bv}}(p_v p_e)^i + \frac{1-(p_v p_e)^{m+1}}{1-p_v p_e} \right\}^{-1} \tag{3.5}$$

Let τ_v' denote the transmission probability of AC_v when at least one frame is waiting in the queue. Then, τ_v' can be derived as follow:

$$\tau_v' = \sum_{i=0}^{m} b_{i,0,0} = b_{0,0,0}\sum_{i=0}^{m}(p_v p_e)^i = \frac{1-(p_v p_e)^{m+1}}{1-p_v p_e} b_{0,0,0} \tag{3.6}$$

Therefore, the transmission probability of AC_v under the unsaturated traffic condition, τ_v, can be derived as follow:

$$\tau_v = \tau_v'(1-P_{0v}) \tag{3.7}$$

where P_{0v} denotes the probability that the transmission queue is empty, which will be derived in the section of queuing model. If an HoB frame attempts to be transmitted from the same AC in multiple stations simultaneously or from an AC with higher priority in the same station, a collision occurs. Thus, the collision probability of AC_v, p_v, can be calculated as follow:

$$p_v = 1 - \prod_{a=0}^{A}(1-\tau_a)^{n-1}\prod_{a>v}^{A}(1-\tau_a) \tag{3.8}$$

where A is the number of the AC queues, and n is the number of vehicles.

If the channel is sensed idle for a time slot during the AIFS period of the AC_v, it means that all of the other ACs with higher priority are not transmitting in the current time slot. Hence, let p_{bv} to be this probability, and p_{tv} can be calculated as follow:

$$p_{tv} = \prod_{a>v}(1-\tau_a)^n \tag{3.9}$$

If the channel is sensed idle for a time slot after the AIFS period of the AC_v, it means that all of the other ACs are not transmitting in the current time slot. Hence, let p_{bv} be this probability, and p_{bv} can be calculated as follow:

$$p_{bv} = (1-\tau_v)^{n-1}\prod_{a\neq v}(1-\tau_a)^n \tag{3.10}$$

3.2.2 Analysis of the service time

In this section, we analyze the mean service time of each frame. The service time is combined with the transmission delay and channel access delay. The transmission delay means the time duration of a packet transmitting over the channel. The value of this time duration has two possible cases: the packet is delivered to the receiver, or the transmission fails due to an internal collision. Note that the transmission delay for an erroneous transmission is equal to a successful one. Hence, let T_v^{tr} represent the first case and T_v^{col} for the second. We have:

$$\begin{cases} T_v^{tr} = AIFS_v + T_{header} + T_{SIFS} + T_{ACK} + T_L \\ T_v^{col} = AIFS_v + T_{header} + T_{SIFS} + T_{ACK} \end{cases} \tag{3.11}$$

where T_{header}, T_{ACK} and T_L represent the time duration of transmitting the header, ACK and payload, respectively, and the T_{SIFS} and $AIFS_v$ denote for the time duration of SIFS and AIFS deferring of AC_v.

Let α_v represent the probability that the channel is occupied by another AC_a during AC_v in the backoff procedure. This probability is mutually inverse of the probability of the channel being in idle status, pb_v. Also, β_a denotes the probability that transmission of this AC_a experienced a transmission without any internal collision. From (3. 11), the value of α_v and β_a are given by:

$$\begin{cases} \alpha_v = 1 - p_{bv} \\ \beta_a = n\tau_a(1-\tau_v)^{(n-2)} \prod_{b\neq v}(1-\tau_b)^{n-1} \prod_{b>a}^{A}(1-\tau_b) \end{cases} \tag{3.12}$$

Therefore, the expression of the mean duration of a time slot, $\overline{\sigma}_v$, is given as follows:

$$\overline{\sigma}_v = \sum_{a=0}^{A} \beta_a T_a^{tr} + (\alpha_v - \sum_{a=0}^{A} \beta_a) T_v^{col} + (1-\alpha_v)\sigma + \alpha_v T_v^A \tag{3.13}$$

where T_v^A is the time duration spent on the AIFS deferring period of AC_v, and σ is the duration of a physical time slot defined in the 802.11p protocol [5]. Hence, the third term calculates the average time if the channel is idle during AC_v in the backoff procedure. The last term calculates the average time during the backoff counter frozen and AC_v in the AIFS deferring period. Moreover, during the period of the backoff counter of AC_v being frozen, it must go through from the beginning of the AIFS period again and again once it senses a busy channel. Therefore, this period consists of many potential attempts. Let T_v^a stand for the time

cost for each attempt. From the Markov chain shown in Fig. 3.1, we have:

$$T_v^A = \sum_{z=1}^{\infty} p_{tv}^{d_v}(1-p_{tv}^{d_v})^{z-1} z T_v^a \tag{3.14}$$

where z is the number of attempts.

When AC_v in the AIFS deferring procedure, let $\overline{\alpha}_v$ represent the probability that at least one of another AC_a transmits, and $\overline{\beta}_a$ denotes the probability that the packet of this transmission is received by the destination in a given slot. The value of $\overline{\alpha}_v$ and $\overline{\beta}_a$ are given by:

$$\begin{cases} \overline{\alpha}_v = 1 - p_{tv} \\ \overline{\beta}_a = n\tau_a \prod_{b>v}(1-\tau_b)^{(n-1)} \prod_{b>max\{a,v\}}^{A}(1-\tau_b) \end{cases} \tag{3.15}$$

Therefore, T_v^a can be calculated as follows:

$$T_v^a = \sum_{a>v}^{A} \overline{\beta}_a T_a^{tr} + (\overline{\alpha}_v - \sum_{a>v}^{A} \overline{\beta}_a) T_v^c + \sigma \sum_{x=1}^{d_v-1} x p_{tv}^x \tag{3.16}$$

where the last term calculates the average time spent on a failed attempt for the remaining time slots during the AIFS period of the AC_v after $AIFS_{min}$.

Note that the infinite summation in (3.14) can be solved by the summation of the series formula. Therefore, from (3.11)-(3.16), the mean duration of a time slot can be expressed by τ_v and p_v with constants.

Turn to the analysis of the mean channel access time. Similar to the transmission time, the channel access time also has two possibilities: the packet is received successfully or discarded due to the retry limit reached. Let $\overline{D}_v^a$ represent the mean value for the first case, and $\overline{D}_v^b$ for the second. Therefore, the expressions of $\overline{D}_v^a$ is given as follows:

$$\begin{aligned} \overline{D}_v^a = \left[(1-p_e)T_v^{col} + p_e T_v^{tr}\right] \sum_{i=0}^{m} \frac{i(p_v p_e)^i(1-p_v p_e)}{1-(p_v p_e)^{m+1}} + \\ \overline{\sigma}_v \sum_{i=0}^{m}\sum_{j=0}^{i} \frac{(W_{jv}-1)(p_v p_e)^i(1-p_v p_e)}{2\left[1-(p_v p_e)^{m+1}\right]} \end{aligned} \tag{3.17}$$

Similarly, the expressions of $\overline{D}_v^b$ is given as follows:

$$\overline{D}_v^b = (m+1)\left[(1-p_e)T_v^{col} + p_e T_v^{tr}\right] + \overline{\sigma}_v \sum_{i=0}^{m} \frac{W_{jv}-1}{2} \tag{3.18}$$

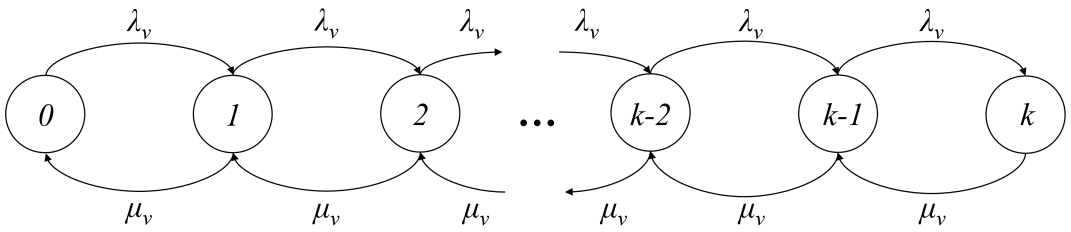

Fig. 3.2 M/M/1/k queue of the MAC buffer.

Finally, the mean service time can be calculated by summing up the transmission time and the mean channel access time. Hence, let D_v^s denote the mean service time of a frame transmitted successfully, and D_v^f stands for the mean service time of a frame discarded due to the retry limit reached. Therefore, D_v^s and D_v^f can be calculated as follows:

$$\begin{cases} D_v^s = \overline{D}_v^a + T_v^{tr} \\ D_v^f = \overline{D}_v^b \end{cases} \tag{3.19}$$

3.2.3 Queuing analysis

In this section, we discuss the throughput and end-to-end delay calculation based on the Queuing analysis. Since the traffic of packets arriving follows Poisson Distribution, the queue of AC_v can be modelled as an $M/M/1/k$ queuing system. As shown in Fig.3.2, k equals the MAC buffer size, and the arrival rate equals λ_v. The mean service rate μ_v is composed of two components: the service rate of the frame is transmitted successfully, μ_{sv}; and the service rate of the frame is removed due to the retry limit reached, μ_{fv}. The mean service rate is defined as the reciprocal of the mean service time. Therefore, from (3.19), μ_{sv} and μ_{fv} are given as follow:

$$\begin{cases} \mu_{sv} = \frac{1}{D_v^s} \\ \mu_{fv} = \frac{1}{D_v^f} \end{cases} \tag{3.20}$$

From the Markov chain shown in Fig.3.2, μ_v can be calculated as follows:

$$\mu_v = \mu_{fv}(p_v p_e)^{m+1} + \mu_{sv}[1 - (p_v p_e)^{m+1}] \tag{3.21}$$

Therefore, the probability that no frame is waiting in the queue, P_{0v}, and the probability that a frame is discarded due to the finite buffer being full, P_{Kv}, can be calculated by the

queuing system theories [134]:

$$P_{0v} = \frac{1 - \frac{\lambda_v}{\mu_v}}{1 - (\frac{\lambda_v}{\mu_v})^{k+1}} \tag{3.22}$$

$$P_{Kv} = P_{0v}(\frac{\lambda_v}{\mu_v})^k \tag{3.23}$$

Note that from (3.1) to (3.23), all variables can be expressed by τ_v and p_v with constants. Moreover, the relationships between τ_v and p_v are shown in (8) and (9). Thus, the value of τ_v and p_v can be solved by a numerical method. Therefore, the throughput of AC_v, S_v, can be calculated as follow:

$$S_v = \lambda_v L(1 - P_{Kv})[1 - (p_v p_e)^{m+1}] \tag{3.24}$$

where L is the size of the payload.

Then, turn to the calculation of the end-to-end delay. The end-to-end delays of AC_v, D_v, mean the total time duration that a frame of AC_v spends on the MAC layer. It comprises the service delay, D_v^s, and the queue delay, D_v^q. Hence, $D_v = D_v^s + D_v^q$. First, the mean service delay is equal to the reciprocal of the mean service rate. Therefore, $D_v^s = \frac{1}{\mu_v}$. The expression of μ_v has already been expressed in (3.21). Second, the queue delay and total delay can be calculated by the queue theory of $M/M/1/k$ queues [134]. Hence, we have:

$$D_v^q = \frac{\frac{\frac{\lambda_v}{\mu_v}}{1-\frac{\lambda_v}{\mu_v}} - \frac{(k+1)\frac{\lambda_v}{\mu_v}^{(k+1)}}{1-(\frac{\lambda_v}{\mu_v})^{k+1}} - (1 - P_{0v})}{\lambda_v(1 - P_{Kv})} \tag{3.25}$$

3.3 Model validation

Table 3.2 SYSTEM PARAMETERS

Frame payload	500 Bytes	PHY header	192 bits
MAC header	224 bits	ACK	304 bits
Data rate	6 Mbit/s	Buffer size	50 frames
Slot time	13 µs	Retry limit	7
SIFS	32 µs	Number of vehicles	10 vehicles

In this section, the effectiveness and precision of our analytical model are verified by a series of simulation results. As shown in Fig. 3.3, the simulation is conducted using a real map of a part of the urban area in Liverpool, UK. The map is extracted from OpenStreetMap

Table 3.3 EDCA PARAMETERS

	AIFSN	CW_{min}	CW_{max}
AC_BK	9	3	7
AC_BE	6	7	15
AC_VI	3	15	1023
AC_VO	2	15	1023

[135]. The network simulation experiments are designed with the simulation tool ns-3 (ns-3 3.30) [136]. We consider an urban environment with 10 OBUs (vehicles) running in a 360m $\times$ 360m rectangular map. Each vehicle is moving around with a constant velocity of 10 m/s following the Random Way Point model. The mobility of vehicles is generated by SUMO [137]. One RSU is at the centre of this map. All vehicles install four AC queues and transmit frames to the RSU. The transmission power is set strong enough to cover all of the maps. The packet arrival rates of four ACs are equal and follow a Poisson Process with a mean value λ_v. We ran multiple times of simulations with different random seeds and calculated average results. The simulation time of each simulation is 300 s. Other parameters follow the definition in the IEEE 802.11p protocol[5] and showing in Table 3.2 and Table 3.3.

Fig. 3.3 Simulation map.

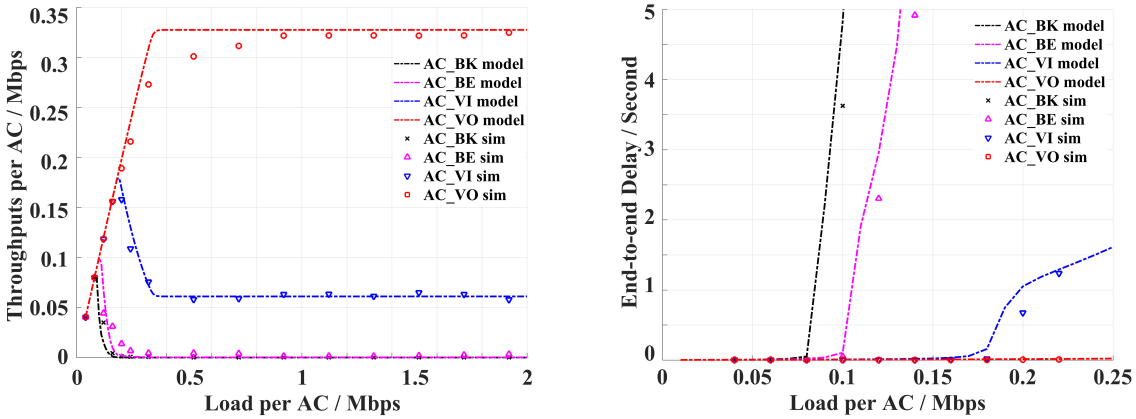

Fig. 3.4 Throughput and end-to-end delay vs. load per AC under an error-free channel.

Fig. 3.4 demonstrates the throughput and end-to-end delay versus the offered loads per AC under a perfect channel condition. In this case, the channel error is zero. This assumption was utilized in most of the existing models. From the left figure of Fig. 3.4, we can see that the throughputs of all four ACs grow linearly at first as the channel is unsaturated and then drops except for AC_VO. The saturation throughput under a perfect channel is about 0.055 Mbps and 0.33 Mbps for AC_VI and AC_VO, respectively. Thus, the throughputs of higher ACs, which have stringent throughput requirements, can be ensured.

Meanwhile, the saturation throughputs for AC_BK and AC_BE are all very low. However, the non-saturation throughputs for AC_BK and AC_BE can reach 0.085 Mbps and 0.1 Mbps, respectively, when the loads are lower than 0.16 Mbps. Also, the peak throughput of AC_VI is about 0.18 Mbps which is about three times as high as the saturation throughput. Therefore, the throughputs of all four ACs with non-saturation loads significantly differ from those with saturation loads.

From the right figure of Fig. 3.4, we can see that the end-to-end delays for all four ACs are very low at the beginning. However, for AC_BK and AC_BE, the end-to-end delays grow sharply to more than 5 seconds when the load increases. Meanwhile, the end-to-end delays for AC_VI also increase to more than 1.5 seconds. By contrast, the end-to-end delays for AC_VO keep at a reasonable level. Thus, the low delay requirement can be ensured for AC_VO.

Generally, it is clear that the results of the proposed analytical model closely match the results obtained from the simulation experiments. In addition, due to the dramatic changes in the throughput during the transition period, the differences between the results of the proposed analytical model and the results of simulation experiments are noteworthy.

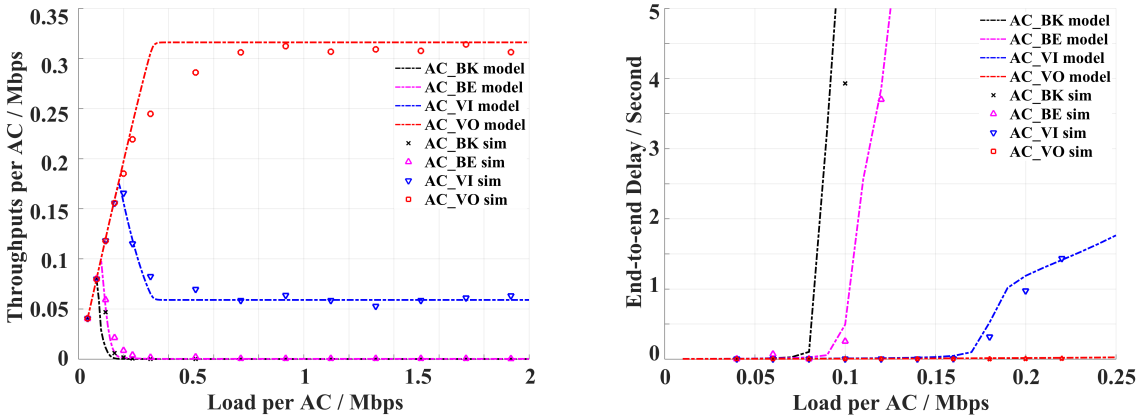

Fig. 3.5 Throughput and end-to-end delay vs. load per AC under an error-prone channel with $BER = 10^{-5}$.

Fig. 3.5 demonstrates the throughput and end-to-end delay versus the offered loads per AC via an error-prone channel with $BER = 10^{-5}$. Both of the figures indicate the influence of channel errors as the channel error slightly decreased the throughput and enlarged the end-to-end delay. From the left figure of Fig. 3.5, we can observe a similar tendency to the above that the throughputs of all four ACs grow linearly at first as the channel is unsaturated and then drops except for AC_VO. The saturation throughput under a benign erroneous channel is about 0.05 Mbps and 0.31 Mbps for AC_VI and AC_VO, respectively. Thus, the throughputs of higher ACs are minorly down due to the impact of channel errors.

Meanwhile, the saturation throughputs for lower ACs are similar to the performance under a perfect channel. For example, the peak throughputs for AC_BK and AC_BE can still reach 0.085 Mbps and 0.1 Mbps, respectively, when the loads are lower than 0.16 Mbps. Also, the saturation throughputs for AC_BK and AC_BE are near zero. Consequently, the throughputs of lower ACs are close to the throughputs under a perfect channel.

From the right figure of Fig. 3.5, we can also observe a similar tendency. The end-to-end delays for all four ACs are very low at the beginning and then grow sharply to more than 5 seconds for lower ACs when the load increases. Meanwhile, the end-to-end delays for AC_VI and AC_VO are also similar to the above because the impact of channel errors is mild.

Generally, the proposed analytical model results are also very close to the results obtained from the simulation experiments. Moreover, each AC's transition period also shows a similar tendency to the curves in the above figures.

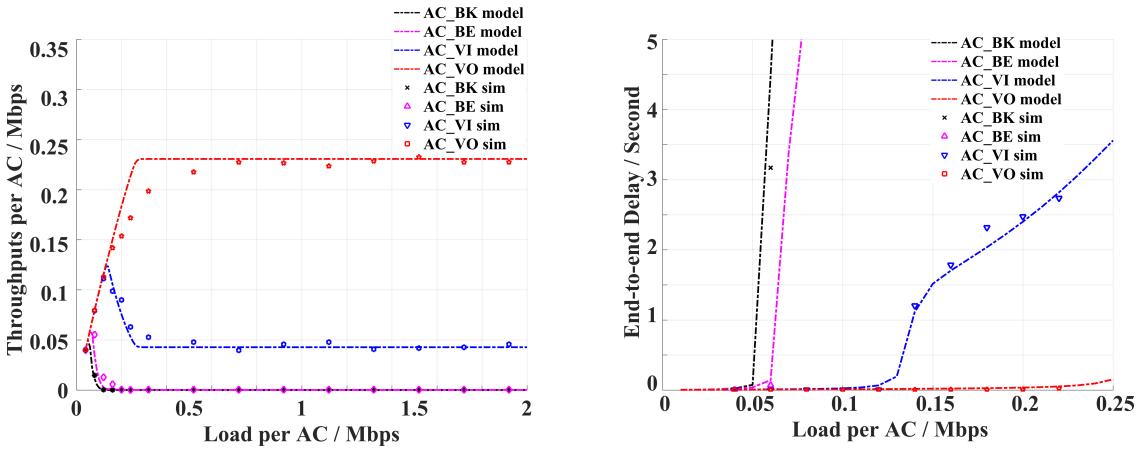

Fig. 3.6 Throughput and end-to-end delay vs. load per AC under an error-prone channel with $BER = 10^{-4}$.

Fig. 3.6 demonstrates the throughput results versus the offered loads per AC via an error-prone channel with $BER = 10^{-4}$. In this case, the channel error significantly decreased the throughput, and the end-to-end delay for all four ACs is considerable. From the left figure of Fig. 3.6, we can find that the saturation throughputs of all four ACs vastly decrease due to the strong impact of channel errors. For example, the saturation throughput under the error-prone channel is about 0.045 Mbps and 0.235 Mbps for AC_VI and AC_VO, respectively. Thus, the saturation throughputs of the higher ACs almost dropped by about 35%.

Meanwhile, the saturation throughputs for lower ACs are significantly lower than the performance under a perfect channel. For example, the peak throughputs for AC_BK and AC_BE decrease to 0.04 Mbps and 0.06 Mbps, respectively, when the loads are lower than 0.16 Mbps. Still, the saturation throughputs for AC_BK and AC_BE are near zero. Consequently, the throughputs of all the networks drop vastly compared to the throughputs under a perfect channel due to the impact of channel errors.

From the right figure of Fig. 3.6, we can also observe that the end-to-end delays are primarily increased due to the influence of channel errors. As a result, the end-to-end delays for the lower ACs soon become enormous. Meanwhile, the end-to-end delays for AC_VI and AC_VO also become considerable due to frequent channel errors.

Generally, the proposed analytical model precisely predicts this case's throughputs and end-to-end delays. All the differences between the results from the model and simulation are low.

Moreover, from Fig. 3.4 to Fig. 3.6, first, the throughput of the ACs with higher priorities is much larger than the ACs with higher priorities. Second, the end-to-end delay of the highest priority, AC_VO, is steady. Therefore, it can support applications with stringent real-time requirements or high throughput. Furthermore, the maximum throughput of

AC_BK, AC_BK, and AC_VI are remarkably higher than their saturation throughput. This phenomenon indicates that the unsaturation analysis of the EDCA mechanism of IEEE 802.11p is worthy.

Overall, the results obtained from the simulation experiments through the ns-3 prove the correctness and effectiveness of our model. Meanwhile, the results generated from both the model and the simulation experiments suggest the powerful influences of channel errors on the performance of IEEE 802.11p.

3.4 Performance evaluation

In this section, we investigate the impact of channel errors and MAC buffer size, which are neglected in many existing models.

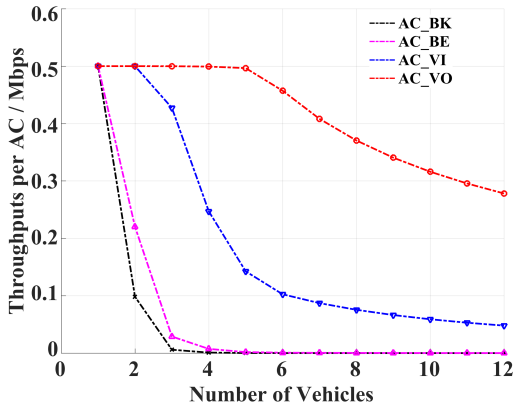

Fig. 3.7 Throughput vs. the number of vehicles.

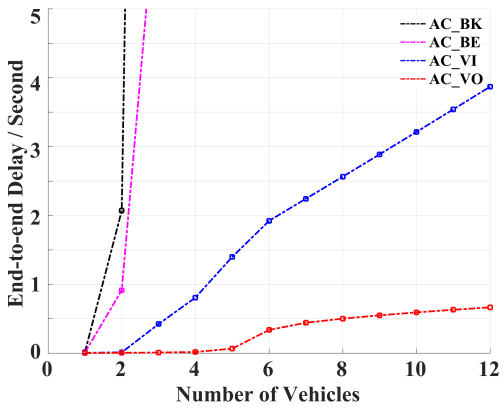

Fig. 3.8 End-to-end delay vs. the number of vehicles.

Fig. 3.7, Fig. 3.8 and Fig. 3.9 display the throughput, end-to-end delays, and packet loss rate versus the number of vehicles, respectively. In this case, the packet arrival rate is set to 0.5 Mbps. Unlike the above, the tendency shows that the network's throughput increases initially as the contention is limited and then drops with the increasing contention. Meanwhile, the end-to-end delay goes sharply, especially for AC_BE and AC_BK. In addition, the end-to-end delay of AC_VI and AC_VO also grows very fast. In addition, the packet loss rates also grow dashingly when the number of vehicles increases. For example, the packet loss rates increase almost linearly when the number of vehicles is larger than 5. This phenomenon indicates that a crowded urban environment could strongly impact the performance of an IoV system.

Fig. 3.10 shows the impact of bit errors on the throughput. In this case, the packet arrival rate is set to 1Mbps. It means that an imperfect channel can result in significant influences

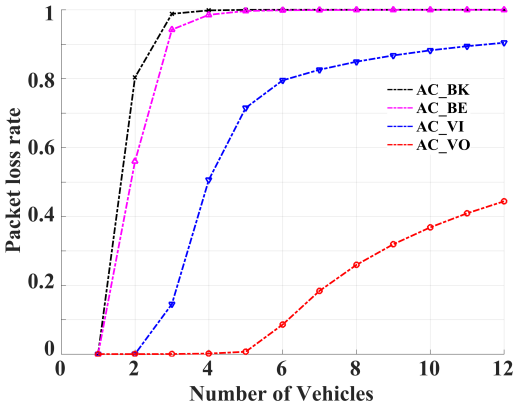

Fig. 3.9 Packet loss rate vs. the number of vehicles under an error-prone channel with $BER = 10^{-5}$.

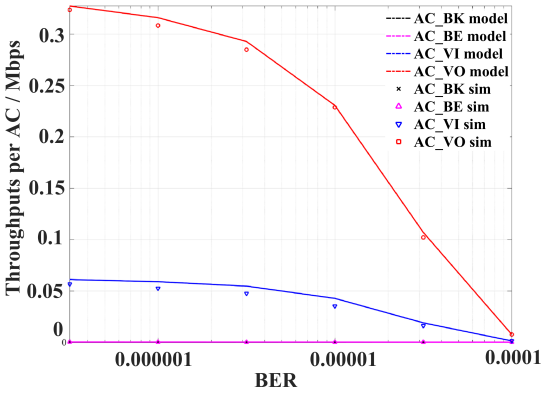

Fig. 3.10 Throughput vs. BER.

on the performance of the network. In an IoV environment composed of the high mobility of vehicles, this impact is remarkable due to the Doppler spread. We can see that while the growth of BER, the throughput drops sharply. First, for AC 3, when the BER is 0, the throughputs reach about 0.33 Mbps. Then it drops sharply to about 0.01 Mbps when the BER equals 0.001.

Second, we can also observe a similar tendency for AC_VI. The peak throughput is 0.06 Mbps. However, the throughput decreased to near zero under an error-prone channel, with the BER equaling 0.001. Consequently, the influence of the channel error is significant for IEEE 802.11p and cannot be ignored in the performance modelling.

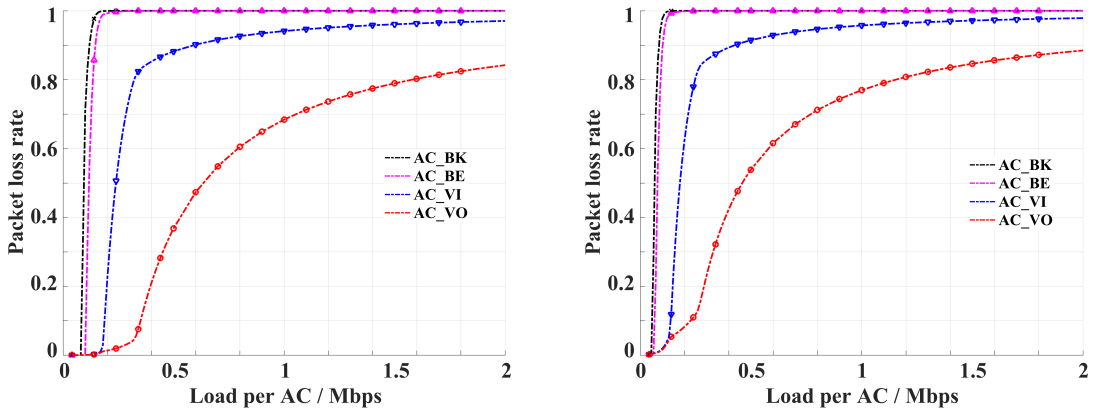

Fig. 3.11 Packet loss rate vs. load per AC under an ideal channel and an error-prone channel with $BER = 10^{-4}$.

Fig. 3.11 illustrates the packet loss rate versus the offered loads per AC via a perfect channel and an error-prone channel with $BER = 10^{-4}$, respectively. The packet loss rates indicate the reliability of the network. Therefore, from the left figure of Fig. 3.11, we can find that the packet loss rates grow sharply for all four ACs. The packet loss rates for lower ACs reach almost 100% when the offered loads are high. This phenomenon means that almost all of the packets of lower ACs are undelivered under saturation conditions.

Nonetheless, by contract, the higher ACs are much more reliable. For example, more than 90% of packets of AC_VO are delivered successfully when the offered loads are lower than 0.38 Mbps. Moreover, about half of the packets of AC_VI are lost when the offered loads are equal to 0.22 Mbps. Turn to the right figure of Fig. 3.11. It indicates that the packet loss rates for all four ACs are significantly larger than those shown on the left side of Fig. 3.11. It is because of the impact of channel errors. For example, when the offered load is equal to 0.22 Mbps, the packet loss rates for AC_VI increase to about 78%, which is 153% as influential as the packet loss rates under a perfect channel. In short, the channel errors significantly impact the reliability of IEEE 802.11p.

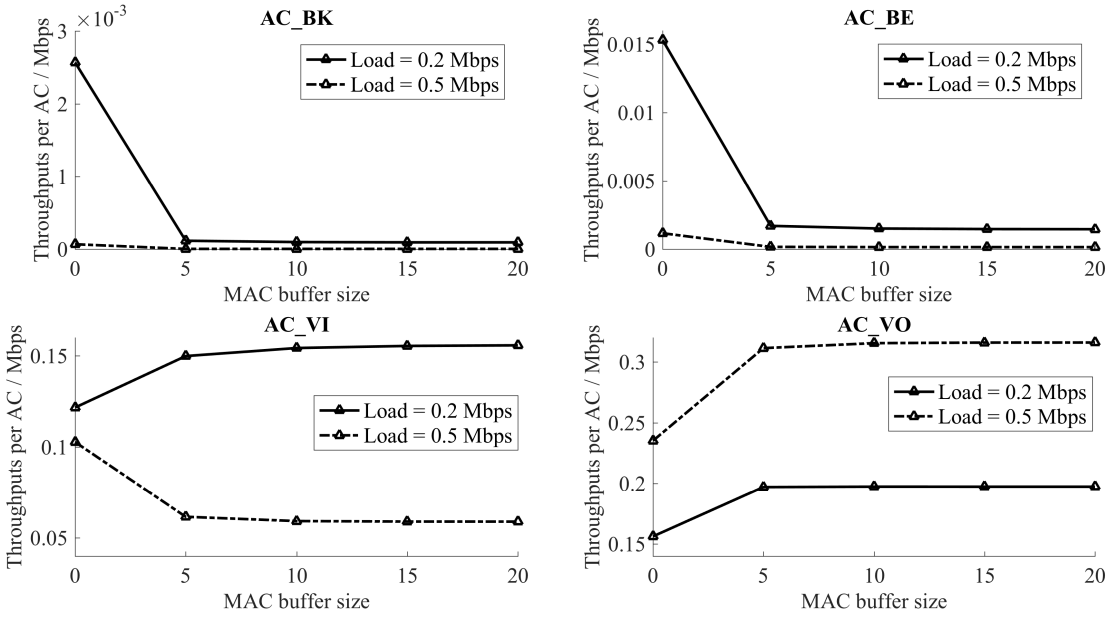

Fig. 3.12 Throughput vs. MAC buffer size.

Fig. 3.12 and Fig. 3.13 display the influence of the MAC buffer size. We use two different input traffic loads, $\lambda = 0.2$ and $\lambda = 0.5$. In this case, the BER is set to $BER = 10^{-5}$. First, Fig. 3.12 shows the influence of the buffer size on the throughputs. We can see that the throughputs experience significant changes with the different buffer sizes, especially for the lower ACs. For example, the throughput of the AC_BE achieves 0.0153 Mbps with no MAC

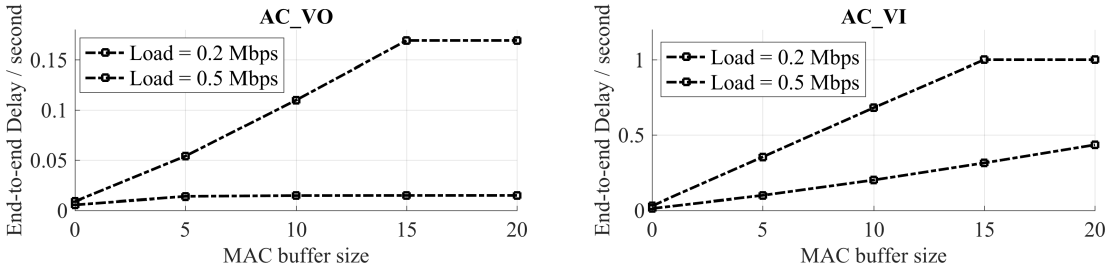

Fig. 3.13 End-to-end delay vs. MAC buffer size.

buffer under the offered load is 0.2 Mbps. However, it drops to almost zero when the buffer size increase. The throughput of the AC_BK also shows a similar tendency.

Meanwhile, the throughputs of higher ACs display different trends. For the AC_VO, the throughput indicates a revised tendency of lower ACs. It goes up fast while the buffer increase and then become steady but still increases. For example, the throughput arrives at 0.127 and 0.195 Mbps under the no buffer condition, with the offered load equal to 0.2 and 0.5 Mbps. Then it rises and becomes stable.

Furthermore, the throughputs of the AC_VI illustrate the opposite tendency when the offered loads are equal to 0.2 and 0.5 Mbps. It grows with the buffer sizes increasing under the offered load is 0.2 Mbps. However, it shows a downing tendency with buffer sizes increasing under the offered load is 0.5 Mbps. Accordingly, this phenomenon suggests that the assumption of an infinite buffer size can result in immense errors.

Fig. 3.13 shows the end-to-end delay versus buffer sizes. We only display the AC_VI and AC_VO here. It is clear that the end-to-end delay climbs while the buffer size increases. It is because of the longer queuing delay with less possibility to discard packets due to a full buffer. However, the end-to-end delays of both ACs become steady after the buffer size is larger than 15.

In short, the effects of the channel errors and MAC buffer size are noteworthy in the performance evaluation of IEEE 802.11p. Moreover, these results indicate the significant effect of the buffer.

3.5 Conclusion

In this chapter, we presented a new analytical model based on a 3-D Markov chain and Queuing analysis for the IEEE 802.11p EDCA mechanism in IoV under imperfect channel conditions. This analytical model combined the CW backoff and AIFS deferring procedures within one model. Specially, all of the major factors, including the backoff counter freezing, AIFS defers, and internal collision, have also been taken into account under error-prone

channels with both saturated and unsaturated traffic. The effectiveness and accuracy of the proposed model have been validated through the ns-3 simulation experiments. In addition, the combined results of the proposed model and the simulation experiments demonstrated a significant impact on the performance due to channel errors and MAC buffer size.

Although the presented model has comprehensively described the IEEE 802.11p EDCA mechanism, it could still be improved. First, this model assumes that all packet errors follow the Bit Error Rate model. However, the packet error rates can be various due to the influence of the physical surrounding, especially for vehicles moving in urban areas. Second, this model assumes the traffic loads follow the Poison Distribution. Nevertheless, modelling the network traffic for the Internet of Vehicles is controversial. Arguably, other traffic models are more representative than Poison Distribution.

Chapter 4

Modelling and Performance Analysis of IEEE 802.11p for Internet of Vehicles with Bursty Error Transmissions

4.1 Introduction

In recent years, intelligent connected vehicle systems have drawn a great deal of attention from both academia and vehicle manufacturers. Intelligent connected vehicle systems require vehicles and roadside infrastructures to communicate wirelessly with each other, called the Internet of Vehicles (IoV). In an ideal intelligent connected vehicle system, OBUs and RSUs can exchange safety messages and traffic management information for collision avoidance and auto-driving systems wirelessly through the IoV. IoV plays a vital role in the future Smart City structure of its potential for traffic management and public safety. However, the network structure of such an intelligent connected vehicle system could be very complex as the devices use various communication protocols. Therefore, as a unified protocol for vehicular networks, IEEE 802.11p has been designed to provide standardised services and interfaces for intelligent connected vehicle systems.

Unlike other WLAN environments, wireless channels of IEEE 802.11p are significantly influenced by the obstacles and the movement in vehicular environments. Moreover, vehicles' physical surroundings are ever-changing within urban environments, affecting packet transmissions [138, 9]. For example, the wireless channel could be utterly unavailable while vehicles pass a tunnel or enter a parking garage. Furthermore, modern cities intend to construct more and more skyscrapers. Those buildings with a very high altitude affect wireless networks with worsened path loss than lower buildings [139]. By contrast, the channel status

can be much better when a vehicle communicates to another within a line-of-sight range, which is also a ubiquitous scene of IoV [10, 140]. Thus, the channel status can change dramatically during driving in urban environments. Consequently, the channel error rates can also alter from one extreme to the other. However, the influences of the altering channel status due to the realistic physical environments are still underestimated.

4.2 Bursty error channel modelled by a two-state continuous-time Markov chain

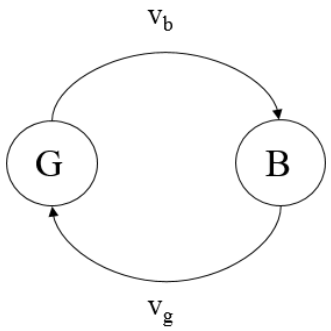

Fig. 4.1 Two-state continuous-time Markov chain channel model

In this section, we introduce an analytical model based on the Gilbert-Elliot model of a bursty error channel. The Gilbert-Elliot model is a two-state Markov chain model that can model the bursty characteristics of channel errors. As shown in Fig. 4.1, the wireless channel of IEEE 802.11p is characterised by a continuous two-state Markov chain rotating between a good state and a bad state. These two states model the current physical surroundings of the vehicles. For example, on the one hand, if the vehicle is going through a tunnel or other cases that can cause a worse wireless channel, we assume the channel is in a bad state. On the other hand, if the vehicle operates on a highway or in other conditions with no negative communication factors, we assume the channel is in a good state.

The transition rate from a good to a bad state is represented by v_g, while that from a bad to a good state is denoted as v_b. Therefore, assuming these two values are available, the duration of the good state and bad state are exponential random variables with means v_g^{-1} and v_b^{-1}. Therefore, the probability that the channel stays in a good or bad state for a duration t, $P_g(t)$ or $P_b(t)$, can be expressed as follows:

$$\begin{cases} P_g(t) = e^{-v_g t} \\ P_b(t) = e^{-v_b t} \end{cases} \tag{4.1}$$

The steady-state probabilities of the channel being in the good and bad state, π_g and π_b , can be given by:

$$\begin{cases} \pi_g = \frac{v_g}{v_g+v_b} \\ \pi_b = \frac{v_b}{v_g+v_b} \end{cases} \tag{4.2}$$

Assuming it is in a good state, the channel is perfect, and no packet error occurs. By contrast, if it is in a bad state, all packets are erroneous. Moreover, an erroneous packet is considered a failed transmission and a retransmission is required until the retry limit. Let the probability of a packet being transmitted with errors be p_e, and we have:

$$p_e = \begin{cases} 0, & \text{if the channel state is good} \\ 1, & \text{if the channel state is bad} \end{cases} \tag{4.3}$$

4.3 Analytical model

4.3.1 Analysis of the backoff procedure

In this section, we introduce a developed 3-D discrete-time Markov Chain to analyze the EDCA mechanism in IEEE 802.11p based on our analytical model presented in Chapter 3 and [50].

Let p_v represent the probability that the transmission failed due to a collision or packet error of the AC_v. p_{bv} stands for the probability of the channel being sensed idle for a time slot after the AIFS period of the AC_v. p_{tv} indicates the probability that the channel is sensed idle for a time slot within the AIFS period of the AC_v. m is the retry limit defined in the protocol of IEEE 802.11p. d_v represents the difference between the AIFS value of the current AC between the minimal value of AIFSN. Accordingly, $d_v = AIFS_v - AIFS_{min}$. W_{iv} represents the current CW value after i times failed transmission. Let τ'_v represent the transmission probability of AC_v when at least one frame is waiting in the queue. According to [50] and Chapter 3, the expression of τ'_v is showing as follow:

$$\begin{aligned} \tau'_v = \frac{1-p_v^{m+1}}{1-p_v} \Bigg\{ & \frac{(1-p_{tv}^{d_v})}{(1-p_{tv})p_{tv}^{d_v}}[(1-p_{bv})\sum_{i=0}^{m}\frac{W_{iv}-1}{2p_{bv}}p_v^i \\ & + \sum_{i=0}^{m}\frac{p_v^i}{W_{iv}}] + \sum_{i=0}^{m}\frac{W_{iv}-1}{2p_{bv}}p_v^i + \frac{1-p_v^{m+1}}{1-p_v} \Bigg\}^{-1} \end{aligned} \tag{4.4}$$

Therefore, the transmission probability of AC_v under the unsaturated traffic condition, τ_v, can be derived as follow:

$$\tau_v = \tau'_v(1 - P_{0v}) \tag{4.5}$$

where P_{0v} denotes the probability that the transmission queue is empty, which will be derived in the section on queuing analysis. Moreover, a collision occurs if a frame attempts to be transmitted from the same AC in multiple stations simultaneously or from an AC with higher priority in the same station. Let the collision probability of AC_v be p'_v. It can be calculated as follow:

$$p'_v = 1 - \prod_{a=0}^{A}(1-\tau_a)^{n-1}\prod_{a>v}^{A}(1-\tau_a) \tag{4.6}$$

where A is the number of AC queues, and n is the number of vehicles.

Note that p_v is different from the collision probability p'_v because transmissions could fail due to collisions or packet errors. Therefore:

$$p_v = p'_v + (1 - p'_v)p_e \tag{4.7}$$

Since the channel is perfect when the channel is in a good state, on the one hand, all transmission failures result from internal collisions in a good state, $p_v = p'_v$. On the other hand, if the channel is in a bad state, all transmissions fail due to packet errors. Therefore, p_v can be expressed as follow:

$$p_v = \begin{cases} p'_v, & \text{if the channel state is good} \\ \\ 1, & \text{if the channel state is bad} \end{cases} \tag{4.8}$$

Since the TXOP is not considered here, the channel state is not changing during one transmission. Hence,

$$\begin{aligned} p_v &= \pi_g p_v + \pi_b p_v \\ &= \pi_g p'_v + \pi_b \end{aligned} \tag{4.9}$$

where π_g and π_b are the probabilities of the channel is a good or bad state. If the channel is sensed idle for a time slot during the AIFS period of the AC_v, it means that all of the other ACs with higher priority are not transmitting in the current time slot. Hence, let p_{bv} to be this probability, and p_{tv} can be calculated as follow:

$$p_{tv} = \prod_{a>v}(1-\tau_a)^n \tag{4.10}$$

If the channel is sensed idle for a time slot after the AIFS period of the AC_v, it means that all of the other ACs are not transmitting in the current time slot. Hence, let p_{bv} be this probability, and p_{bv} can be calculated as follow:

$$p_{bv} = (1-\tau_v)^{n-1} \prod_{a \neq v} (1-\tau_a)^n \tag{4.11}$$

4.3.2 Analysis of the service time

In this section, we analyze the mean service time of each packet. The service time is combined with the transmission delay and channel access delay. The transmission delay means the time duration of a packet transmitting over the channel. The value of this time duration has two possible cases: the packet is delivered to the receiver, or the transmission fails due to an internal collision. Note that the transmission delay for an erroneous transmission is equal to a successful one. Hence, let T_v^{tr} represent for the first case and T_v^{col} for the second. We have:

$$\begin{cases} T_v^{tr} = AIFS_v + T_{header} + T_{SIFS} + T_{ACK} + T_L \\ T_v^{col} = AIFS_v + T_{header} + T_{SIFS} + T_{ACK} \end{cases} \tag{4.12}$$

where T_{header}, T_{ACK} and T_L represent the time duration of transmitting the header, ACK and payload, respectively, and the T_{SIFS} and $AIFS_v$ denote for the time duration of SIFS and AIFS deferring of AC_v.

Let α_v characterise the probability that the channel is occupied by another AC_a during AC_v in the backoff procedure. This probability is mutually inverse of the probability of the channel being in idle status, pb_v. Also, β_a denotes the probability that transmission of this AC_a experienced a transmission without any internal collision. The value of α_v and β_a are given by:

$$\begin{cases} \alpha_v = 1 - p_{bv} \\ \beta_a = n\tau_a(1-\tau_v)^{(n-2)} \prod_{b \neq v}(1-\tau_b)^{n-1} \prod_{b>a}^{A}(1-\tau_b) \end{cases} \tag{4.13}$$

Therefore, the expression of the mean duration of a time slot, $\overline{\sigma}_v$, is given as follows:

$$\overline{\sigma}_v = \sum_{a=0}^{A} \beta_a T_a^{tr} + (\alpha_v - \sum_{a=0}^{A} \beta_a) T_v^{col} + (1-\alpha_v)\sigma + \alpha_v T_v^A \tag{4.14}$$

where T_v^A is the time duration spent on the AIFS deferring period of AC_v, and σ is the duration of a physical time slot defined in the 802.11p protocol. Hence, the third term calculates the average time if the channel is idle during AC_v in the backoff procedure. The last term calculates the average time during the backoff counter frozen and AC_v in the AIFS deferring

period. Moreover, during the period of the backoff counter of AC_v being frozen, it must go through from the beginning of the AIFS period again and again once it senses a busy channel. Therefore, this period consists of many potential attempts. Let T_v^a stand for the time cost for each attempt. The expression of T_v^a is shown as follows:

$$T_v^A = \sum_{z=1}^{\infty} p_{tv}^{d_v}(1-p_{tv}^{d_v})^{z-1} z T_v^a \tag{4.15}$$

where z is the number of attempts. When AC_v in the AIFS deferring procedure, let $\overline{\alpha}_v$ represent the probability that at least one of another AC_a transmits, and $\overline{\beta}_a$ denotes the probability that the packet of this transmission is received by the destination in a given slot. The value of $\overline{\alpha}_v$ and $\overline{\beta}_a$ are given by:

$$\begin{cases} \overline{\alpha}_v = 1 - p_{tv} \\ \overline{\beta}_a = n\tau_a \prod_{b>v}(1-\tau_b)^{(n-1)} \prod_{b>max\{a,v\}}^{A}(1-\tau_b) \end{cases} \tag{4.16}$$

Therefore, T_v^a can be calculated as follow:

$$T_v^a = \sum_{a>v}^{A} \overline{\beta}_a T_a^{tr} + (\overline{\alpha}_v - \sum_{a>v}^{A} \overline{\beta}_a) T_v^c + \sigma \sum_{x=1}^{d_v-1} x p_{tv}^x \tag{4.17}$$

where the last term calculates the average time spent on a failed attempt for the remaining time slots during the AIFS period of the AC_v after $AIFS_{min}$.

Note that the summation of the series formula can solve the infinite summation in (4.15). Therefore, from all equations above, the mean duration of a time slot can be expressed by τ_v and p_v with constants.

Turn to the analysis of the mean channel access time. Similar to the transmission time, the channel access time also has two possibilities: the packet is received successfully or discarded due to the retry limit reached. Let $\overline{D}_v^a$ represent the mean value for the first case, and $\overline{D}_v^b$ for the second. Both $\overline{D}_v^a$ and $\overline{D}_v^b$ should be expressed by the conditions of the channel state. Therefore, the expressions of $\overline{D}_v^a$ and is given as follows:

$$\begin{aligned} \overline{D}_v^a = \overline{\sigma_v} \sum_{i=0}^{m} \sum_{j=0}^{i} \frac{(W_{jv}-1)p_v^i(1-p_v)}{2[1-p_v^{m+1}]} + \\ \{\pi_g T_v^{col} + \pi_b[p_v' T_v^{col} + (1-p_v')T_v^{tr}]\} \sum_{i=0}^{m} \frac{i p_v^i (1-p_v)}{1-p_v^{m+1}} \end{aligned} \tag{4.18}$$

Similarly, the expressions of $\overline{D}_v^b$ is given as follow:

$$\overline{D}_v^b = \overline{\sigma_v} \sum_{i=0}^{m} \frac{W_{jv}-1}{2} + \{\pi_g T_v^{col} + \pi_b [p'_v T_v^{col} + (1-p'_v) T_v^{tr}]\}(m+1) \tag{4.19}$$

Finally, the mean service time can be calculated by summing up the transmission time and the mean channel access time. Hence, let D_v^s characterise the mean service time of a frame is transmitted successfully, and D_v^f stands for the mean service time of a frame is discarded due to the retry limit reached. Therefore, D_v^s and D_v^f can be calculated as follows:

$$\begin{cases} D_v^s = \overline{D}_v^a + T_v^{tr} \\ D_v^f = \overline{D}_v^b \end{cases} \tag{4.20}$$

4.3.3 Queuing analysis

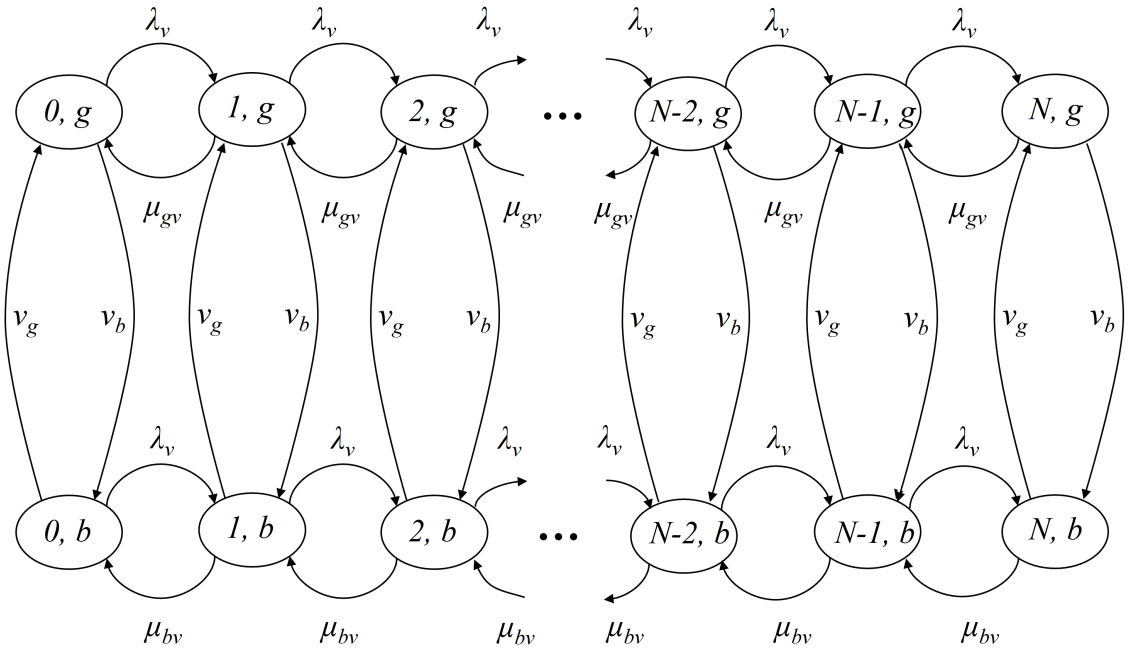

Fig. 4.2 M/G/1/K queuing system

In this section, we discuss the throughput and end-to-end delay calculation based on the Queuing analysis. Since the traffic of packets arriving follows Poisson Distribution, the queue of AC_v can be modelled as an $M/G/1/K$ queuing system. As shown in Fig.4.2, K equals the

MAC buffer size, and the arrival rate equals λ_v. The mean service rate μ_v is composed of four components. First, if the channel is in a good state, the mean service rate can be two possibilities: the service rate of the frame is transmitted successfully, μ_{gv}^s; and the service rate of the frame is removed due to the retry limit reached, μ_{gv}^f. The mean service rate is defined as the reciprocal of the mean service time. Therefore, from (4.20), μ_{gv}^s and μ_{gv}^f are given as follow:

$$\begin{cases} \mu_{gv}^s = \frac{1}{D_v^s} \\ \mu_{gv}^f = \frac{1}{D_v^f} \end{cases} \tag{4.21}$$

μ_{gv} can be calculated as follow:

$$\mu_{gv} = \mu_{gv}^f p_d + \mu_{gv}^s (1 - p_d) \tag{4.22}$$

where p_d is the probability that the packet is discarded due to the retry limit reached. It can be calculated conditioned on the channel state as follow:

$$\begin{aligned} p_d = {} & \pi_g [e^{-\nu_g \overline{D}_v^f} {p'_v}^{m+1} + (1 - e^{-\nu_g \overline{D}_v^f}) p_v^{m+1}] \\ & + \pi_b [e^{-\nu_g \overline{D}_v^f} {p'_v}^{m+1} + (1 - e^{-\nu_g \overline{D}_v^f}) p_v^{m+1}] \end{aligned} \tag{4.23}$$

Similarly, if the channel is in a bad state, the mean service rate, μ_{bv}, also can be two possibilities: the service rate of the frame is transmitted successfully, μ_{bv}^s; and the service rate of the frame is removed due to the retry limit reached, μ_{bv}^f. Note that in this case, a packet cannot be transmitted successfully. Hence, μ_{bv}^s and μ_{bv}^f can be expressed as follows:

$$\begin{cases} \mu_{bv}^s = 0 \\ \mu_{bv}^f = \mu_{bv} = \frac{1}{D_v^f} \end{cases} \tag{4.24}$$

The state transition probabilities of this $M/G/1/K$ queue are demonstrated as follows:

$$\begin{cases} P_{\{i,b|i,g\}} = \pi_b, & i \in [0,K] & \text{(a)} \\ P_{\{i,g|i,b\}} = \pi_g, & i \in [0,K] & \text{(b)} \\ P_{\{i+1,g|i,g\}} = \lambda_v, & i \in [0,K-1] & \text{(c)} \\ P_{\{i+1,b|i,b\}} = \lambda_v, & i \in [0,K-1] & \text{(d)} \\ P_{\{i-1,g|i,g\}} = \mu_{gv}, & i \in [1,K] & \text{(e)} \\ P_{\{i-1,b|i,b\}} = \mu_{bv}, & i \in [1,K] & \text{(f)} \end{cases} \tag{4.25}$$

Hence, let $p_{i,j}$ stand for the stationary distribution of the Markov chain above. The $p_{i,j}$ satisfies the following normalization condition:

$$1 = \sum_{i=0}^{k} p_{i,g} + \sum_{i=0}^{k} p_{i,b}, \qquad i \in [0,K] \tag{4.26}$$

To solve this Markov chain, we assume:

$$P_i = p_{i,g} + p_{i,b}, \qquad i \in [0,K] \tag{4.27}$$

Accordingly, P_i also satisfies the normalization condition. Therefore, we have:

$$\sum_{i=0}^{k} P_i = 1, \qquad i \in [0,K] \tag{4.28}$$

Therefore, the balance equation of this Markov chain can be listed as follow:

$$\begin{cases} 2\lambda_v P_0 = (\mu_{gv} + \mu_{bv})P_1 \\ 2\lambda_v P_1 + (\mu_{gv} + \mu_{bv})P_1 = 2\lambda_v P_0 + (\mu_{gv} + \mu_{bv})P_2 \\ 2\lambda_v P_2 + (\mu_{gv} + \mu_{bv})P_2 = 2\lambda_v P_1 + (\mu_{gv} + \mu_{bv})P_3 \\ ....., \\ 2\lambda_v P_{K-2} + (\mu_{gv} + \mu_{bv})P_{K-2} = 2\lambda_v P_{K-3} + (\mu_{gv} + \mu_{bv})P_{K-1} \\ 2\lambda_v P_{K-1} + (\mu_{gv} + \mu_{bv})P_{K-1} = 2\lambda_v P_{K-2} + (\mu_{gv} + \mu_{bv})P_K \\ (\mu_{gv} + \mu_{bv})P_K = 2\lambda_v P_{K-1} \end{cases} \tag{4.29}$$

Hence, from the regularity of the balance equations above, we can derive the expressions of the probability P_0 and P_K summing up the equations in (4.28) and (4.29).

$$\begin{cases} P_0 = \frac{1-\frac{2\lambda_v}{\mu_{gv}+\mu_{bv}}}{1-(\frac{2\lambda_v}{\mu_{gv}+\mu_{bv}})^{K+1}} \\ P_K = P_{0v}(\frac{2\lambda_v}{\mu_{gv}+\mu_{bv}})^K \end{cases} \tag{4.30}$$

Here, P_0 is equal to the probability that no frame is waiting in the queue for AC_v, P_{0v}, whereas P_K is equal to the probability that a frame is discarded due to the finite buffer is full for AC_v, P_{Kv}.

Note that from (4.1) to (4.30), all variables can be expressed by τ_v and p_v with constants. Moreover, the relationships between τ_v and p_v are shown in (4.5) and (4.6). Thus, the value of τ_v and p_v can be solved by a numerical method. Therefore, the throughput of AC_v, S_v, can be calculated as follow:

$$S_v = \lambda_v L(1 - P_{Kv})(1 - p_d) \tag{4.31}$$

where L is the size of the payload.

Then, turn to the calculation of the end-to-end delay. The end-to-end delays of AC_v, D_v, mean the total time duration that a frame of AC_v spends on the MAC layer. It is composed of the service time of a packet transmitted to the destination successfully, D_v^s, and the queue delay, D_v^q. Hence, the expression of the end-to-end delays is:

$$D_v = D_v^q + D_v^s. \tag{4.32}$$

Observing the regularity from Equation (4.28) to (4.30), this queuing system can be equivalent to a $M/M/1/K$ queuing system with the arriving rate equals to $2\lambda_v$, and the service rate equals to $\mu_{gv} + \mu_{bv}$. Hence, Let ρ_v stand for the ratio of the equivalent arrival rate and service rates. Then, the queuing delay D_v^q can be calculated following the formulas of the queuing theory as follows:

$$D_v^q = \frac{\frac{\rho_v}{1-\rho_v} - \frac{(K+1)\rho_v^{(K+1)}}{1-\rho_v^{K+1}} - (1-P_{0v})}{2\lambda_v(1-P_{Kv})} \tag{4.33}$$

Note that the expression of D_v^s has already been displayed in (4.20). Therefore, all variables for the end-to-end delays can also be e expressed by τ_v and p_v with constants. Finally, we can calculate the end-to-end delays by solving the τ_v and p_v with a numerical method.

4.4 Model validation

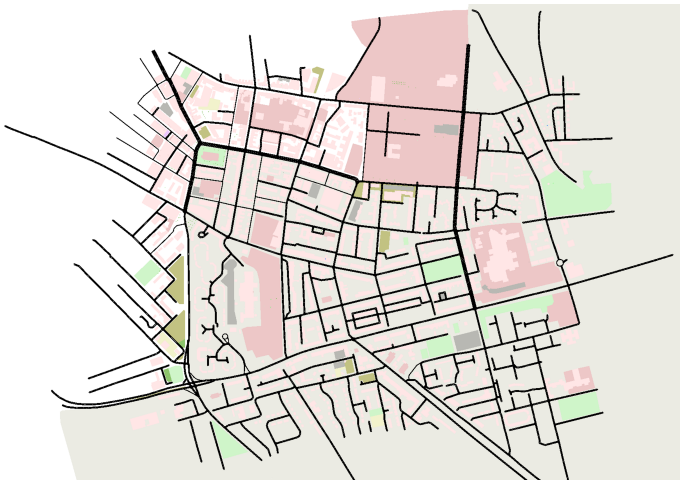

Fig. 4.3 Simulation map.

In this section, we validate the efficacy and accuracy of our analytical model with a series of simulation results. We designed a simulation environment with a real map of a part of the urban area in Liverpool, UK. The detail of this map is according to OpenStreetMap [135]. The network simulation experiments are designed with the simulation tool ns-3 (ns-3 3.30) [136]. We consider an urban environment with 10 OBUs (vehicles) running in a 360m $\times$ 360m rectangular map. Each vehicle moves around with a constant velocity of 10 m/s following the Random Way Point model. The mobility and traffic of all vehicles are generated by SUMO [137]. One RSU stands at the centre of this map. The device of all OBUs installs four AC queues and transmits frames to the RSU. The transmission power has been adjusted to be strong enough to cover the area. The packet arrival rates of four ACs follow a Poisson Process with a mean value λ_v. We have tested enough times of simulations with multiple random seeds and calculated average results. The simulation time of each simulation has been set to 300 s. Other parameters follow the definition in the IEEE 802.11p protocol [5] and showing in Table 4.1 and Table 4.2

Table 4.1 SYSTEM PARAMETERS

Frame payload	500 Bytes	PHY header	192 bits
MAC header	224 bits	ACK	304 bits
Data rate	6 Mbit/s	Buffer size	50 frames
Slot time	13 µs	Retry limit	7
SIFS	32 µs	Number of vehicles	10 vehicles

Table 4.2 EDCA PARAMETERS

	AIFSN	CW_{min}	CW_{max}
AC_BK	9	3	7
AC_BE	6	7	15
AC_VI	3	15	1023
AC_VO	2	15	1023

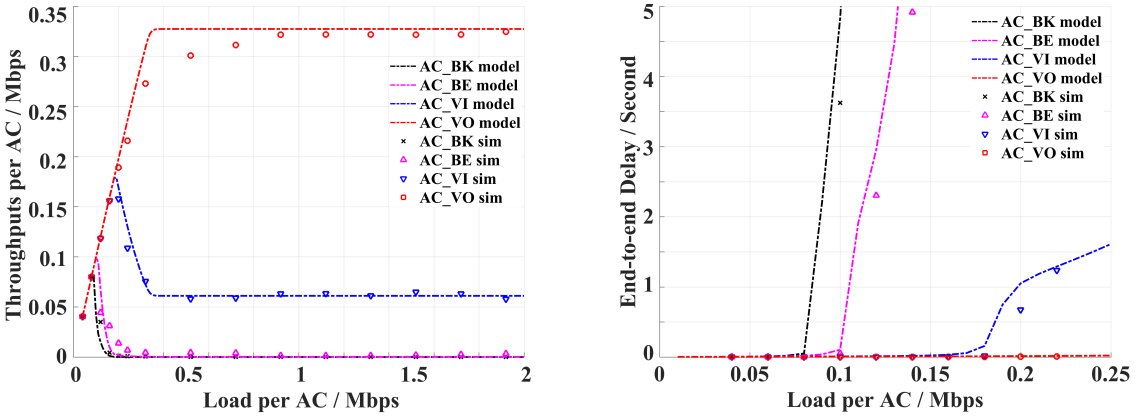

Fig. 4.4 Throughput and end-to-end delay vs. load per AC with $v_g = 1$ and $v_b = 0$.

Fig. 4.4 demonstrates the throughput and end-to-end delay, respectively, versus the offered loads per AC under an ideal channel. In this case, the channel status does not alter. Therefore, in this case, the packet loss due to the channel error is zero. This assumption was utilized in most of the existing models. From the left figure of Fig. 4.4, we can see that the throughputs of all four ACs grow linearly at first as the channel is unsaturated and then drops except for AC_VO. The saturation throughput under a perfect channel is about 0.055 Mbps and 0.33 Mbps for AC_VI and AC_VO, respectively. Thus, the throughputs of higher ACs, which have stringent throughput requirements, can be ensured.

Meanwhile, the saturation throughputs for AC_BK and AC_BE are all very low. However, the non-saturation throughputs for AC_BK and AC_BE can reach 0.085 Mbps and 0.1 Mbps, respectively, when the loads are lower than 0.16 Mbps. Also, the peak throughput of AC_VI is about 0.18 Mbps which is about three times as high as the saturation throughput. Therefore, the throughputs of all four ACs with non-saturation loads significantly differ from those with saturation loads.

From the right figure of Fig. 4.4, we can see that the end-to-end delays for all four ACs are very low at the beginning. However, for AC_BK and AC_BE, the end-to-end delays grow sharply to more than 5 seconds when the load increases. Meanwhile, the end-to-end delays for AC_VI also increase to more than 1.5 seconds. By contrast, the end-to-end delays for AC_VO keep at a reasonable level. Thus, the low delay requirement can be ensured for AC_VO.

Generally, it is clear that the results of the proposed analytical model closely match the results obtained from the simulation experiments. In addition, due to the dramatic changes in the throughput during the transition period, the differences between the proposed analytical model results and the simulation experiments results are noteworthy.

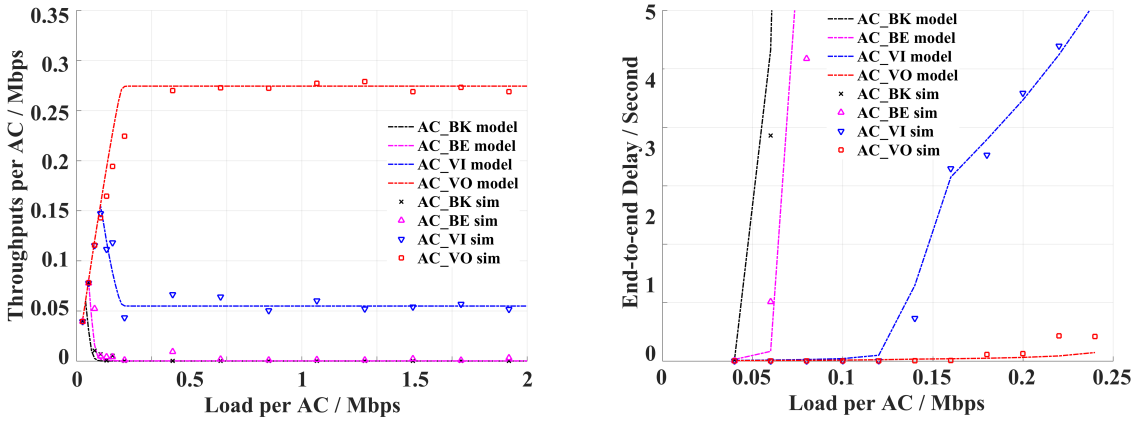

Fig. 4.5 Throughput and end-to-end delay vs. load per AC with $v_g = 0.9$ and $v_b = 0.1$.

Fig. 4.5 illustrates the throughputs and end-to-end delay, respectively, versus the offered loads per AC for bursty error transmissions with $v_g = 0.9$ and $v_b = 0.1$. In this case, the bursty errors decreased the throughput and significantly enlarged the end-to-end delay. Both figures indicate the influence of bursty errors as the bursty errors slightly decreased the throughput and enlarged the end-to-end delay. From the left figure of Fig. 4.5, we can observe a similar tendency to the above that the throughputs of all four ACs grow linearly at first as the channel is unsaturated and then drops except for AC_VO. The saturation throughput under a benign erroneous channel is about 0.055 Mbps and 0.26 Mbps for AC_VI and AC_VO, respectively. Thus, the throughputs of higher ACs are minorly down due to the impact of channel errors.

Meanwhile, the saturation throughputs for lower ACs are also worse than the performance under a perfect channel. For example, the peak throughputs for AC_BK and AC_BE can only reach 0.06 Mbps and 0.07 Mbps, respectively, when the loads are lower than 0.16 Mbps. Also, the saturation throughputs for AC_BK and AC_BE are near zero. Consequently, the throughputs of lower ACs went down faster than the throughputs under an ideal channel.

From the right figure of Fig. 4.5, we can observe a much worse end-to-end delay performance. The end-to-end delays for all four ACs are higher than the above. For example, the end-to-end delays grow dashingly to more than 5 seconds for lower ACs when the load increases. Meanwhile, the end-to-end delays for AC_VI are also much worse than the above. The value of the delays increases quickly to more than 5 seconds while the offered loads rise. The end-to-end delays AC_VO also experience a rise, even though the increases are small. Compared to the BER results in Chapter 3, the impact on the end-to-end delays with bursty error transmissions is much more powerful.

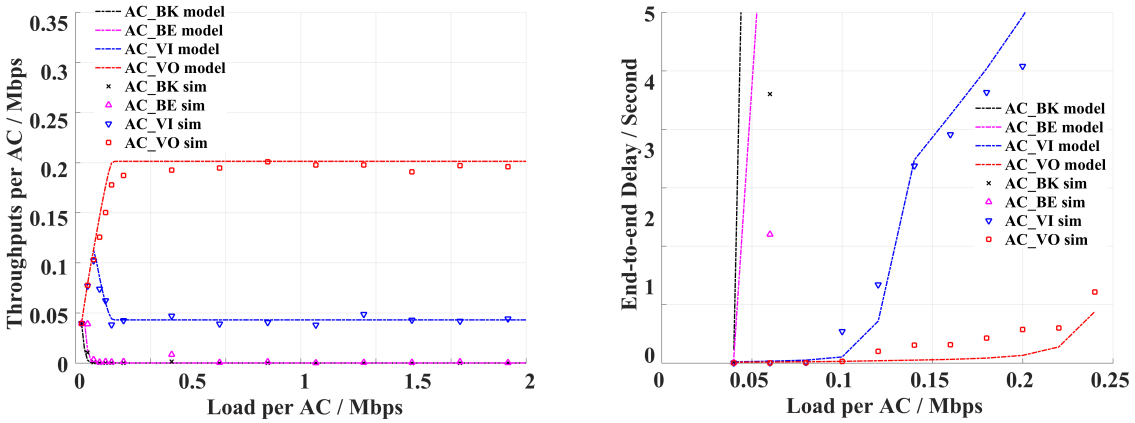

Fig. 4.6 Throughput and end-to-end delay vs. load per AC with $v_g = 0.7$ and $v_b = 0.3$.

Fig. 4.6 illustrates the throughputs versus the offered loads per AC for bursty error transmissions with $v_g = 0.7$ and $v_b = 0.3$. In this case, the bursty errors significantly decreased the throughput, and the end-to-end delay for all four ACs is significant. Also, the proposed analytical model precisely predicts this case's throughput and end-to-end delay. From the left figure of Fig. 4.6, we can find that the saturation throughputs of all four ACs vastly decrease due to the strong impact of channel errors. For example, the saturation throughput under the error-prone channel is about 0.045 Mbps and 0.2 Mbps for AC_VI and AC_VO, respectively. Thus, the saturation throughputs of the higher ACs almost dropped by about 43%.

Meanwhile, the saturation throughputs for lower ACs are significantly lower than the performance under a perfect channel. For example, the peak throughputs for AC_BK and AC_BE decrease to 0.04 Mbps when the loads are lower than 0.16 Mbps. Still, the saturation throughputs for AC_BK and AC_BE are near zero. Consequently, the throughputs of all the networks drop vastly compared to the throughputs under a perfect channel due to the impact of bursty errors.

From the right figure of Fig. 4.6, we can also observe that the end-to-end delays are primarily increased due to the influence of channel errors. As a result, the end-to-end delays for the lower ACs soon become enormous. Furthermore, the end-to-end delays for AC_VI also rise sharply while the offered loads increase. Meanwhile, the end-to-end delays for AC_VO also become considerable due to the frequent channel status changes.

Generally, the proposed analytical model precisely predicts this case's throughputs and end-to-end delays. All the differences between the results from the model and simulation are low.

Moreover, from Fig. 4.4 to Fig. 4.6, first, the throughput of the ACs with higher priorities is much larger than the ACs with higher priorities. Second, the end-to-end delay of the

highest priority, AC_VO, is steady. Therefore, it can support applications with stringent real-time requirements or high throughput. Furthermore, the maximum throughput of AC_BK, AC_BK, and AC_VI are remarkably higher than their saturation throughput. This phenomenon indicates that the unsaturation analysis of the EDCA mechanism of IEEE 802.11p is worthy.

Overall, the results obtained from the simulation experiments through the ns-3 prove the correctness and effectiveness of our model. Meanwhile, the results generated from both the model and the simulation experiments suggest the powerful influences of bursty errors on the performance of IEEE 802.11p.

4.5 Performance evaluation

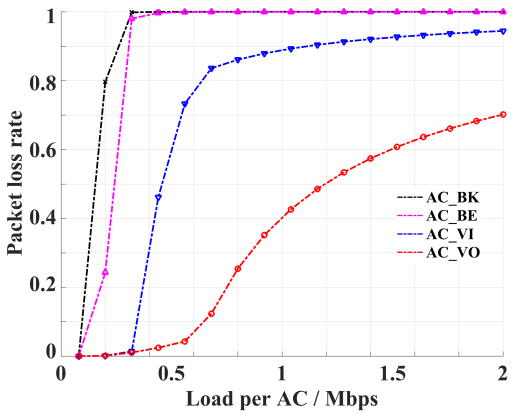

Fig. 4.7 Throughput vs. the number of vehicles.

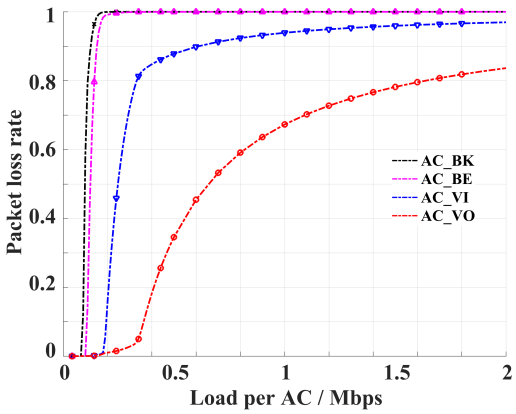

Fig. 4.8 End-to-end delay vs. the number of vehicles.

In this section, we investigate the impact of channel errors and MAC buffer size, which are neglected in many existing models.

Fig. 4.7 and Fig. 4.8 illustrate the packet loss rate versus the offered loads per AC via a perfect channel and an error-prone channel with $v_g = 0.7$ and $v_b = 0.3$, respectively. The packet loss rates indicate the reliability of the network. Therefore, from Fig. 4.7, we can find that the packet loss rates grow sharply for all four ACs. The packet loss rates for lower ACs reach almost 100% when the offered loads are high. This phenomenon means that almost all of the packets of lower ACs are undelivered under saturation conditions.

Nonetheless, by contract, the higher ACs are much more reliable. For example, more than 90% of packets of AC_VO are delivered successfully when the offered loads are lower than 0.38 Mbps. Moreover, about half of the packets of AC_VI are lost when the offered

loads are equal to 0.22 Mbps. Turn to Fig. 4.8. It indicates that the packet loss rates for all four ACs are significantly larger than those shown in Fig. 4.7. This is because of the impact of channel errors. For example, when the offered load is equal to 0.22 Mbps, the packet loss rates for AC_VI increase to about 69%, which is 142% as influential as the packet loss rates under a perfect channel. In short, the bursty errors significantly impact the reliability of IEEE 802.11p.

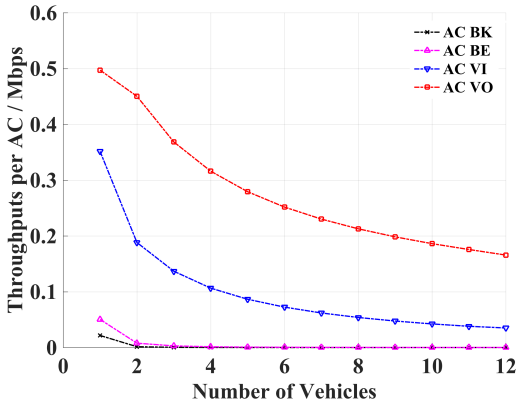

Fig. 4.9 Throughput vs. the number of vehicles.

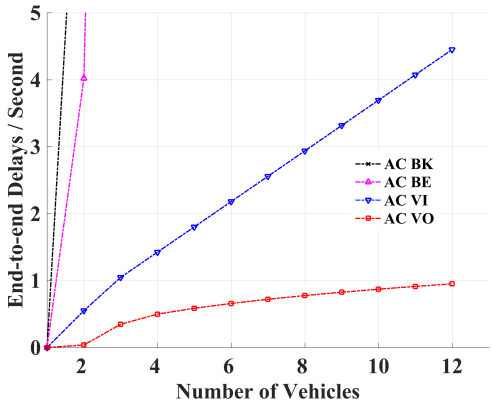

Fig. 4.10 End-to-end delay vs. the number of vehicles.

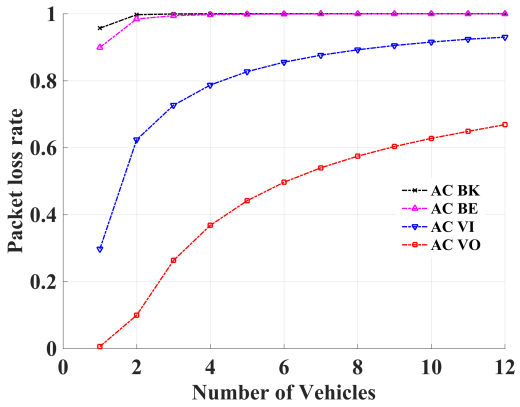

Fig. 4.11 Packet loss rate vs. the number of vehicles.

Fig. 4.9, Fig. 4.10 and Fig. 4.11 display the throughput, end-to-end delays, and packet loss rate versus the number of vehicles, respectively. In this case, the packet arrival rate is set to 0.5 Mbps. Unlike the above, the tendency shows that the network's throughput increases initially as the contention is limited and then drops with the increasing contention. Meanwhile, the end-to-end delay goes high sharply, especially for AC_BE and AC_BK. In addition, the end-to-end delay of AC_VI and AC_VO also grows very fast. In addition, the packet loss

rates also grow dashingly when the number of vehicles increases. This phenomenon indicates that a crowded urban environment could strongly impact the performance of an IoV system.

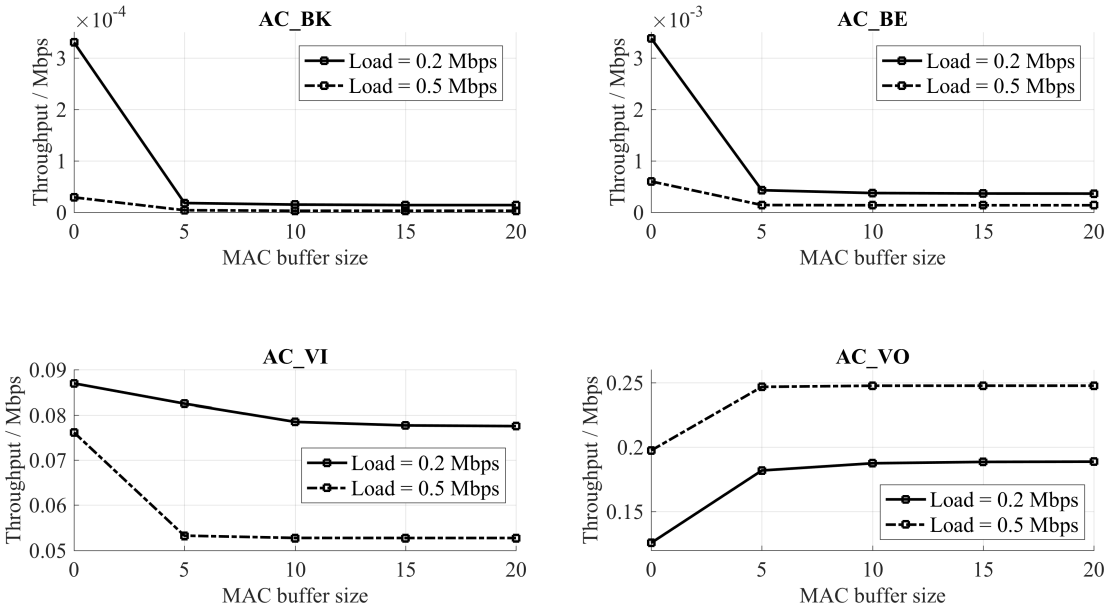

Fig. 4.12 Throughput vs. MAC buffer size.

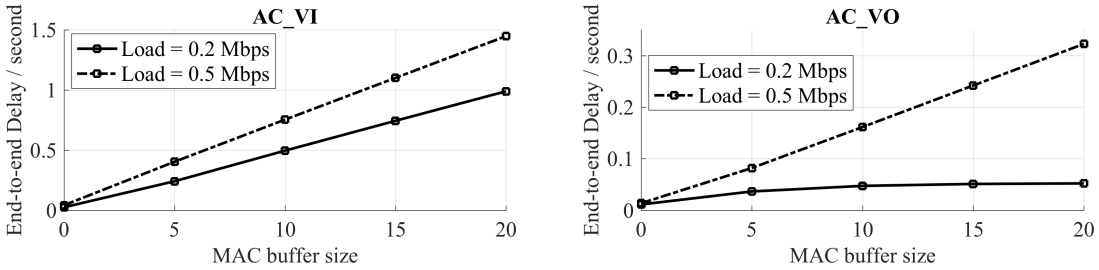

Fig. 4.13 End-to-end delay vs. MAC buffer size.

Fig. 4.12 and Fig. 4.13 display the influence of the MAC buffer size. We use two different input traffic loads, $\lambda = 0.2$ and $\lambda = 0.5$. In this case, the channel alters rate is set to $v_g = 0.9$ and $v_b = 0.1$. First, Fig. 4.12 shows that while the buffer size increases, the throughputs drop for the ACs with lower priorities. For example, the throughput of the AC_VI achieves 0.078 Mbps with no MAC buffer under the offered load is 0.2 Mbps. However, it drops to 0.052 Mbps while the buffer size increase. The throughput of the AC_BK and AC_BE also shows a similar tendency with more significant decreases.

Meanwhile, the throughputs of AC_VO display different trends. For the AC_VO, the throughput indicates a revised tendency of lower ACs. It goes up fast while the buffer increases and then becomes steady but still increases. The throughput arrives at 0.127 and

0.195 Mbps under the no buffer condition, with the offered load equal to 0.2 and 0.5 Mbps. Then it rises and becomes stable. This phenomenon suggests that the assumption of an infinite buffer size can result in immense errors.

Fig. 4.13 shows the end-to-end delay versus buffer sizes. We only display AC_VI and AC_VO here. It is clear that the end-to-end delay climbs while the buffer size increases. It is because of a long queuing delay. However, the end-to-end delays of both ACs become steady after the buffer size is larger than 15.

In short, the effects of the channel errors and MAC buffer size are noteworthy in the performance evaluation of IEEE 802.11p.

4.6 Conclusion

In this chapter, we developed an analytical model based on a 3-D Markov chain and Advanced Queuing analysis in IEEE 802.11p for IoV with bursty error transmissions. The proposed analytical model specially modelled the channel state with a two-state continuous-time Markov chain. The effectiveness and accuracy of the proposed model have been validated through the ns-3 simulation experiments. Furthermore, the powerful impact of the bursty error transmissions has been evaluated by the proposed model.

The presented model is developed based on the one introduced in Chapter 3. However, compared to the previous one, this model considered the influences due to the physical surrounding and vehicles' mobility with the Bursty Error model. Consequently, this model works under more realistic urban areas. Furthermore, this model also described the influences of the buffer queues in depth, which were widely ignored by other works.

Several issues still limit the presented model. First, this model assumes the traffic loads follow the Poison Distribution. Nevertheless, modelling the network traffic for the Internet of Vehicles is controversial. Arguably, other traffic models are more representative than Poison Distribution. Second, the traffic of an IoV can be more complex due to the traffic lights and traffic jams. For example, the density of vehicles in a city centre can be much higher than on a highway. This phenomenon leads to higher network demands. In this case, the presented model can be less accurate because of the various node densities.

Chapter 5

A Simulation Study of the Performance of IEEE 802.11ah for Internet of Things

5.1 Introduction

The development of the Internet of Things has made Smart Cities possible. Smart Cities aim to connect all movable and immovable nodes, including vehicles, buildings, and factories, in the urban area through an autonomic, self-controlled network with information collecting and processing. Therefore, the scale of the sensor networks in Smart Cities would be much larger than traditional WLAN. It means that such a network could be composed of thousands of nodes. As a result, the network congestion and contention could be fierce, which led to significantly low performance.

Moreover, the energy consumption of the wireless networks in Smart Cities is also a bottleneck. As a result, the performance of networks can be substantially poorer with a steep reduction in throughput with current wireless protocols. Consequently, IEEE 802.11ah was developed as the best solution for Smart Cities by IEEE Task Group AH (TGah). The IEEE 802.11ah standard is designed to meet the requirements of large-scale, low-energy consumption sensor networks for the Internet of Things. It takes advantage of both low-power networks and Wi-Fi technologies. Therefore, it is valuable to study the performance of IEEE 802.11ah.

5.2 The RAW mechanism of the MAC layer of IEEE 802.11ah

In the MAC layer of IEEE 802.11ah, the RAW access scheme is employed to moderate the contention among the massive number of nodes. The RAW access scheme separates all the

nodes into groups based on Terminal ID (TID) or spatial location. The nodes which belong to a particular group can only access the channel at specific RAW time slots. The RAW time slots are predefined by splitting the beacon interval. Meanwhile, the beacon interval carries a RAW parameter set (RPS) information element, which defines the interval start time and other parameters, including the number of slots, slot format and slot duration, for all stations that belong to the group. The duration of a RAW interval is equal, which is calculated as follows:

$$D_{RAW} = 500 + 120 \times C_{RAW} \tag{5.1}$$

where C_{RAW} symbolises the slot duration count sub-field. The slot duration count sub-field value is either 11 or 8 bits long if the slot format sub-field is set to 1 or 0, respectively.

When a RAW slot completes, nodes belonging to this specific group can go to doze mode. With the TWT mechanism, they will be wakened up at the start of the following assigned RAW slot. Therefore, the energy consumption of a node can be much lower than using other IEEE 802.11 protocols.

The MAC layer of IEEE 802.11ah also utilises the DCF contention mechanism. However, the back-off scheme is different from IEEE 802.11e or IEEE 802.11p. In previous IEEE 802.11 protocol families, channel contentions begin once a frame reaches the head of queues for all nodes. Therefore, if the number of nodes in a network is enormous, the contentions become fierce. Consequently, the strong contentions result in more collisions, longer end-to-end delays and significantly lower performances.

By contrast, as in IEEE 802.11ah, the contention mechanism is different because all nodes can only access the channel during specific RAW slots. In detail, the contention mechanism comprises two cases: the time during the assigned RAW slot and the time outside the assigned RAW slot. To achieve this, each node in the network uses two back-off states: one for the first case and one for the second. Therefore, the first back-off state decreases if the time is outside the assigned RAW slot. In this case, the channel is unavailable for this node, irrelevant to the stage of the second back-off counter. After that, when the assigned RAW time slot comes, the first back-off counter is frozen, and the second back-off counter starts to operate.

The second back-off counter operates following the DCF mechanism. Thus, the second back-off counter follows a uniform distribution within the $[0, CW]$. In the beginning, the value of CW equals CW_{min}. After encountering a transmission failure due to a collision or packet error, the CW doubles until it reaches CW_{max}. If the transmission is successful or the retry limit is reached, the value of CW is reset to CW_{min}. The station keeps sensing the channel status during the back-off procedure. Once the channel is idle for a time slot, the second back-off counter decreases by one. Otherwise, the back-off counter freezes until the

channel is sensed idle continuously for an AIFS. The AC attempts to transmit the packets when the second back-off counter becomes zero. Finally, the second back-off counter and the back-off stage are reset at the end of this RAW slot. Then, the first back-off counter is restarted. Once the next assigned RAW slot comes, the value of CW of the secondary back-off is reset to CW_{min}.

5.3 Simulation design and implementation

In this section, we present the design and implementation of the simulation of IEEE 802.11ah. This simulation environment is developed based on ns-3 [136]. ns-3 is an open-source discrete-event network simulator. The reliability of ns-3 has been widely proved by academia. Currently, ns-3 supports multiple wireless network standards of IEEE 802.11 families, including IEEE 802.11a, 802.11b, 802.11g, 802.11n and s 802.11p. However, the implementation of IEEE 802.11ah in the original ns-3 needs to be completed. Therefore, we introduce an extension of ns-3 [141]. In this extension, it proposed a framework for the implementation of IEEE 802.11ah. The framework for implementing IEEE 802.11ah is shown in Fig. 5.1 [142].

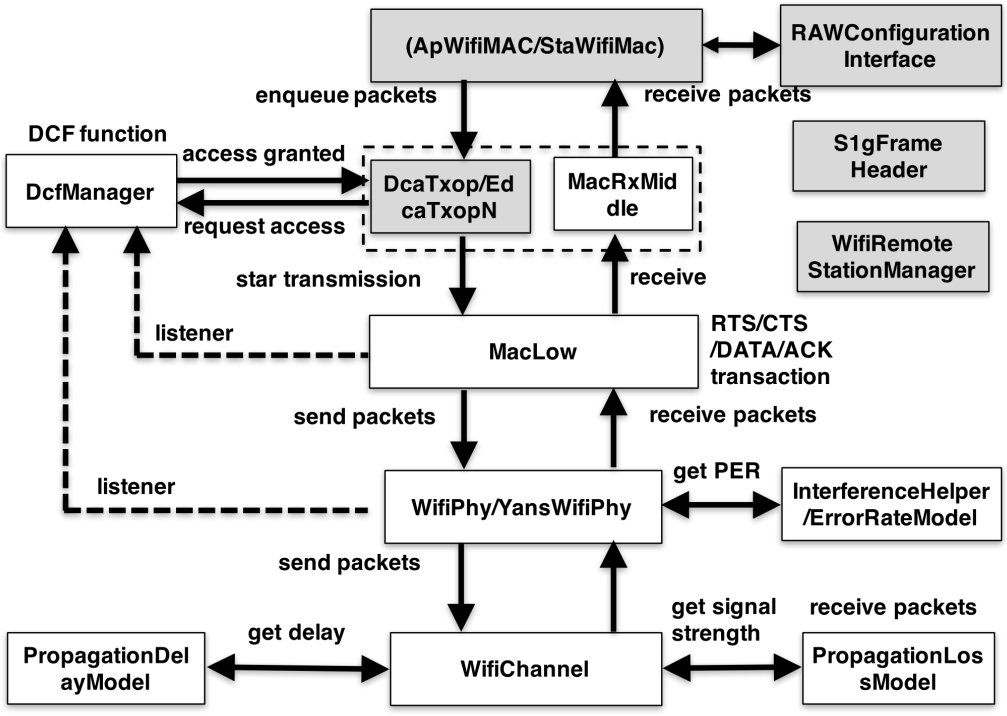

Fig. 5.1 The framework of the IEEE 802.11ah models in the extended ns-3.

In Fig. 5.1, the white components are the modules in the original ns-3. The grey components are the modules created or modified by an extension of ns-3 [141]. We implement the protocol of IEEE 802.11ah and develop our simulations based on this framework. Furthermore, both the PHY and MAC layers have been improved. Therefore, our implementation is more suitable for achieving the simulations of the performance of IEEE 802.11ah.

5.3.1 The implementation of the PHY layer of IEEE 802.11ah

The implementation of the PHY layer of IEEE 802.11ah has two main components: *WifiChannel* and *WifiPhy*. These two components are mainly kept as the original structure in ns-3. The former achieves an analytical approximation of the physical medium of the wireless network. Also, the channel error models are included here. The latter defines the PHY part of the protocol. These two components determine packet loss due to interference. Originally, the channel error models utilized *YansErrorRateModel* and *NistErrorRateModel*. Furthermore, we design two new error models based on *NistErrorRateModel*. The first error module is called *BitErrorRateModel* according to [50]. Therefore, the input of it is a fixed error rate. Correspondingly, this model determines whether a packet is erroneous according to the fixed error rate.

Meanwhile, we implement a *BurstyErrorRateModel* with a two-state continuous-time Markov chain according to the Gilbert-Elliot model [143]. The algorithm of this bursty error rate mode is shown below:

Algorithm 1 Two state bursty error model

Input: p_e
Output: $PacketErrorRate$
  $Call : X \Leftarrow ns3 :: RandomVariableStream(0,1)$
  if $p_e == 0$ **then**
    if $X \leq v_b$ **then**
      $PacketErrorRate \Leftarrow 1$
    else
      $PacketErrorRate \Leftarrow 0$
    end if
  else
    if $X \leq v_g$ **then**
      $PacketErrorRate \Leftarrow 0$
    else
      $PacketErrorRate \Leftarrow 1$
    end if
  end if

As shown in Algorithm 1, this model alters the channel status between two different possibilities: a good or a bad state. In detail, the probability that the channel is in a good state is v_g, while the probability that the channel is in a bad state is v_b. On the one hand, if the channel status is good, the probability of receiving an erroneous packet is zero. On the other hand, if the channel status is bad, all received packets are faulty, and all transmissions are failed.

5.3.2 The implementation of the MAC layer of IEEE 802.11ah

The MAC layer of the simulation of IEEE 802.11ah is designed to support the new features of IEEE 802.11ah, including the RAW and TWT. We develop the MAC layer based on [141, 142, 144]. The RAW and TWT mechanisms are implemented with the RAW information recognition module. Moreover, we also develop a RAW parameters table which defines the RAW information. Some important parameters are displayed in Table 5.1.

Table 5.1 DATA STRUCTURE OF THE RAW PARAMETERS

Name	Data type	Meaning
RAWnum	double	The number of the RAW group
STAnum	double	The number of the STAs in the RAW group
CountRAW	double	The slot duration count sub-field
Erroneous	bool	Whether the channel errors is considered
ErrorModel	bool	The error model if channel errors is considered

As shown in Table 5.1, *RAWnum* defines the number of the RAW group in the network. *STAnum* defines the number of STAs within this RAW group. The *CountRAW* defines the slot duration count sub-field. Hence, the duration of a RAW slot can be calculated following the equation 5.1. Moreover, we also implemented and included the channel error models here. Here, *Erroneous* determines whether the channel error models are utilized, and the model can be selected with *ErrorModel*. The possible error models are the Bit Error Rate model with a fixed error rate and the Bursty error model.

Fig. 5.2 illustrates the flow diagram of the implemented IEEE 802.11ah. First, the RAW parameters are defined in *RAWConfigurationInterface* component. It works correspondingly with *ApWifiMac* and *StaWifiMac* to achieve the configuration of both APs and STAs in IEEE 802.11ah, including the RAW grouping, the duration, start and end time of each RAW slot, and the start and end time of the TWT. The configuration process is accomplished at the

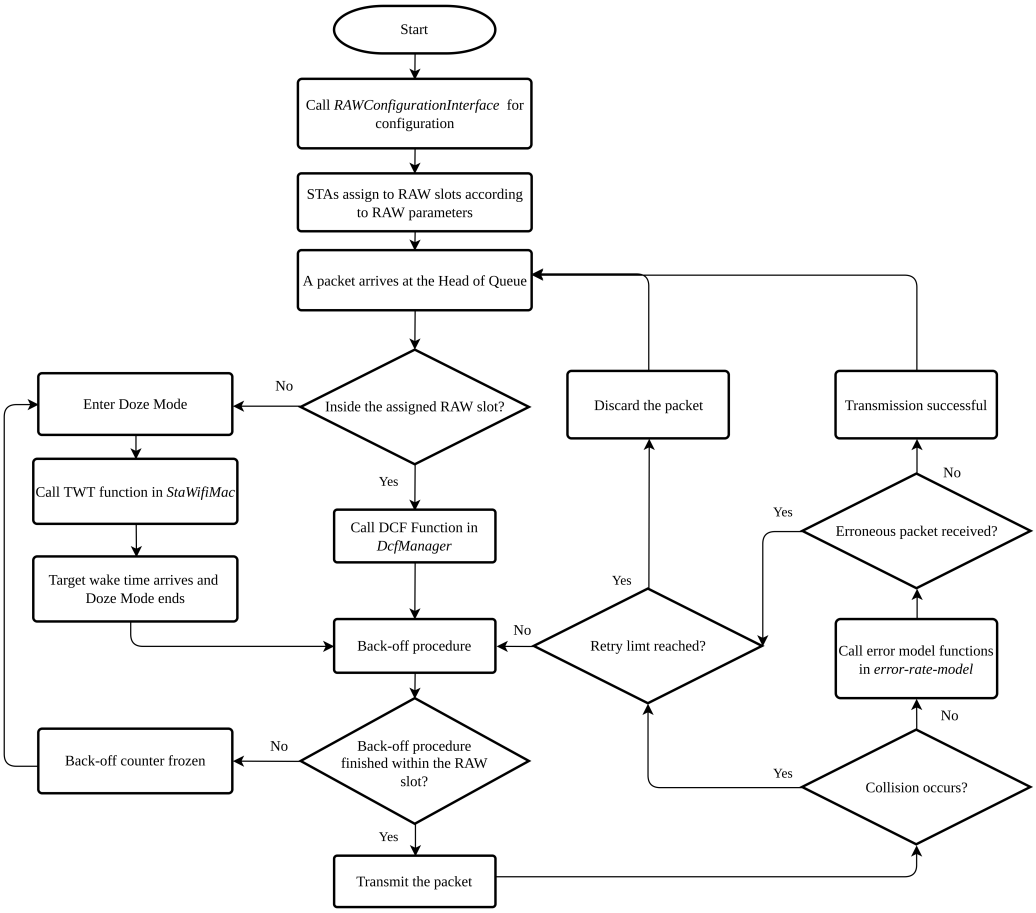

Fig. 5.2 The structure of the implemented MAC layer of IEEE 802.11ah.

STAs receiving the first beacon from the AP. After that, each STA checks if the current time is inside its assigned RAW time slot. If not, this STA goes to Doze mode to save energy.

When a packet arrives at the Head of Queue (HoQ), the STA does not become aware if it is in the Doze mode. However, once the assigned RAW slot comes, the STA is wakened up due to the TWT mechanism and checks the transmission queue. If at least one packet is waiting in the buffer queue, the DCF function is called, and the contention process starts. The DCF function is utilized the original one defined in *DcfManager* module ns-3. Therefore, the process of contenting for the medium is generally very similar to other IEEE 802.11 protocols. Nonetheless, if the back-off process is ongoing while the current RAW slot ends, the CW back-off counter is frozen. The back-off procedure will resume when the next assigned RAW slot comes.

Meanwhile, after the STA has won the contention and transmitted a packet to the destination, the *error-rate-model* is called to determine whether it is an erroneous one. The *error-rate-model* has already been developed in the implementation of the PHY layer. Therefore, it calculates probabilities of channel errors according to the *BitErrorRateModel* or *BurstyErrorRateModel*. The algorithms of these two error models have been described in Section 5.3.1. If the packet is received with errors, retransmission is required until the retry limit is reached.

Furthermore, if the packet at the HoQ is transmitted successfully or discarded due to too many failed transmissions, and the STA is still within the assigned time slot, it proceeds to the transmission process of the next packet. At the end of the current RAW time slot, the STA enters the Doze mode regardless of the transmission process and buffer queue. The detail of the Doze mode is defined in the function *MacLow::GetPhy()->SetDozeMode()* in the *MacLow* module. Then, the back-off counter for outside the RAW slot duration starts according to the TWT mechanism. Finally, the STA will be wakened up at the Target Wake Time. The start and the end time of the Doze mode have already been calculated during the configuration process.

5.4 Performance analysis of IEEE 802.11ah

In this section, we present the simulation results of the performance of IEEE 802.11ah. The network simulation experiments are designed using the tool ns-3 (ns-3 3.23)[136]. We consider an urban environment with a number of stations (STAs) located randomly on a circle map with a 200 m radius. One Access Point (AP) stands at the centre of this map. The topology of the simulation is shown in Fig. 5.3. All of the STAs are uploading frames to the AP. The transmission power has been adjusted to be strong enough to cover the area. The packet arrival rates of four ACs follow a Poisson Process with a mean value λ_v. We have tested enough times of simulations with multiple random seeds and calculated average results. The simulation time of each simulation has been set to 300 s. Other parameters follow the definition in the IEEE 802.11ah protocol [13] and showing in Table 5.2.

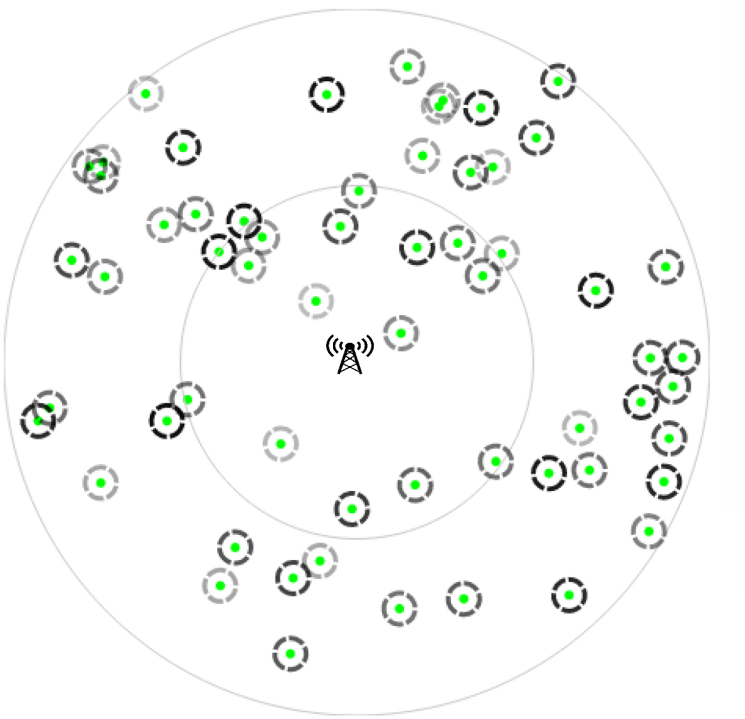

Fig. 5.3 Simulation topology.

Table 5.2 SYSTEM PARAMETERS

Frame payload	500 Bytes	PHY header	192 bits
MAC header	224 bits	ACK	304 bits
RTS	20	CTS	14
Data rate	6 Mbit/s	Buffer size	50 frames
Slot time	13 µs	Retry limit	7
SIFS	32 µs	Number of STAs	10-100
CW_{min}	15	CW_{max}	1023
Frequency	900 Mhz	Access Categories	*AC_BE*
Cross boundary transmission	Disabled	RAW groups	2, 5

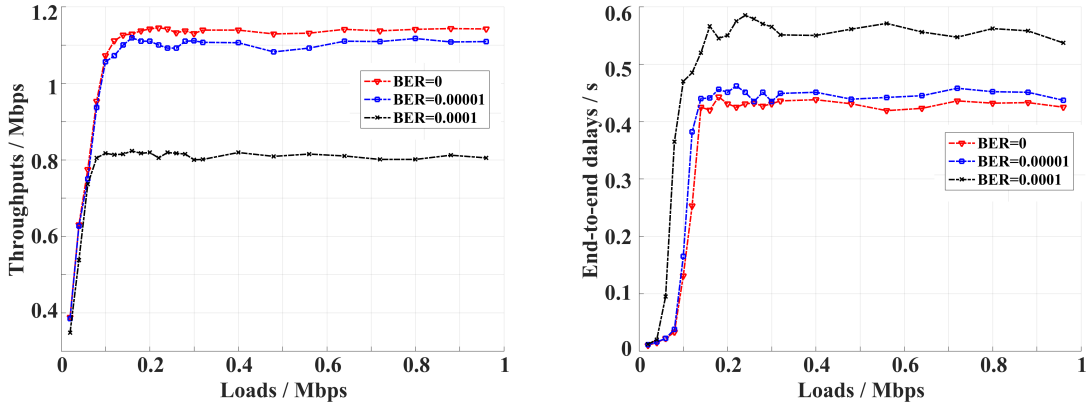

Fig. 5.4 Throughput and end-to-end delay vs. load with 2 RAW groups.

Fig. 5.4 demonstrates the throughput and end-to-end delay versus the offered load with 2 RAW groups. The Bit Error Rate $BER = 0, 10^{-5}, 10^{-4}$ respectively. In this case, the channel status does not alter. Moreover, the channel error is a fixed value. From the left figure of Fig. 5.4, we can see that all of the throughputs grow until they reach saturation. However, saturation throughputs are significantly influenced by channel errors. If the channel is an ideal one, the saturation throughputs are able to reach 1.15 Mbps. In contrast, the saturation throughputs are much lower with imperfect channels. For the case of $BER = 10^{-5}$, the saturation throughputs can still reach 1.11 Mbps. Hence, the throughputs are 2.5% lower. Furthermore, for the case of $BER = 10^{-4}$, the saturation throughputs are only 0.81 Mbps. Thus, the throughputs experienced a 29.5% cut due to the strong impact of channel errors. Therefore, the impact of channel errors on the throughput is powerful and cannot be neglected.

From the right figure of Fig. 5.4, we can see a similar tendency of end-to-end delays. The end-to-end delays climb steadily at first; after that, the end-to-end delays rise sharply until they reach saturation. The average end-to-end saturation delay of an ideal channel is 0.432 seconds. Meanwhile, the performance slightly increases to 0.453 seconds under a mild erroneous channel with $BER = 10^{-5}$. However, the average end-to-end saturation delay rises to 0.565 seconds under an error-prone channel with $BER = 10^{-4}$, which is 25.2% worse than under a perfect channel. Therefore, the impact of channel errors on latency performance is also significant.

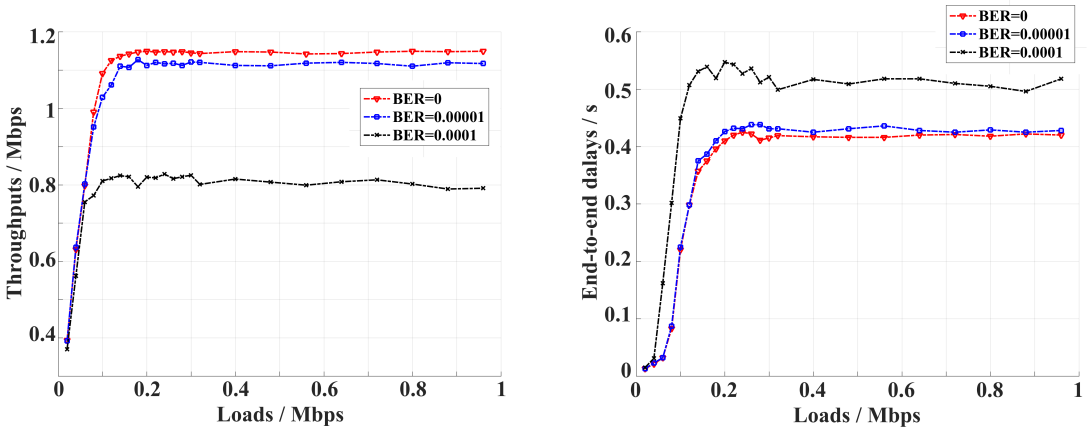

Fig. 5.5 Throughput and end-to-end delay vs. load with 5 RAW groups.

Fig. 5.5 demonstrates the throughput and end-to-end delay versus the offered load with 5 RAW groups, respectively. The Bit Error Rate $BER = 0, 10^{-5}, 10^{-4}$ respectively. Still, the channel error is a fixed value. From the left figure of Fig. 5.4, we can observe a similar tendency to the above as all of the throughputs grow linearly until they reach saturation. Also, saturation throughputs are significantly influenced by channel errors. However, in this case, it achieves a better performance due to lower packet loss of contention. First, the saturation throughput can reach 1.16 Mbps if the channel is perfect. Therefore, it is higher than the case with 2 RAW groups. Second, the saturation throughputs are much lower with imperfect channels. For the case of $BER = 10^{-5}$, the saturation throughputs can still reach 1.08 Mbps. Hence, the throughputs are 6.3% lower. Furthermore, for the case of $BER = 10^{-4}$, the saturation throughputs are only 0.81 Mbps. Thus, the throughputs experienced a 30.5% cut due to the strong impact of channel errors. The results also indicate the unneglectable effect on the throughputs of channel errors.

From the right figure of Fig. 5.5, we can catch a similar tendency of end-to-end delays as the channel is perfect or the channel error is small. The end-to-end delays climb steadily at first; after that, they rise sharply until they reach saturation. The average end-to-end saturation delay of an ideal channel is 0.425 seconds. Meanwhile, the performance slightly increases to 0.430 seconds under a mild erroneous channel with $BER = 10^{-5}$. However, the average end-to-end saturation delay rises to 0.515 seconds under an error-prone channel with $BER = 10^{-4}$, which is 21.1% worse than under a perfect channel. Compared to the throughput performance, the average end-to-end delays with 5 RAW groups are 9.7% better than the values with 2 RAW groups. Therefore, the influence of the RAW mechanism is more noteworthy for the delay performance, especially under an error-prone channel.

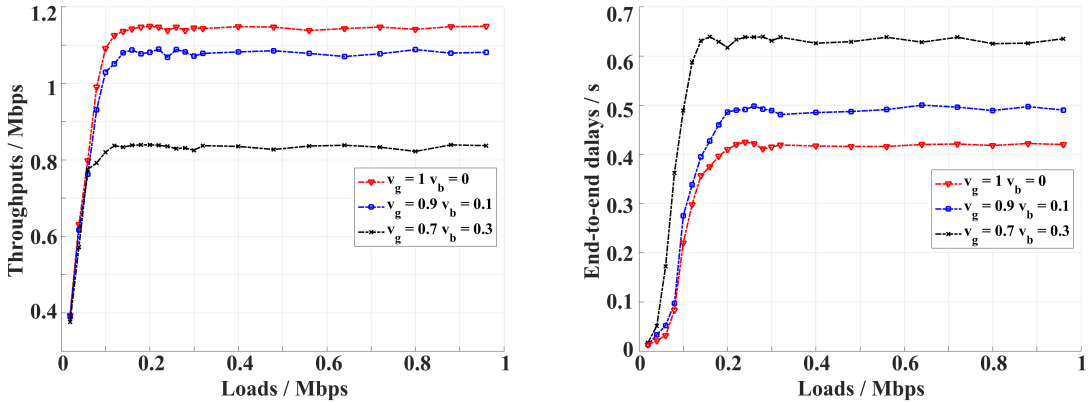

Fig. 5.6 Throughput and end-to-end delay vs. load with 2 RAW groups.

Fig. 5.6 displays the throughput and end-to-end delay versus the offered load with 2 RAW groups. In this case, we investigate the impact of bursty error transmissions. The transition rate of the channel status from a good to a bad state $v_g = 1, 0.9, 0.7$, and from a bad to a good state $v_b = 0, 0.1, 0.3$, respectively. From the left figure of Fig. 5.6, we can find that the impact on the throughputs is more influential than the fixed BER. First and similarly, all the throughputs rise until they reach saturation. However, the saturation throughputs are significantly impacted by bursty errors. For the case of $v_g = 1, v_b = 0$, the throughputs are 1.15 Mbps, the same as the perfect channel in Fig. 5.4. Moreover, for the case of $v_g = 0.9, v_b = 0.1$, the average saturation throughput can achieve as high as 1.078 Mbps. Thus, the throughputs are decreased by 6.3%. Furthermore, for the case of $v_g = 0.7, v_b = 0.3$, the saturation throughputs are just able to arrive at 0.836 Mbps. Consequently, the throughputs encountered a 27.3% drop due to the powerful influence of the bursty errors. Therefore, the impact of the bursty channel errors on the throughput is influential and noteworthy.

From the right figure of Fig. 5.6, we can witness a trend of end-to-end delays similar to the left one. The end-to-end delays ascend linearly until they reach saturation. The average end-to-end saturation delay of an ideal channel is 0.430 seconds, the same as shown in Fig. 5.4. Meanwhile, the end-to-end delays narrowly grow to 0.495 seconds with bursty error transmissions when $v_g = 0.9, v_b = 0.1$. Hence, it is grown for 15.1%. Moreover, the average end-to-end saturation delay rises to 0.638 seconds with bursty error transmissions when $v_g = 0.7, v_b = 0.3$, which is 36.7% worse than under a perfect channel. Therefore, the impact of bursty error transmissions on the latency performance is also significant.

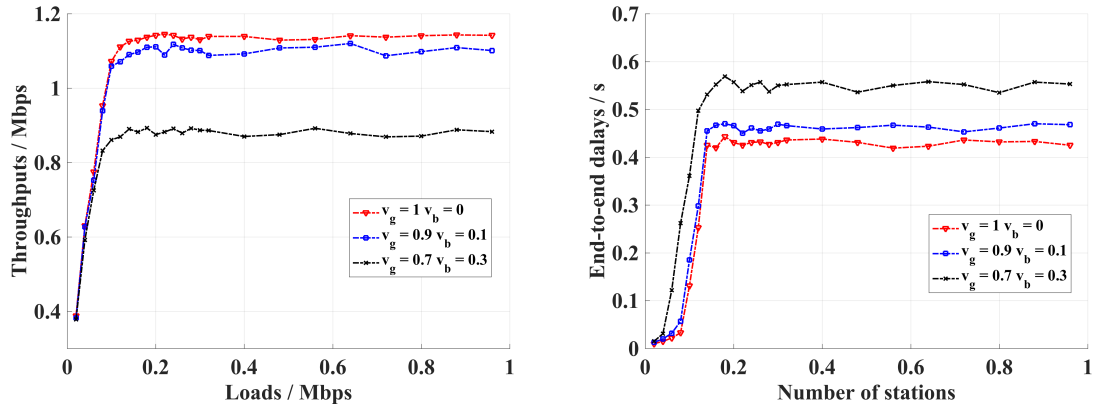

Fig. 5.7 Throughput and end-to-end delay vs. load with 5 RAW groups.

Fig. 5.7 shows the throughput and end-to-end delay versus the offered load with 5 RAW groups. Again, the transition rate of the channel status from a good to a bad state $v_g = 1$, 0.9, 0.7, and from a bad to a good state $v_b = 0$, 0.1, 0.3, respectively. In this case, the performance is significantly better than the case above with 2 RAW groups due to lower packet loss of contention. From the left figure of Fig. 5.7, we can still see a similar tendency to the above as all of the throughputs grow linearly until they reach saturation. Also, saturation throughputs are seriously affected by bursty errors. In detail, first, for the saturation throughputs of a perfect channel with $v_g = 1$, $v_b = 0$, the throughput can reach 1.16 Mbps, equal to the results shown in Fig. 5.5. Second, the saturation throughputs for the case of $v_g = 0.9$, $v_b = 0.1$, the saturation throughputs can still reach 1.10 Mbps, which is 5.3% lower than the above. Therefore, compared to Fig. 5.6, the decrease due to the burst errors is mitigated. Furthermore, for the case of $BER = 10^{-4}$, the saturation throughput is able to arrive at 0.891 Mbps. Thus, although the throughputs fall for 23.2% due to the effect of bursty errors, the decreases are lighter than the case with 2 RAW groups. Therefore, the RAW mechanism shows a better performance improvement with bursty error transmissions.

From the right figure of Fig. 5.6, we can see a trend of end-to-end delays similar to the left one. Again, the impact on the latency performance is extenuated due to the RAW mechanism. First, the average end-to-end saturation for the case of $v_g = 1$, $v_b = 0$ is 0.425 seconds, the same as shown in Fig. 5.5. Meanwhile, the end-to-end delays slightly grow to 0.495 seconds with bursty error transmissions when $v_g = 0.9$, $v_b = 0.1$. Therefore, it is 15.1% higher than the case with a perfect channel. Moreover, the average end-to-end saturation delay rises to 0.556 seconds with bursty error transmissions when $v_g = 0.7$, $v_b = 0.3$, which is 30.8% worse than under a perfect channel. Nonetheless, compared to the case with 2 RAW groups, the increase in end-to-end delay is 5.9% smaller. Consequently, more RAW groups also achieve better performance in latency with the impact of bursty errors.

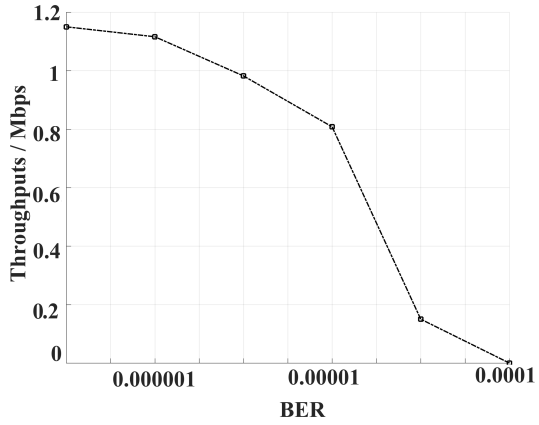

Fig. 5.8 Throughput vs. BER.

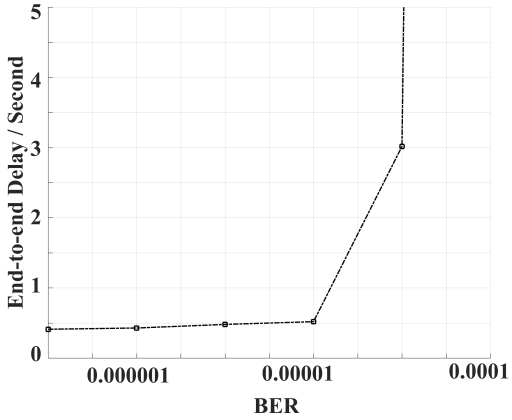

Fig. 5.9 End-to-end delay vs. BER.

Fig. 5.8 and Fig. 5.9 show the throughputs and end-to-end delays, respectively, versus the Bit Error Rates with the RAW groups equal to 5. From Fig. 5.8, again, we can observe a sharp drop due to the impact of channel errors. In the beginning, the peak throughputs can reach 1.16 Mbps without any channel error. After that, however, the throughputs decrease quickly while the channel errors increase. Finally, the significant channel errors lead to zero throughputs for the whole network. Meanwhile, from Fig. 5.9 the end-to-end delays experience exponential growth during the BER climb. When the BER is higher than 0.0005, we can find that the average end-to-end delays are too high, which results in significant packet loss. Consequently, the BER shows a decisive impact on the QoS performance of IEEE 802.11ah.

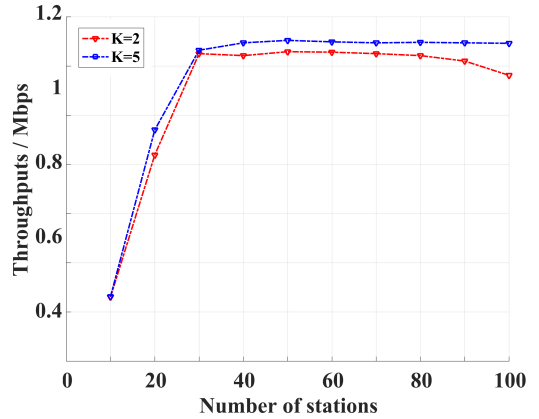

Fig. 5.10 Throughput vs. the number of STAs.

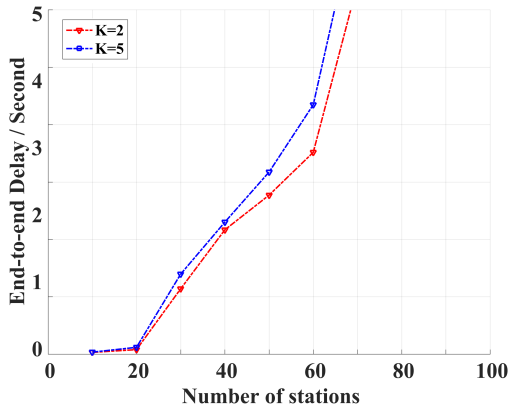

Fig. 5.11 End-to-end delay vs. the number of STAs.

Fig. 5.10 and Fig. 5.11 illustrate the throughputs and end-to-end delays, respectively, versus the number of STAs with the RAW groups equal to 2 and 5. Compared to Fig. 5.4 to Fig. 5.7, the performance improvement is more significant with more RAW groups. This is because while the number of STAs increases, the contention becomes more influential and results in more packet loss. From Fig. 5.10, we can observe that the throughputs of the number of RAW groups, $K = 5$, is clearly higher than it is with $K = 2$. Moreover, while the number of STAs increases, the advantages also increase. For example, the throughputs with 2 RAW groups reach 1.11 Mbps, whereas the throughputs with 5 RAW groups arrive at 1.15 Mbps. However, when the number of STAs grows to 100, the throughputs of 2 RAW groups drop to 1.08 Mbps. Meanwhile, the throughputs of 5RAW groups keep at 1.15 Mbps. Therefore, the case of $K = 5$ achieves 6.5% higher performance than the case of $K = 2$.

From Fig. 5.11, again, we can observe that more RAW groups achieve more satisfactory end-to-end delay performance. Similar to the above, while the number of STAs increases, the advantages also increase. For instance, the average end-to-end delays with 2 RAW groups reach 0.7 seconds, whereas the throughput with 5 RAW groups is only 0.56 seconds. Furthermore, when the number of STAs grows to 60, the throughputs of 2 RAW groups rise to 2.25 seconds. Meanwhile, the throughputs of 5RAW groups stand at 1.75 seconds. Therefore, the case of $K = 5$ achieves 28.6% lower end-to-end delay than the case of $K = 2$. In short, the RAW mechanism improves the performance of IEEE 802.11ah, particularly when the number of stations is enormous.

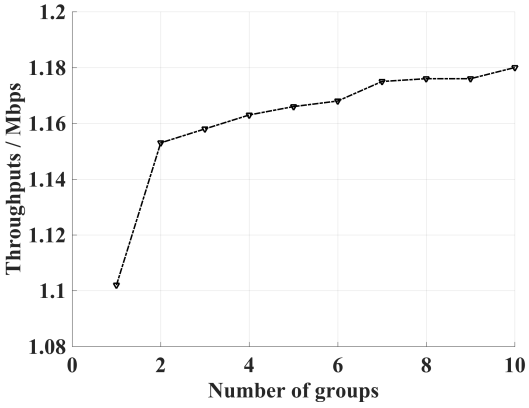

Fig. 5.12 Throughput vs. the number of RAW groups.

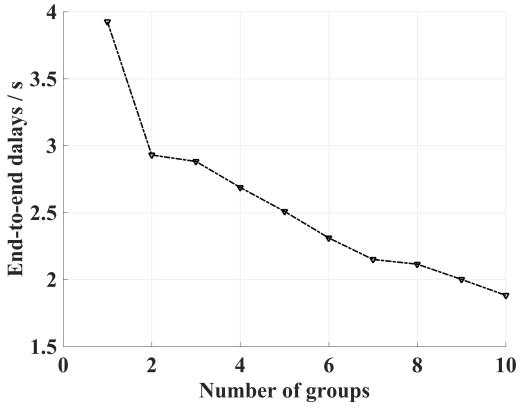

Fig. 5.13 End-to-end delay vs. the number of RAW groups.

Fig. 5.12 and Fig. 5.13 demonstrate the throughputs and end-to-end delays, respectively, versus the number of RAW groups. The effect of the RAW mechanism is tested for a larger-scale network. Therefore, the number of nodes is set to 100. From Fig. 5.12, we can observe the throughputs increase while the number of RAW groups grows. In the beginning, the

number of RAW groups is equal to 1. Therefore, all nodes are kept awake and contend for the wireless channel. In this case, the throughput is 1.10 Mbps. Then, when the number of RAW groups increases, the competition intensity becomes lower. As a result, the throughputs rise higher. The peak throughputs can reach 1.16 Mbps when the number of RAW groups is equal to 10.

Meanwhile, from Fig. 5.13, the end-to-end delays go down while the number of RAW groups grows. Similarly, when the number of RAW groups is low, the strong contention leads to very high end-to-end delays. The highest end-to-end delays appear when the number of RAW groups is equal to 1, which is 3.9s. By contrast, the lowest end-to-end delays, 1.88s, are achieved when the number of the RAW groups is equal to 10. In short, the RAW mechanism can achieve better performance with higher throughputs and lower end-to-end delays for large-scale sensor networks.

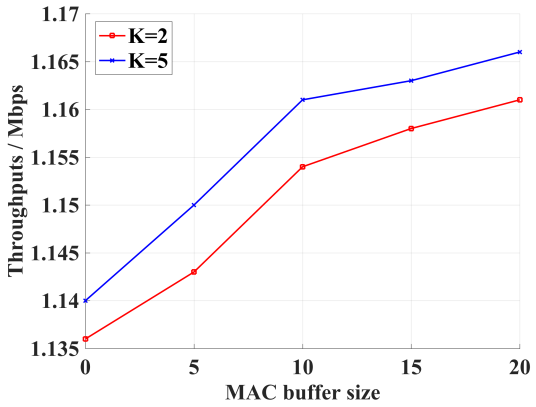

Fig. 5.14 Throughput vs. MAC buffer size.

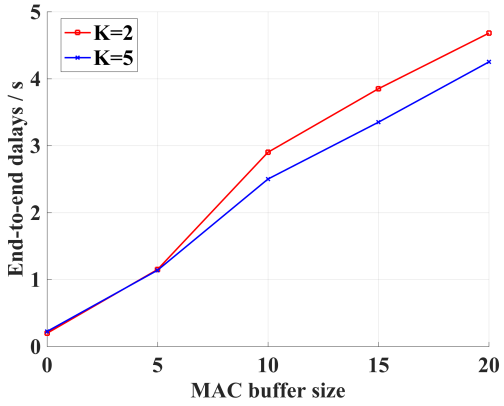

Fig. 5.15 End-to-end delay vs. MAC buffer size.

Fig. 5.14 and Fig. 5.15 indicate the influence of the MAC buffer size on the performance of IEEE 802.11ah. In this case, the number of nodes is equal to 100, and the number of RAW groups is set to 2 and 5. First, Fig. 5.14 shows that while the buffer size increases, the throughputs experience a minor growth tendency. It is because a smaller buffer size leads to more packet drops, and fewer packets are able to be transmitted successfully. Meanwhile, Fig. 5.15 shows the end-to-end delay versus buffer sizes. It is clear that the end-to-end delay climbs while the buffer size increases. It is because of the longer queuing delay with less possibility to discard packets due to a full buffer. In short, the effects of the channel errors and MAC buffer size are noteworthy in the performance evaluation of IEEE 802.11ah.

5.5 Conclusion

In this chapter, we proposed a simulation study of the performance of IEEE 802.11ah with error-prone transmissions. First, the RAW and TWT mechanisms were introduced. Second, the implementation of the RAW mechanism of IEEE 802.11ah was presented. Third, the simulation results of the performance of IEEE 802.11ah was demonstrated. The simulation results clearly indicate the performance improvement due to the RAW mechanism, as it can achieve higher throughputs and lower end-to-end delays. Furthermore, the simulation results also indicate the impact on the performance of channel errors. Moreover, performance improvement is more significant when the number of stations or channel errors grows. Therefore, IEEE 802.11ah and the RAW mechanism are valuable for the IoT as the scale of IoT in Smart Cities can be enormous.

The results of this simulation study give insights into the impact of channel errors, bursty errors and MAC buffer sizes on the performance of IEEE 802.11ah. Moreover, the tendencies for the performance with channel errors and limited buffer sizes are similar to those shown in Chapters 3.5 and 4.5. Therefore, it suggests the probability of analysing the performance of the MAC protocol of IEEE 802.11ah with a similar analytical model proposed in Chapter 3.2.

Some limitations are still needed to be improved. First, the simulation study used a random distribution of the node density. However, it is arguable that a random distribution may not be able to reflect the real operating environments. Second, this simulation study considered non-QoS packets in IEEE 802.11ah. It is considerable to examine the performance of QoS scenarios.

Chapter 6

Conclusion and Future Work

6.1 Conclusion

To conclude, first, this research presented a comprehensive analytical model for IEEE 802.11p under imperfect channels. Second, this research presented an improved analytical model of IEEE 802.11p with bursty error transmissions. Third, this research proposed a set of simulation studies of the performance of IEEE 802.11ah.

In Chapter 2, the background knowledge of this thesis has been introduced. First, the characteristics of IEEE 802.11p have been discussed. Second, the related works of the performance analysis of IEEE 802.11p have been analysed. Third, the characteristics of IEEE 802.11ah have been introduced. Also, a detailed literature review on related works of IEEE 802.11ah has been given.

In Chapter 3, we presented a new analytical model based on 3-D Markov Chain and Queuing analysis to analyse the performance of IEEE 802.11p under imperfect channels. First, we began by analysing the EDCA mechanism of IEEE 802.11p. Second, we proposed an analytical model which comprehensively describes the CW back-off and AIFS deferring procedure for all four AC queues simultaneously within one 3-D Markov Chain. As a comprehensive model, all influential factors, including back-off counter freezing, AIFS deferring and internal collisions, are mathematically included. Third, we validated our model through a series of simulations. The results proved the efficiency and accuracy of the presented model. After that, the performances of IEEE 802.11p were evaluated in terms of throughputs, end-to-end delays and packet loss rate. Specially, the impact of channel errors and buffer sizes were analysed, which were widely ignored in previous works. The results of the presented model indicate their decisive effects of them.

In Chapter 4, we presented an improved analytical model of the performance of IEEE 802.11p with bursty error transmissions. First, a two-state continuous-time Markov chain

was introduced to model the channel status within the urban area. Second, the improved analytical model was presented. Also, a detailed analysis of the buffer queues of the MAC layer of IEEE 802.11p was proposed. Third, we validated this improved model through a series of simulations. At last, we used the presented model to evaluate the performance of IEEE 802.11p with bursty error transmissions.

In Chapter 5, we proposed a simulation study of the performance analysis of IEEE 802.11ah. First, we introduced the unique mechanisms of IEEE 802.11ah, including the grouping, RAW, and TWT. Second, we discussed the implementation and simulation design of IEEE 802.11ah. Third, the performances of IEEE 802.11ah were analysed regarding the throughputs, end-to-end delays and packet loss rates. Finally, the simulation results suggest the powerful influence of channel errors and the RAW mechanism. Remarkably, the improvement in performance due to the RAW mechanism indicates the great potential of IEEE 802.11ah in Smart Cities.

6.2 Future work

6.2.1 Extending the proposed analytical model of IEEE 802.11p with other traffic models

Although the efficiency of the proposed 3-D Markov chain analytical model in Chapter 3 and Chapter 4 has already been proven, nevertheless, there is still room for improvement. Therefore, some approaches that can improve the proposed model are conceivable.

Traffic models are a vital component of the performance analysis of IEEE 802.11p. However, the reliability of different traffic models has been controversial since the network was invented. Since it is the most widely used and oldest traffic model [145], the Poisson Model is assumed as the traffic of the proposed models in this research. Nonetheless, it is criticised for failing to model the multimedia traffic in the modern network uses [146]. Moreover, some researchers suggested the bursty traffic loads in wireless networks [147, 148]. Thus, modelling the performance of IEEE 802.11p with bursty traffics is an attractive direction.

Many research efforts on the performance analysis of wireless networks have already been presented. For example, [149] compared the throughput estimation with an on-off traffic model for IEEE 802.11b. Furthermore, [83] proposed an analytical model to evaluate the throughputs based on burst traffic transmissions for IEEE 802.11e. Moreover, [150] examined the latency performance for IEEE 802.11 with a Markov-modulated Poisson process (MMPP) model. However, all of the works above are not designed for IEEE 802.11p.

Few papers considered bursty traffic of the performance analysis for IEEE 802.11p. It is because the vehicular environment of IEEE 802.11p brings more uncertainty to the traffics. However, some works still discussed the conceivable traffic models in IEEE 802.11p. For instance, [48] proposed an analysis of unbalanced traffics in different priorities. However, the back-off counter freezing was ignored. Moreover, [151] evaluated the performance of IEEE 802.11p under the assumption of finite traffics. Furthermore, [152] analysed vehicular networks' performance under on-off traffic. Nevertheless, it assumed a different vehicle network architecture based on cellular networks. In short, there is a clear gap in the existing studies on the influences of load traffic on the performance of IEEE 802.11p. Therefore, evaluating the performance of IEEE 802.11p under busty traffic can be a good development for this research.

6.2.2 Performance optimization of IEEE 802.11p

The proposed analytical model is able to precisely evaluate the influence of factors on the performance of IEEE 802.11p. Therefore, it can be a good fundamental to optimise the QoS of IEEE 802.11p.

Many research works aimed to improve the QoS of IEEE 802.11p with data-driven approaches. For example, [153] introduced a Q-Learning method of the back-off procedure of the MAC layer in IEEE 802.11p. It utilised a Learning-based decision process instead of the exponential increase of the contention window. However, this method entirely dismissed the EDCA mechanism in IEEE 802.11p. Therefore, it can support only one AC simultaneously and cannot achieve prioritised medium access. Besides, [154] proposed a Q-Learning method to improve efficiency and access fairness according to the contention status. It developed a Machine-Learning based method to adjust the contention window size, including the maximum and minimum value of the contention window. Nevertheless, this work also ignored the EDCA mechanism in IEEE 802.11p. As a result, it failed to meet the differentiated QoS requirements, which are vital in IoV.

Moreover, [155] took the bit error rates into consideration. It designed a Deep Learning process to estimate the channel status of vehicular networks. However, as it has been analysed in Chapter 2 and Chapter 4, the channel errors of the IoV are bursty and complex. Likewise, [156] presented a Neural Network approach to achieve a lower bit error rate in IEEE 802.11p. Nevertheless, it failed to link the MAC layer with the mechanism.

Meanwhile, [157] proposed a Deep Learning approach to improve the reliability of IEEE 802.11p. Nonetheless, it considered only safety applications and ignored the multiple non-safety applications, which are also supposed to require high reliability. Similarly, [158] also presented a Machine-Learning method to decrease the latency for safety applications.

Correspondingly, it estimated the impact of channel errors. Again, it operates only for broadcasting and safety applications.

Based on the discussion above, the proposed analytical model is vital for the data-driven approaches to optimise the QoS of IEEE 802.11p. First, with the proposed model, the linkage effects of the EDCA parameters on the performance of IEEE 802.11p. Therefore, it is possible to combine a Learning-based decision-making method for the EDCA mechanism based on the results of the performance evaluations of the proposed analytical model. Second, our model also indicated the impact of BER and bursty errors on the performance of IEEE 802.11p. Thus, it is valuable to utilise the proposed model to estimate the effect of a Learning-based approach on the PHY layer of IEEE 802.11p. In short, the presented analytical model is beneficial for data-driven approaches to achieve better performance.

6.2.3 Modelling of the MAC protocol of IEEE 802.11ah

With the proposed analytical model for IEEE 802.11p and simulation study IEEE 802.11ah, it is valuable to migrate the analytical model to evaluate the performance of IEEE 802.11ah.

Although some primary research on the performance analysis of IEEE 802.11ah has already been presented, they are insufficient and incomplete. For instance, [159] introduced a 2-D Markov Chain model to estimate the throughputs of the DCF mechanism for IEEE 802.11ah. In addition, it analysed the influences on the saturation throughputs of the RAW mechanism. Based on [159], [160] proposed a similar model to evaluate the throughputs with two different priorities for the MAC layer of IEEE 802.11ah. However, this work did not consider all four AC queues in the EDCA mechanism. Besides, [161] offered an analytical model to evaluate the RAW mechanism's effect based on a 2-D Markov Chain. However, the RAW mechanism is different from the definition in the IEEE 802.11ah protocol. In short, the existing studies on the performance analysis of IEEE 802.11ah are inadequate and unfinished.

Consequently, due to the commonalities in the MAC layer of the two standards, it is possible to develop a comprehensive analytical model for IEEE 802.11ah based on the proposed analytical model for IEEE 802.11p. Although it is a challenge caused by the grouping and RAW mechanism, it is achievable according to the implementation of the simulation study of IEEE 802.11ah.

References

[1] F. Akhter, S. Khadivizand, H. R. Siddiquei, M. E. E. Alahi, and S. Mukhopadhyay, "IoT enabled intelligent sensor node for smart city: Pedestrian counting and ambient monitoring," *Sensors*, vol. 19, no. 15, p. 3374, 2019.

[2] S. Latif, H. Afzaal, and N. A. Zafar, "Intelligent traffic monitoring and guidance system for smart city," pp. 1–6, 2018.

[3] V. Chamola, F. R. Yu, B. Sikdar, S. Kanhere, and M. Guizani, "Guest editorial: Internet of drones: Novel applications, recent deployments, and integration," *IEEE Internet of Things Magazine*, vol. 4, no. 4, pp. 8–10, 2021.

[4] D. Evans, "How the next evolution of the internet is changing everything," 2011.

[5] "IEEE standard for information technology– local and metropolitan area networks– specific requirements– part 11: Wireless lan medium access control (MAC) and physical layer (phy) specifications amendment 6: Wireless access in vehicular environments," *IEEE Std 802.11p-2010 (Amendment to IEEE Std 802.11-2007 as amended by IEEE Std 802.11k-2008, IEEE Std 802.11r-2008, IEEE Std 802.11y-2008, IEEE Std 802.11n-2009, and IEEE Std 802.11w-2009)*, pp. 1–51, 2010.

[6] M. A. Togou, L. Khoukhi, and A. S. Hafid, "Throughput analysis of the IEEE802.11p EDCA considering transmission opportunity for non-safety applications," pp. 1–6, 2016.

[7] J. Du, X. Liu, and L. Rao, "Proactive doppler shift compensation in vehicular cyber-physical systems," *IEEE/ACM Transactions on Networking*, vol. 26, no. 2, pp. 807–818, 2018.

[8] N. Wang and J. Hu, "Performance analysis of the IEEE 802.11p for vehicular networks with bursty packet errors," *2022 IEEE International Conference on Trust, Security and Privacy in Computing and Communications (TrustCom): Workshop 5: Next Generation Data-driven Networks (NGDN-2022)*, 2022.

[9] K. T. Herring, J. W. Holloway, D. H. Staelin, and D. W. Bliss, "Path-loss characteristics of urban wireless channels," *IEEE Transactions on Antennas and Propagation*, vol. 58, no. 1, pp. 171–177, 2010.

[10] J. Karedal, N. Czink, A. Paier, F. Tufvesson, and A. F. Molisch, "Path loss modeling for vehicle-to-vehicle communications," *IEEE Transactions on Vehicular Technology*, vol. 60, no. 1, pp. 323–328, 2011.

[11] D. Shukla, V. Kumar, e. D. Prakash, Arun", H. Kar, C. Kumar, and V. Bhadauria, "Performance evaluation of IEEE 802.11p physical layer for efficient vehicular communication," *Advances in VLSI, Communication, and Signal Processing*, pp. 51–60, 2020.

[12] J. Gopinath and B. Nithya, "Mathematical and simulation analysis of contention resolution mechanism for IEEE 802.11ah networks," *Computer Communications*, vol. 124, pp. 87–100, 2018.

[13] "IEEE standard for information technology–telecommunications and information exchange between systems - local and metropolitan area networks–specific requirements - part 11: Wireless lan medium access control (MAC) and physical layer (phy) specifications amendment 2: Sub 1 GHz license exempt operation," *IEEE Std 802.11ah-2016 (Amendment to IEEE Std 802.11-2016, as amended by IEEE Std 802.11ai-2016)*, p. 1–594, 2017.

[14] Z. Wang, S. Jin, L. Liu, C. Fang, M. Li, and S. Guo, "Design of intelligent connected cruise control with vehicle-to-vehicle communication delays," *IEEE Transactions on Vehicular Technology*, pp. 1–1, 2022.

[15] C. Sun, S. Zheng, and Y. Ma, "An active safety control method of collision avoidance for intelligent connected vehicle based on driving risk perception," *Journal of Intelligent Manufacturing*, vol. 32, p. 1249–1269, 2021.

[16] P. Arthurs, L. Gillam, P. Krause, N. Wang, K. Halder, and A. Mouzakitis, "A taxonomy and survey of edge cloud computing for intelligent transportation systems and connected vehicles," *IEEE Transactions on Intelligent Transportation Systems*, vol. 23, no. 7, pp. 6206–6221, 2022.

[17] M. Aloqaily, S. Otoum, Ridhawi, and Y. Jararweh, "An intrusion detection system for connected vehicles in smart cities," *Ad Hoc Networks*, vol. 90, pp. 101–142, 2019.

[18] B. Fiebig, "European traffic accidents and purposed solutions," *Proc. ITU-T Workshop on Standardisation in Telecommunication for motor vehicles*, vol. 90, pp. 101–142, 2003.

[19] S. Yogarayan, "Wireless ad hoc network of manet, vanet, fanet and sanet: A review," *Journal of Telecommunication, Electronic and Computer Engineering (JTEC)*, vol. 90, pp. 13–78, 2021.

[20] S. Fatih and S. Sevil, "A survey of attacks and detection mechanisms on intelligent transportation systems," *Ad Hoc Network.*, vol. 61, pp. 33–50, 2017.

[21] A. Sumalee and H. Ho, "Smarter and more connected: Future intelligent transportation system," *in IATSS Research*, vol. 42, pp. 67–71, 2018.

[22] O. Kaiwartya and et al., "Internet of vehicles: Motivation, layered architecture, network model, challenges, and future aspects," *IEEE Access*, vol. 4, pp. 5356–5373, 2016.

[23] H. Yu, R. Liu, Z. Li, Y. Ren, and H. Jiang, "An RSU deployment strategy based on traffic demand in vehicular Ad Hoc Networks (vanets)," *IEEE Internet of Things Journal*, vol. 9, no. 9, pp. 6496–6505, 2022.

[24] W. Shi, H. Zhou, J. Li, W. Xu, N. Zhang, and X. Shen, "Drone assisted vehicular networks: Architecture, challenges and opportunities," *IEEE Network*, vol. 32, pp. 130–137, 2018.

[25] M. Baqer and A. Krings, "On the reliability of vanet safety applications for bicycles," *2019 IEEE International Conference on Connected Vehicles and Expo (ICCVE)*, pp. 1–6, 2019.

[26] S. Y. Gelbal, S. Arslan, H. Wang, B. Aksun-Guvenc, and L. Guvenc, "Elastic band based pedestrian collision avoidance using V2X communication," *2017 IEEE Intelligent Vehicles Symposium (IV)*, pp. 270–276, 2017.

[27] F. Arena, G. Pau, and A. Severino, "V2X communications applied to safety of pedestrians and vehicles," *Journal of Sensor and Actuator Networks*, vol. 9, pp. 2224–2708, 2020.

[28] S. Kohler, B. Schreiner, S. Ronalter, K. Doll, U. Brunsmann, and K. Zindler, "Autonomous evasive maneuvers triggered by infrastructure-based detection of pedestrian intentions," *2013 IEEE Intelligent Vehicles Symposium (IV)*, pp. 519–526, 2013.

[29] S. S. F. Sakiz, "A survey of attacks and detection mechanisms on intelligent transportation systems: Vanets and iov," *Ad Hoc Networks*, vol. 61, pp. 33–50, 2017.

[30] K. Z. Zhenyu. Liu, Lin. Pu and L. Zhang, "Design and evaluation of V2X communication system for vehicle and pedestrian safety," *The Journal of China Universities of Posts and Telecommunications*, vol. 22, pp. 18–26, 2015.

[31] H. Gao, C. Liu, Y. Li, and X. Yang, "V2vr: Reliable hybrid-network-oriented v2v data transmission and routing considering RSUs and connectivity probability," *IEEE Transactions on Intelligent Transportation Systems*, vol. 22, pp. 3533–3546, 2021.

[32] M. M.Bayat, M.Pournaghi, "Nera: A new and efficient RSU based authentication scheme for vanets," *Wireless Networks*, vol. 26, p. 3083–3098, 2020.

[33] W. S. Atoui, W. Ajib, and M. Boukadoum, "Offline and online scheduling algorithms for energy harvesting RSUs in vanets," *IEEE Transactions on Vehicular Technology*, vol. 67, pp. 6370–6382, 2018.

[34] A. Pundir, S. Singh, M. Kumar, A. Bafila, and G. J. Saxena, "Cyber-physical systems enabled transport networks in smart cities: Challenges and enabling technologies of the new mobility era," *IEEE Access*, vol. 10, pp. 16350–16364, 2022.

[35] S. Chen, J. Hu, Y. Shi, L. Zhao, and W. Li, "A vision of c-V2X: Technologies, field testing, and challenges with chinese development," *IEEE Internet of Things Journal*, vol. 7, no. 5, pp. 3872–3881, 2020.

[36] M. Hasan, S. Mohan, T. Shimizu, and H. Lu, "Securing vehicle-to-everything (V2X) communication platforms," *IEEE Transactions on Intelligent Vehicles*, vol. 5, pp. 693–713, 2020.

[37] G. S. Khekare and A. V. Sakhare, "A smart city framework for intelligent traffic system using vanet," *in 2013 International Mutli-Conference on Automation, Computing, Communication, Control and Compressed Sensing (iMAC4s)*, pp. 302–305, 2013.

[38] X. Li, B.-J. Hu, H. Chen, G. Andrieux, Y. Wang, and Z.-H. Wei, "An RSU-coordinated synchronous multi-channel MAC scheme for vehicular Ad Hoc Networks," *IEEE Access*, vol. 3, pp. 2794–2802, 2015.

[39] H. Zhou, W. Xu, J. Chen, and W. Wang, "Evolutionary V2X technologies toward the internet of vehicles: Challenges and opportunities," *Proceedings of the IEEE*, vol. 108, no. 2, pp. 308–323, 2020.

[40] Z. Wu, J. Zhao, Y. Zhu, K. Lu, and F. Shi, "Research on in-vehicle key management system under upcoming vehicle network architecture," *Electronics*, vol. 8, no. 9, 2019.

[41] H. Guo and S. Mahmud, "In-vehicle network architecture for the next-generation vehicles," *Automotive Informatics and Communicative Systems*, vol. 8, pp. 283–302, 01 2009.

[42] J. Huang, M. Zhao, Y. Zhou, and C.-C. Xing, "In-vehicle networking: Protocols, challenges, and solutions," *IEEE Network*, vol. 33, no. 1, pp. 92–98, 2019.

[43] D. Vadhwani and D. Thakor, "Statistical analysis of vehicle detection in the its application for monitoring the traffic and road accident using internet of things," *Advances in VLSI and Embedded Systems*, pp. 55–70, 2021.

[44] E. Kidando, R. Moses, M. Ghorbanzadeh, and E. E. Ozguven, "Traffic operation and safety analysis on an arterial highway: Implications for connected vehicle applications," *2018 21st International Conference on Intelligent Transportation Systems (ITSC)*, pp. 2753–2758, 2018.

[45] Z. H. Mir, J. Toutouh, F. Filali, and Y.-B. Ko, "Enabling dsrc and c-V2X integrated hybrid vehicular networks: Architecture and protocol," *IEEE Access*, vol. 8, pp. 180909–180927, 2020.

[46] Q. Xu, T. Mak, J. Ko, and R. Sengupta, "Vehicle-to-vehicle safety messaging in dsrc," *Proceedings of the 1st ACM International Workshop on Vehicular Ad Hoc Networks*, p. 19–28, 2004.

[47] Y. Li, "An overview of the dsrc/wave technology," *Quality, Reliability, Security and Robustness in Heterogeneous Networks*, pp. 544–558, 2012.

[48] C. Han, M. Dianati, R. Tafazolli, R. Kernchen, and X. Shen, "Analytical study of the IEEE 802.11p MAC sublayer in vehicular networks," *IEEE Transactions on Intelligent Transportation Systems*, vol. 13, no. 2, pp. 873–886, 2012.

[49] W. W. Pamungkas, T. Suryani and A. Affandi, "Doppler effect mitigation on v2v channels with moving scatterers using dynamic equalization based on the coherence time," *International Journal of Wireless Information Networks*, vol. 28, p. 332–343, 2021.

[50] N. Wang and J. Hu, "Performance analysis of the IEEE 802.11p EDCA for vehicular networks in imperfect channels," *20th International Conference on Ubiquitous Computing and Communications (IUCC/CIT/DSCI/SmartCNS)*, pp. 535–540, 2021.

[51] F. Zeng, C. Li, and H. Wang, "Performance evaluation of different fading channels in vehicular Ad Hoc Networks," pp. 356–361, 2018.

[52] C. Chen, L. Liu, T. Qiu, J. Jiang, Q. Pei, and H. Song, "Routing with traffic awareness and link preference in internet of vehicles," *IEEE Transactions on Intelligent Transportation Systems*, vol. 23, no. 1, pp. 200–214, 2022.

[53] P. Li, Y. Zeng, C. Li, L. Chen, H. Wang, and C. Chen, "A probabilistic broadcasting scheme for emergent message dissemination in urban internet of vehicles," *IEEE Access*, vol. 9, pp. 113187–113198, 2021.

[54] T. Qiu, X. Liu, K. Li, Q. Hu, A. K. Sangaiah, and N. Chen, "Community-aware data propagation with small world feature for internet of vehicles," *IEEE Communications Magazine*, vol. 56, no. 1, pp. 86–91, 2018.

[55] K. Zrar Ghafoor, L. Kong, S. Zeadally, A. S. Sadiq, G. Epiphaniou, M. Hammoudeh, A. K. Bashir, and S. Mumtaz, "Millimeter-wave communication for internet of vehicles: Status, challenges, and perspectives," *IEEE Internet of Things Journal*, vol. 7, no. 9, pp. 8525–8546, 2020.

[56] A. Karim, "Development of secure internet of vehicle things (iovt) for smart transportation system," *Computers and Electrical Engineering*, vol. 102, p. 108101, 2022.

[57] J. Wang, C. Jiang, Z. Han, Y. Ren, and L. Hanzo, "Internet of vehicles: Sensing-aided transportation information collection and diffusion," *IEEE Transactions on Vehicular Technology*, vol. 67, no. 5, pp. 3813–3825, 2018.

[58] L. Zhao, W. Zhao, A. Hawbani, A. Y. Al-Dubai, G. Min, A. Y. Zomaya, and C. Gong, "Novel online sequential learning-based adaptive routing for edge software-defined vehicular networks," *IEEE Transactions on Wireless Communications*, vol. 20, no. 5, pp. 2991–3004, 2021.

[59] G. Bianchi, "Performance analysis of the IEEE 802.11 distributed coordination function," *IEEE Journal on Selected Areas in Communications*, vol. 18, pp. 535–547, 2000.

[60] K. Duffy, D. Malone, and D. Leith, "Modeling the 802.11 distributed coordination function in non-saturated conditions," *IEEE Communications Letters*, vol. 9, no. 8, pp. 715–717, 2005.

[61] J. R. Norris, "Markov chains," vol. 1, 1998.

[62] J. Hui and M. Devetsikiotis, "A unified model for the performance analysis of IEEE 802.11e EDCA," *IEEE Transactions on Communications*, vol. 53, pp. 1498–1510, 2005.

[63] J. Hu, G. Min, W. Jia, and M. Woodward, "Comprehensive qos analysis of enhanced distributed channel access in wireless local area networks," *Information Science*, vol. 214, p. 20–34, 2012.

[64] A. V. C. Campolo, A. Molinaro and Y. Zhang, "Modeling prioritized broadcasting in multichannel vehicular networks," *IEEE Transactions on Vehicular Technology*, vol. 61, pp. 687–701, 2012.

[65] J. R. Gallardo, D. Makrakis, and H. T. Mouftah, "Performance analysis of the EDCA medium access mechanism over the control channel of an IEEE 802.11p wave vehicular network," pp. 1–6, 2009.

[66] K. Xu, D. Tipper, Y. Qian, and P. Krishnamurthy, "Time-dependent performance analysis of IEEE 802.11p vehicular networks," *IEEE Transactions on Vehicular Technology*, vol. 65, no. 7, pp. 5637–5651, 2016.

[67] H. J. F. Qiu, I. W.-H. Ho, C. K. Tse, and Y. Xie, "A methodology for studying 802.11p vanet broadcasting performance with practical vehicle distribution," *IEEE Transactions on Vehicular Technology*, vol. 64, no. 10, pp. 4756–4769, 2015.

[68] Y. Harkat, Amrouche, E. Lamini, and M. Kechad, "Modeling and performance analysis of the IEEE 802.11p EDCA mechanism for vanet under saturation traffic conditions and error-prone channel," *AEU - International Journal of Electronics and Communications*, vol. 10, p. 2019, 33-43.

[69] C. Song, "Performance analysis of the IEEE 802.11p multichannel MAC protocol in vehicular Ad Hoc Networks,"

[70] A. A. Almohammedi, N. K. Noordin, A. Sali, F. Hashim, and M. Balfaqih, "An adaptive multi-channel assignment and coordination scheme for IEEE 802.11p/1609.4 in vehicular ad-hoc networks," *IEEE Access*, vol. 6, pp. 2781–2802, 2018.

[71] J. Zheng and Q. Wu, "Performance modeling and analysis of the IEEE 802.11p EDCA mechanism for vanet," *IEEE Transactions on Vehicular Technology*, vol. 65, pp. 2673–2687, 2016.

[72] S. Cao and V. Lee, "An accurate and complete performance modeling of the IEEE 802.11p MAC sublayer for vanet," *Computer Communications*, vol. 149, pp. 107–120, 2020.

[73] R. H. S. Kim and Y. Fang, "Analysis of the IEEE 802.11e EDCA under statistical traffic," *IEEE Transactions on Vehicular Technology*, vol. 2, pp. 855–864, 2008.

[74] O. M. Abu-sharkh and A. H. Tewfik, "Toward accurate modeling of the IEEE 802.11e EDCA under finite load and error-prone channel," *IEEE Transactions on Wireless Communications*, vol. 7, pp. 2560–2570, 2008.

[75] V. V. P. Chatzimisios and A. C. Boucouvalas, "Revisit of fading channel characteristics in IEEE 802.11 wlans: independent and burst transmission errors," *2006 IEEE 17th International Symposium on Personal, Indoor and Mobile Radio Communications*, pp. 1–6, 2006.

[76] S. Pack, X. Shen, J. W. Mark, and L. Cai, "A two-phase loss differentiation algorithm for improving tfrc performance in IEEE 802.11 wlans," *IEEE Transactions on Wireless Communications*, vol. 6, no. 11, pp. 4164–4175, 2007.

[77] D. P. A. Jun Yin, Xiaodong Wang, "Impact of bursty error rates on the performance of wireless local area network (wlan)," *Ad Hoc Networks*, vol. 4, pp. 651–668, 2006.

[78] W.-T. Chen, T.-C. Lin, Y.-C. Chang, and J.-C. Chen, "Dynamic packet selection for h.264 video streaming over IEEE 802.11e wlans," pp. 3133–3138, 2008.

[79] H. Liang, C. Ke, C. Shieh, W. Hwang, and N. Chilamkurti, "Performance evaluation of 802.11e edcf in the ad-hoc mode with real audio/video traffic," pp. 6 pp.–6, 2006.

[80] Q. Pang, V. Leung, and S. Liew, "A rate adaptation algorithm for IEEE 802.11 wlans based on MAC-layer loss differentiation," pp. 659–667 Vol. 1, 2005.

[81] B. Munir, N. K. Chilamkurti, and B. Soh, "A comparative study of voice over wireless networks using ns-2 simulation with an integrated error model," pp. 1–5, 2006.

[82] S. Cristobal Perez, H. Alberto Facchini, L. Alberto Bisaro, and J. Campos, "Tuning mechanism for IEEE 802.11e EDCA optimization," *IEEE Latin America Transactions*, vol. 11, no. 4, pp. 1134–1142, 2013.

[83] G. Min, J. Hu, W. Jia, and M. E. Woodward, "Performance analysis of the txopscheme in IEEE 802.11e wlans with bursty error channels," pp. 1–6, 2009.

[84] V. Shivaldova and C. F. Mecklenbrauker, "A two-state packet error model for vehicle-to-infrastructure communications," pp. 1–5, 2013.

[85] Y. Yao, L. Rao, and X. Liu, "Performance and reliability analysis of IEEE 802.11p safety communication in a highway environment," *IEEE Transactions on Vehicular Technology*, vol. 62, no. 9, pp. 4198–4212, 2013.

[86] Y. Yao, L. Rao, X. Liu, and X. Zhou, "Delay analysis and study of IEEE 802.11p based dsrc safety communication in a highway environment," pp. 1591–1599, 2013.

[87] O. Tickoo and B. Sikdar, "Modeling queueing and channel access delay in unsaturated IEEE 802.11 random access MAC based wireless networks," *IEEE/ACM Transactions on Networking*, vol. 16, no. 4, pp. 878–891, 2008.

[88] W. Zhang and S. A. Y. Aung, N.and Dhelim, "Diftos: A distributed infrastructure-free traffic optimization system based on vehicular Ad Hoc Networks for urban environments," *Sensors*, vol. 18, p. 2567, 2018.

[89] X. L. Y. Yao, L. Rao and X. Zhou, "Delay analysis and study of IEEE 802.11p based dsrc safety communication in a highway environment," *2013 Proceedings IEEE INFOCOM*, p. 2013, 1591-1599.

[90] A. Almohammedi and V. Shepelev, "Saturation throughput analysis of steganography in the IEEE 802.11p protocol in the presence of non-ideal transmission channel," *IEEE Access*, vol. 9, pp. 14459–14469, 2021.

[91] L. D. Xu, W. He, and S. Li, "Internet of things in industries: A survey," *IEEE Transactions on Industrial Informatics*, vol. 10, no. 4, pp. 2233–2243, 2014.

[92] A. Osseiran, O. Elloumi, J. Song, and J. F. Monserrat, "Internet of things," *IEEE Communications Standards Magazine*, vol. 1, no. 2, pp. 84–84, 2017.

[93] K. Kim, Y.-H. Han, and S.-G. Min, "An authentication and key management mechanism for resource constrained devices in IEEE 802.11-based IoT access networks," *Sensors*, vol. 17, p. 2170, 09 2017.

[94] L. C. Püschel, M. Röglinger, and R. Brandt, "Unblackboxing smart things—a multilayer taxonomy and clusters of nontechnical smart thing characteristics," *IEEE Transactions on Engineering Management*, vol. 69, no. 5, pp. 2129–2143, 2022.

[95] Y. Meng, W. Zhang, H. Zhu, and X. S. Shen, "Securing consumer IoT in the smart home: Architecture, challenges, and countermeasures," *IEEE Wireless Communications*, vol. 25, no. 6, pp. 53–59, 2018.

[96] A. Broering, C. Niedermeier, I. Olaru, U. Schopp, K. Telschig, and M. Villnow, "Toward embodied intelligence: Smart things on the rise," *Computer*, vol. 54, no. 7, pp. 57–68, 2021.

[97] P. Chanak and I. Banerjee, "Internet-of-things-enabled smartvillages: An overview," *IEEE Consumer Electronics Magazine*, vol. 10, no. 3, pp. 12–18, 2021.

[98] S. Feng, P. Setoodeh, and S. Haykin, "Smart home: Cognitive interactive people-centric internet of things," *IEEE Communications Magazine*, vol. 55, no. 2, pp. 34–39, 2017.

[99] Y. Mehmood, F. Ahmad, I. Yaqoob, A. Adnane, M. Imran, and S. Guizani, "Internet-of-things-based smart cities: Recent advances and challenges," *IEEE Communications Magazine*, vol. 55, no. 9, pp. 16–24, 2017.

[100] L. Tian, S. Santi, A. Seferagi, J. Lan, and J. Famaey, "Wi-fi halow for the internet of things: An up-to-date survey on IEEE 802.11ah research," *Journal of Network and Computer Applications*, vol. 182, p. 103036, 2021.

[101] E. Ahmed, I. Yaqoob, A. Gani, M. Imran, and M. Guizani, "Internet-of-things-based smart environments: state of the art, taxonomy, and open research challenges," *IEEE Wireless Communications*, vol. 23, no. 5, pp. 10–16, 2016.

[102] M. Singh and G. Baranwal, "Quality of service (qos) in internet of things," pp. 1–6, 2018.

[103] A. Kumar and G. P. Hancke, "A zigbee-based animal health monitoring system," *IEEE Sensors Journal*, vol. 15, no. 1, pp. 610–617, 2015.

[104] Z. Pu, M. Zhu, W. Li, Z. Cui, X. Guo, and Y. Wang, "Monitoring public transit ridership flow by passively sensing wi-fi and bluetooth mobile devices," *IEEE Internet of Things Journal*, vol. 8, no. 1, pp. 474–486, 2021.

[105] H. Mrabet, S. Belguith, A. Alhomoud, and A. Jemai, "A survey of IoT security based on a layered architecture of sensing and data analysis," *Sensors*, vol. 20, no. 13, 2020.

[106] Prahlad, M. Prasanna, V. Rakesh, and M. R. Ahmed, "Design of dual-band microstrip antenna for wimax and x band applications," pp. 598–602, 2018.

[107] A. Sørensen and et al, "Modeling and experimental validation for battery lifetime estimation in NB-IoT and lte-m," *IEEE Internet of Things Journal*, vol. 9, no. 12, pp. 9804–9819, 2022.

[108] B. S. Pavan, M. Mahesh, and V. Harigovindan, "Performance anomaly of group-synchronized distributed coordination function in IEEE 802.11ah based multi-rate IoT networks," pp. 1–5, 2020.

[109] M. Meera and S. N. Rao, "A survey of the state of the art of 802.11ah," pp. 1–4, 2017.

[110] K. H. Chang, "IEEE 802.11 for sub 1 GHz [industry perspectives]," *IEEE Wireless Communications*, vol. 20, no. 5, pp. 8–9, 2013.

[111] M. Park, "IEEE 802.11ah: Energy efficient MAC protocols for long range wireless lan," pp. 2388–2393, 2014.

[112] A. F. Rochim, B. Harijadi, Y. P. Purbanugraha, S. Fuad, and K. A. Nugroho, "Performance comparison of wireless protocol IEEE 802.11ax vs 802.11ac," pp. 1–5, 2020.

[113] A. Sjivo, D. Kerkhove, L. Tian, J. Famaey, A. Munteanu, I. Moerman, J. Hoebeke, and E. De Poorter, "Performance evaluation of IEEE 802.11ah networks with high-throughput bidirectional traffic," *Sensors*, vol. 18, no. 2, p. 325, 2018.

[114] N. Ahmed, D. De, F. A. Barbhuiya, and M. I. Hussain, "MAC protocols for IEEE 802.11ah-based internet of things: A survey," *IEEE Internet of Things Journal*, vol. 9, no. 2, pp. 916–938, 2022.

[115] A. Seferagić, I. Moerman, E. De Poorter, and J. Hoebeke, "Evaluating the suitability of IEEE 802.11ah for low-latency time-critical control loops," *IEEE Internet of Things Journal*, vol. 6, no. 5, pp. 7839–7848, 2019.

[116] N. Ahmed and M. I. Hussain, "Periodic traffic scheduling for IEEE 802.11ah networks," *IEEE Communications Letters*, vol. 24, no. 7, pp. 1510–1513, 2020.

[117] S. M. Soares and M. M. Carvalho, "An analytical model for the aggregate throughput of IEEE 802.11ah networks under the restricted access window mechanism," *Sensors*, vol. 22, p. 15, 2022.

[118] S. Santi, L. Tian, E. Khorov, and J. Famaey, "Accurate energy modeling and characterization of IEEE 802.11ah raw and twt," *Sensors*, vol. 19, no. 11, p. 2614, 2019.

[119] M. Z. Ali, J. Mišić, and V. B. Mišić, "Efficiency of restricted access window scheme of IEEE 802.11ah under non-ideal channel condition," 2018.

[120] T. A. Riza and D. Gunawan, "IEEE 802.11ah network challenges supports covid-19 prevention team," pp. 73–76, 2020.

[121] L. R. Lakshmi and B. Sikdar, "Fair scheduling in IEEE 802.11ah networks for internet of things applications," pp. 1–7, 2019.

[122] S. Aust, R. V. Prasad, and I. G. Niemegeers, "Performance study of mimo-ofdm platform in narrow-band sub-1 GHz wireless lans," pp. 89–94, 2013.

[123] S. KHAN and M. ZEESHAN, "Performance and throughput analysis of IEEE 802.11ah for multiband multimode operation," *2018 21st International Symposium on Wireless Personal Multimedia Communications (WPMC)*, pp. 150–155, 2018.

[124] L. F. Del Carpio, P. Di Marco, P. Skillermark, R. Chirikov, K. Lagergren, and P. Amin, "Comparison of 802.11ah and ble for a home automation use case," pp. 1–6, 2016.

[125] B. Bellekens, L. Tian, P. Boer, M. Weyn, and J. Famaey, "Outdoor IEEE 802.11ah range characterization using validated propagation models," pp. 1–6, 2017.

[126] S. Santi, A. jivo, L. Tian, E. De Poorter, J. Hoebeke, and J. Famaey, "Supporting heterogeneous IoT traffic using the IEEE 802.11ah restricted access window," vol. 7, p. 2, 2017.

[127] E. Khorov, A. Krotov, A. Lyakhov, R. Yusupov, M. Condoluci, M. Dohler, and I. Akyildiz, "Enabling the internet of things with wi-fi halow—performance evaluation of the restricted access window," *IEEE Access*, vol. 7, pp. 127402–127415, 2019.

[128] N. Nawaz, M. Hafeez, S. Zaidi, D. McLernon, and M. Ghogho, "Throughput enhancement of restricted access window for uniform grouping scheme in IEEE 802.11ah," pp. 1–7, 2017.

[129] O. Raeesi, J. Pirskanen, A. Hazmi, J. Talvitie, and M. Valkama, "Performance enhancement and evaluation of IEEE 802.11ah multi-access point network using restricted access window mechanism," pp. 287–293, 2014.

[130] B. Badihi, L. F. Del Carpio, P. Amin, A. Larmo, M. Lopez, and D. Denteneer, "Performance evaluation of IEEE 802.11ah actuators," pp. 1–5, 2016.

[131] O. Raeesi, J. Pirskanen, A. Hazmi, T. Levanen, and M. Valkama, "Performance evaluation of IEEE 802.11ah and its restricted access window mechanism," pp. 460–466, 2014.

[132] A. Hazmi, J. Rinne, and M. Valkama, "Feasibility study of i 802.11ah radio technology for IoT and M2M use cases," *2012 IEEE Globecom Workshops*, pp. 1687–1692, 2012.

[133] A. A. Marwan, D. Perdana, and D. D. Sanjoyo, "Performance analysis of raw impact on IEEE 802.11ah standard affected by doppler effect," *Int. J. Comput. Commun. Control*, vol. 14, pp. 212–219, 2019.

[134] L. Kleinrock, "Queueing systems," vol. 1, 1975.

[135] OpenStreetMap contributors, "Planet dump retrieved from https://planet.osm.org ," *https://www.openstreetmap.org*, 2017.

[136] ns 3 Network Simulator p. Available online: https://www.nsnam.org/ (accessed on 6 June 2021).

[137] P. e. a. Lopez, "Microscopic traffic simulation using sumo," *2018 21st International Conference on Intelligent Transportation Systems (ITSC)*, pp. 2575–2582, 2018.

[138] B. Rashid and M. H. Rehmani, "Applications of wireless sensor networks for urban areas: A survey," *Journal of Network and Computer Applications*, vol. 60, pp. 192–219, 2016.

[139] A. Al-Hourani, S. Kandeepan, and A. Jamalipour, "Modeling air-to-ground path loss for low altitude platforms in urban environments," pp. 2898–2904, 2014.

[140] M. Giordani, T. Shimizu, A. Zanella, T. Higuchi, O. Altintas, and M. Zorzi, "Path loss models for v2v mmwave communication: Performance evaluation and open challenges," pp. 1–5, 2019.

[141] L. Tian, J. Famaey, and S. Latré, "Evaluation of the IEEE 802.11ah restricted access window mechanism for dense IoT networks," *2016 IEEE 17th International Symposium on A World of Wireless, Mobile and Multimedia Networks (WoWMoM)*, pp. 1–9, 2016.

[142] L. Tian, A. ljivo, S. Santi, E. De Poorter, J. Hoebeke, and J. Famaey, "Extension of the IEEE 802.11ah ns-3 simulation module," *Proceedings of the 2018 Workshop on Ns-3*, p. 53–60, 2018.

[143] E. N. Gilbert, "Capacity of a burst-noise channel," *The Bell System Technical Journal*, vol. 39, pp. 1253–1265, 1960.

[144] L. Tian, S. Deronne, S. Latré, and J. Famaey, "Implementation and validation of an IEEE 802.11ah module for ns-3," *Proceedings of the 2016 Workshop on Ns-3*, p. 49–56, 2016.

[145] V. Frost and B. Melamed, "Traffic modeling for telecommunications networks," *IEEE Communications Magazine*, vol. 32, no. 3, pp. 70–81, 1994.

[146] V. Paxson and S. Floyd, "Wide area traffic: the failure of poisson modeling," *IEEE/ACM Transactions on Networking*, vol. 3, no. 3, pp. 226–244, 1995.

[147] K. Lee, J. Lee, Y. Yi, I. Rhee, and S. Chong, "Mobile data offloading: How much can wifi deliver?," *IEEE/ACM Transactions on Networking*, vol. 21, no. 2, pp. 536–550, 2013.

[148] A. Abdrabou, M. S. A. Darei, M. Prakash, and W. Zhuang, "Application-oriented traffic modeling of wifi-based internet of things gateways," *IEEE Internet of Things Journal*, vol. 9, no. 2, pp. 1159–1170, 2022.

[149] Q. Zhao, D. H. Tsang, and T. Sakurai, "A simple model for nonsaturated IEEE 802.11 dcf networks," *IEEE Communications Letters*, vol. 12, no. 8, pp. 563–565, 2008.

[150] A. Abdrabou and W. Zhuang, "Stochastic delay guarantees and statistical call admission control for IEEE 802.11 single-hop Ad Hoc Networks," *IEEE Transactions on Wireless Communications*, vol. 7, no. 10, pp. 3972–3981, 2008.

[151] D. N. M. Dang, H. N. Dang, T. C. Do, and C. S. Hong, "Performance analysis of the IEEE 802.11p under finite traffic conditions," pp. 191–199, 2014.

[152] T. A. Edwan, A. Tahat, H. Yanikomeroglu, and J. Crowcroft, "An analysis of a stochastic on-off queueing mobility model for software-defined vehicle networks," *IEEE Transactions on Mobile Computing*, vol. 21, no. 5, pp. 1552–1565, 2022.

[153] D. j. Lee, Y. Deng, and Y. J. Choi, "Back-off improvement by using Q-learning in IEEE 802.11p vehicular network," pp. 1819–1821, 2020.

[154] A. Pressas, Z. Sheng, F. Ali, and D. Tian, "A Q-Learning approach with collective contention estimation for bandwidth-efficient and fair access control in IEEE 802.11p vehicular networks," *IEEE Transactions on Vehicular Technology*, vol. 68, no. 9, pp. 9136–9150, 2019.

[155] J. Pan, H. Shan, R. Li, Y. Wu, W. Wu, and T. Q. S. Quek, "Channel estimation based on deep learning in vehicle-to-everything environments," *IEEE Communications Letters*, vol. 25, no. 6, pp. 1891–1895, 2021.

[156] S. Stainton, W. Ozan, M. Johnston, S. Dlay, and P. A. Haigh, "Neural network equalisation and symbol detection for 802.11p v2v communication at 5.9GHz," pp. 1–5, 2020.

[157] S. Ding and X. Ma, "Model-based deep learning optimization of IEEE 802.11 vanets for safety applications," pp. 835–840, 2022.

[158] M. Mohammadi, A. Balador, Z. Fernández, and I. Val, "Adaptive distributed beacon congestion control with MAChine learning in vanets," pp. 766–771, 2021.

[159] U. Sangeetha and A. Babu, "Performance analysis of IEEE 802.11ah wireless local area network under the restricted access window-based mechanism," *International Journal of Communication Systems*, vol. 32, no. 4, p. e3888, 2019.

[160] U. Sangeetha and A. Babu, "Service differentiation in IEEE 802.11ah wlan under restricted access window based MAC protocol," *Computer Communications*, vol. 172, pp. 142–154, 2021.

[161] S. P. Badarla and V. P. Harigovindan, "Restricted access window-based resource allocation scheme for performance enhancement of IEEE 802.11ah multi-rate IoT networks," *IEEE Access*, vol. 9, 2021.